



ELSEVIER

Journal of Nuclear Materials 282 (2000) 245–254

Journal of  
nuclear  
materials

www.elsevier.nl/locate/jnucmat

# Thermally induced gallium removal from plutonium dioxide for MOX fuel production

D.G. Kolman <sup>\*</sup>, M.E. Griego, C.A. James, D.P. Butt <sup>1</sup>

*Materials Corrosion and Environmental Effects Laboratory, Nuclear Materials Technology Division, Los Alamos National Laboratory, MS-E530, P.O. Box 1663, Los Alamos, NM 87545, USA*

Received 1 May 2000; accepted 17 July 2000

## Abstract

A dry process for separating Ga<sub>2</sub>O<sub>3</sub> from PuO<sub>2</sub> – 1 wt% Ga<sub>2</sub>O<sub>3</sub> powder was developed. PuO<sub>2</sub>–Ga<sub>2</sub>O<sub>3</sub> powder was exposed to flowing Ar–6% H<sub>2</sub> at 600–1200°C. Under these conditions, Ga<sub>2</sub>O<sub>3</sub> is reduced to Ga<sub>2</sub>O, a volatile species. Ga<sub>2</sub>O, which is stable in a reducing environment at temperatures greater than 800 °C, evolves and is collected downstream. Different process parameters were varied in an effort to optimize thermally induced gallium removal (TIGR). Exposure temperature had the greatest effect on TIGR. Temperatures of at least 1000 °C were required to obtain discernible TIGR. As little as 25 wppm Ga remained after processing PuO<sub>2</sub> at 1200°C. It is likely that a further reduction in retained Ga can be attained by increasing the processing temperature. Ga removal was shown to increase with process time. However, the benefit in processing beyond 4 h is limited for this system. The lack of effect of sample volume and gas flow rate on TIGR suggests that Ga removal is limited by mass transport within the powder particles. The fact that Ga removal is less efficient in more coarse PuO<sub>2</sub> powders supports this hypothesis. © 2000 Elsevier Science B.V. All rights reserved.

## 1. Introduction

Recent arms control initiatives dictate that the United States convert the plutonium metal from weapons into a form that cannot readily be returned to metal and that may be inspected by international organizations. In January 1997, the Secretary of Energy of the United States signed a Record of Decision finalizing a dual-track strategy to irreversibly dispose of the nation's surplus plutonium. The strategy allows for immobilizing plutonium in inert forms or burning plutonium as mixed oxide (MOX) fuel in existing reactors. There is one potential drawback in using weapons grade plutonium as feed for MOX fuel – weapons grade plutonium contains approximately 1 wt% gallium. Gallium is known to degrade the properties of many metallic materials via

corrosion, embrittlement, or intermetallic compound formation [1–17]. Thus, there is significant concern that gallium present in MOX fuel will compromise zirconium-based fuel cladding [16,18]. A second concern is the detrimental effect of 1 wt% Ga on MOX fuel performance and processibility. The level of Ga that can be tolerated in MOX fuel is not known, but levels of 10 ppm in the MOX fuel (approximately 200 ppm in PuO<sub>2</sub> before blending) appear acceptable based on various studies [16,18,19].

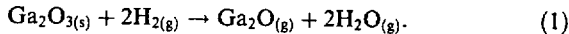
PuO<sub>2</sub>–Ga<sub>2</sub>O<sub>3</sub> particles, which originate from oxidized Pu–Ga alloys, are composed of PuO<sub>2</sub> grains having limited Ga<sub>2</sub>O<sub>3</sub> solubility plus second-phase Ga<sub>2</sub>O<sub>3</sub> grains having limited PuO<sub>2</sub> solubility. Thus, the powder materials are not simple mixtures which can be mechanically separated. Methods for chemically purifying plutonium metal have long been established [20]. These methods use aqueous solutions to dissolve and concentrate the material. Unfortunately, these methods can produce significant mixed waste (i.e., waste containing both radioactive and chemical hazards). The treatment and disposal of the large volume of waste resulting from

<sup>\*</sup> Corresponding author.

<sup>1</sup> Present address: Department of Materials Science and Engineering, Rhines Hall, P.O. Box 116400, University of Florida Gainesville, FL 32611-6400, USA.

aqueous purification of tens of metric tons would be expensive. A new, 'dry' method of purification is required.

$\text{Ga}_2\text{O}$ , a species that is unstable at room temperature, can be stable in the gas phase at elevated temperatures [21,22]. It was hypothesized that  $\text{Ga}_2\text{O}_3$  could be separated from  $\text{PuO}_2$  by passing a reducing gas,  $\text{H}_2$ , over the  $\text{PuO}_2$ - $\text{Ga}_2\text{O}_3$  powder to produce  $\text{Ga}_2\text{O}$  via the reaction



Preliminary experiments indicated that  $\text{Ga}_2\text{O}$  could indeed be vaporized from  $\text{Ga}_2\text{O}_3$  in flowing  $\text{H}_2$  gas and transported downstream [22]. However, it was unclear whether  $\text{Ga}_2\text{O}$  could be vaporized from  $\text{PuO}_2$  incorporating  $\text{Ga}_2\text{O}_3$ . It is the objective of this work to examine the viability of thermally induced gallium removal (TIGR) from  $\text{PuO}_2$  using a reducing gas. A second goal of this work is to determine the factors affecting gallium removal in an effort to optimize the TIGR process.

## 2. Experimental procedure

### 2.1. Material characteristics

Two types of  $\text{PuO}_2$ - $\text{Ga}_2\text{O}_3$  were used for this study. The first was a relatively fine powder produced from Pu-Ga metal using a three-step process, wherein the metal is hydrided, the hydride is nitrided, and the nitride is oxidized [23]. Scattered light analysis of the powder indicated a bimodal particle size distribution with a significant fraction of the powder comprising sub-micron particles (Fig. 1, Lab-Tec particle size analyzer).

An electron micrograph of the three-step powder is shown in Fig. 2. Chemical analysis of this powder indicated a Ga concentration of 0.84 wt% (8400  $\mu\text{g/g}$  (wppm)) or 1.1 at.%. The second type of  $\text{PuO}_2$  (Ga concentration = 8000 wppm) was produced using a direct metal oxidation (DMO) method wherein the metal is converted directly to oxide in air at approximately 600°C. As compared to the three-step process, the DMO method produces a more coarse powder (Fig. 1) having less surface area per gram (Table 1, Quantachrome NOVA-1000 BET surface area analyzer). Loss-on-ignition (LOI) was used to estimate the quantity of water adsorbed on the powder surface. LOI is determined by heating a powder sample to 1000°C for 2 h in air and measuring mass loss [24]. For the three-step and DMO powders, LOI was 0.58% and 0.073%, respectively. Particle size, surface area, and LOI data represent the average of two measurements (measurement errors (S.D.) of 5.8%, 12% and 33%, respectively). The chemical compositions of the powders, determined by a variety of standard analysis techniques (primarily inductively coupled plasma-mass spectroscopy (VG Elemental Plasma Quad 2) and inductively coupled plasma-atomic emission spectroscopy (Thermo Jarrell Ash IRIS CID)), are shown in Table 2. These values are the average of four to seven separate measurements. Commercially pure  $\text{Ga}_2\text{O}_3$  powder (Alfa Aesar) had a reported purity of 99.999% (metal basis).

### 2.2. Test Procedure

TIGR tests comprised the exposure of  $\text{PuO}_2$ - $\text{Ga}_2\text{O}_3$  to high-purity Ar-6%  $\text{H}_2$  gas ( $\text{O}_2 < 8$  ppm,  $\text{H}_2\text{O} < 0.7$

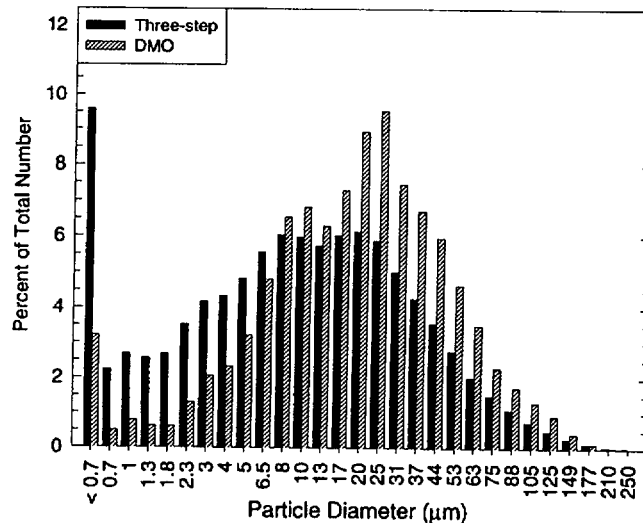


Fig. 1. Particle size distributions of the PuO<sub>2</sub>-Ga<sub>2</sub>O<sub>3</sub> powders used in this study.

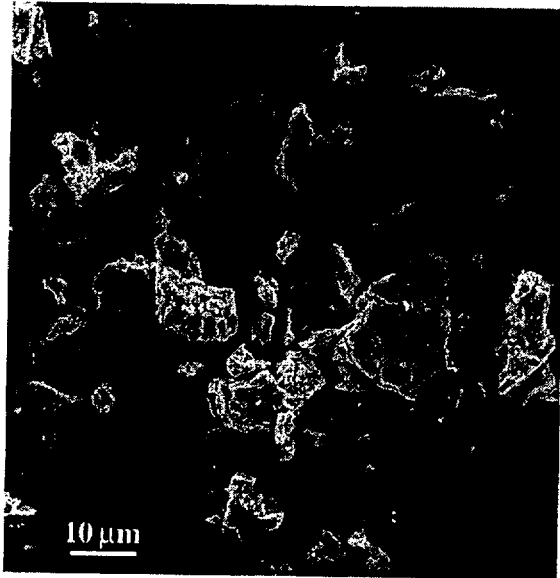


Fig. 2. Micrograph of three-step  $\text{PuO}_2$  powder.

Table 1  
Specific surface areas of various powders

	Three-step	DMO
Untreated	$6.7 \text{ m}^2/\text{g} \pm 0.3$	$1.7 \text{ m}^2/\text{g} \pm 0.2$
Following TIGR (1200°C; 4 h; 1.5 cm/s)	$0.21 \text{ m}^2/\text{g}$	

ppm). Tests were performed within the confines of an Ar-atmosphere glove box. For the majority of small sample tests (typically 0.3, 0.9 and 2.5 g), three samples were simultaneously exposed (see Fig. 3). Simultaneous exposure of three samples yielded results identical to individual exposures. Each  $\text{PuO}_2$  sample was weighed, placed in a nonreactive alumina boat, and then weighed again, noting the total mass of the boat and its contents. These small boats were then placed in a single large alumina boat to facilitate handling. Samples larger than 2.5 g were placed directly in a large boat and exposed individually. The large boat was inserted into the hot zone of a 4.45 cm (1.75 in.) I.D. tube furnace. The hot zone temperature was uniform. The temperature was ramped at a rate of 20°C/min until the temperature of

Table 2  
Primary impurity concentrations in three-step and DMO powders. Values are  $\mu\text{g/g}$  of  $\text{PuO}_2$ . Standard deviations are given as percent of average values

	Ga	H	N	C	Fe	U	Ca	Si	Ni	Cl	Cr	F	Zr	Al	Cu	S
Three-step	8400	510	360	330	240	160	89	79	91	75	48	45	36	27	25	8
DMO	8000	180	320	130	360	98	130	83	95	110	110	34	17	20	24	6
S.D. (%)	7.3	9.2	11	55	34	6.8	41	11	31	68	23	57	21	48	20	59

interest was reached. The samples were held at this temperature for a fixed period of time. At the end of this period, the furnace was turned off and the samples were allowed to cool while maintaining gas flow. Reported test durations include only time at temperature and do not incorporate ramp time. Following cooling to nearly room temperature (<50°C), the samples were removed from the furnace and the gross mass of the boats recorded. Temperature, exposure duration, sample mass, and gas flow velocity were varied in an effort to determine the rate limiting step and thus optimize Ga removal. Two to four replicate tests were performed for most combinations of time, temperature, flow velocity and sample size. A total of 270 experiments were performed. Reproducibility was  $\pm 8\%$  for mass loss values and  $\pm 50\%$  for Ga concentration values based on statistical analyses of experiments that incorporated four replicate tests.

### 3. Results

#### 3.1. Effect of temperature

The remaining Ga concentration in three-step  $\text{PuO}_2$  powder following exposure to Ar–6%  $\text{H}_2$  at different temperatures is shown in Fig. 4. 0.5 h exposures at 600°C and 800°C resulted in essentially no measurable Ga removal, and 900°C exposures yielded only slight Ga removal. Fig. 4 indicates that a temperature of at least 1000°C is required to obtain significant Ga removal. At 1200°C, the Ga concentration was reduced to approximately 150 ppm for a 0.5 h exposure.

Processing at 1200°C resulted in coarsening of the powders, as determined by scattered light particle size analysis (Figs. 5 and 6). Processing also resulted in a dramatic reduction in surface area (Table 1).

#### 3.2. Effect of time

The effect of test duration on TIGR is shown in Fig. 7. Increasing exposure time reduces the concentration of Ga remaining in the samples. For the 24 h exposure (Fig. 7), the Ga concentration is reduced by greater than two orders of magnitude (from 8400 to 33 ppm). However, increasing test duration yields

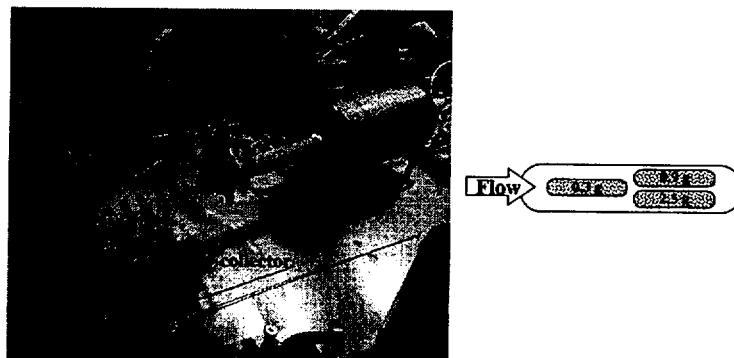


Fig. 3. Picture of furnace setup (left), drawing of boat placement within furnace (top right), and arrangement of small boats within the large boat (bottom right).

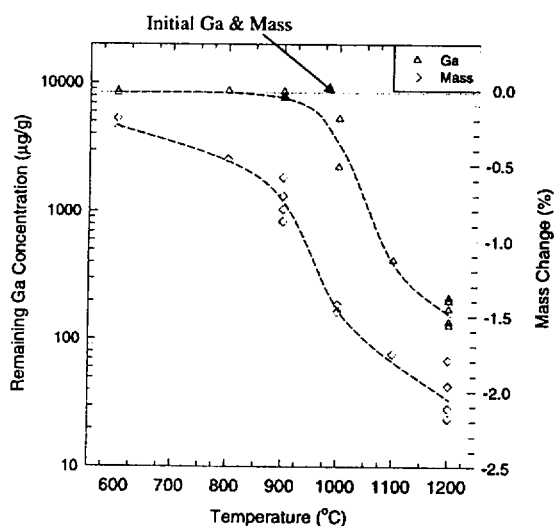


Fig. 4. Remaining Ga concentration in, and mass loss from, three-step powder as a function of exposure temperature in flowing Ar-6% H<sub>2</sub>. Test duration: 0.5 h; sample mass: 2.5 g; flow velocity: 1.5 cm/s.

diminishing returns with respect to Ga removal. For instance, the majority of the Ga is removed during the first 0.5 h (Ga concentration = 110–270 ppm). The asymptotic limit under these test conditions is not clear but testing beyond 4 h provides only a modest reduction of the Ga concentration in PuO<sub>2</sub>-Ga<sub>2</sub>O<sub>3</sub> powder.

### 3.3. Effect of sample mass

The effect of sample mass (and thus sample volume) on Ga removal is shown in Fig. 8. It is seen that the quantity of sample processed at one time has no effect on the Ga removal rate or on mass loss for sample sizes of

0.22–25 g. Linear regression of the data supports this conclusion.<sup>2</sup>

### 3.4. Effect of flow rate

Ga concentration and mass change are plotted as a function of gas flow velocity in Fig. 9 for 2.5 g samples exposed at 1200°C for 4 h. Between 1.5 and 26 cm/s, gas flow rate has no discernible effect on the remaining Ga concentration. In contrast, increasing flow rate increases the mass loss during processing. Linear regression of the data supports the assertion that flow rate affects mass loss but not Ga removal. For 143 observations, it cannot be stated with 95% confidence that flow rate has an effect on the remaining Ga concentration (confidence = 39%). However, for 156 observations, it can be stated with >99.999% confidence that flow rate has an effect on mass change. Similar values are obtained following statistical analysis of DMO material (Ga concentration: 35% confidence, 71 observations; Mass change: >99.995% confidence, 72 observations).

### 3.5. TIGR from different powders

The Ga concentrations within three-step and DMO powders following processing at 1200°C for 4 h are compared in Fig. 10. The DMO material retained slightly more Ga following exposure for the same duration, even though DMO powder had a smaller starting concentration of Ga. Statistical analysis of the data (student *t*-test, 44 observations) indicates a greater than 99% confidence that the retained Ga concentrations are

<sup>2</sup> Note that linear regression of the data is only a semi-quantitative means for assessing the effects of variables on Ga removal because it is clear that there is no linear relationship between temperature or duration and Ga removal.

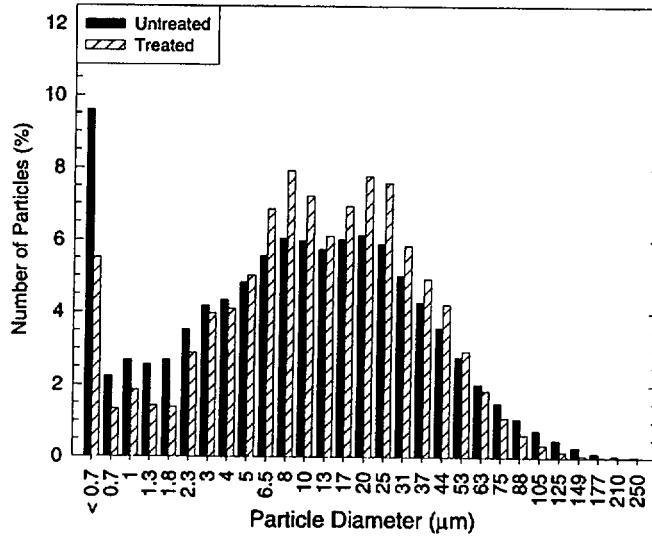


Fig. 5. Three-step powder particle size distribution before and after TIGR (1200°C; 4 h; 1.5 cm/s).

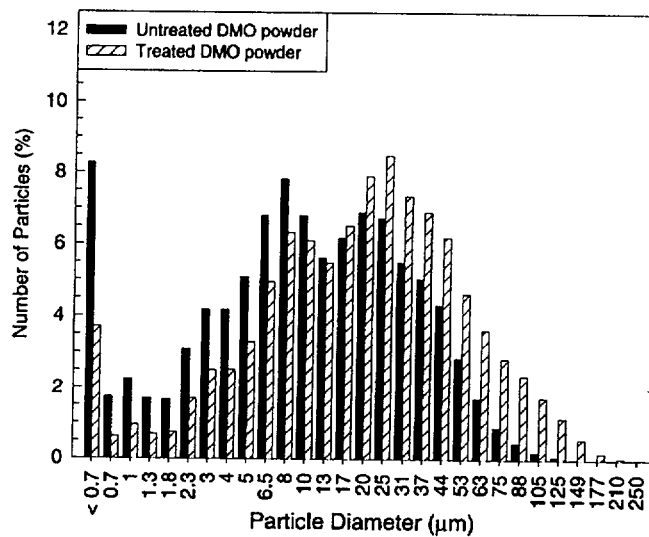


Fig. 6. DMO powder particle size distribution before and after TIGR (1200°C; 4 h; 1.5 cm/s).

different. In contrast to the Ga data, there is a very dramatic difference in the mass changes of the DMO and three-step PuO<sub>2</sub> powders following exposure (Fig. 11). The DMO powder experienced far less mass loss (approximately 1.3%) than the three-step (approximately 2.1%) following a 1200°C exposure for 4 h.

Tests on 2.5 g samples of commercially pure Ga<sub>2</sub>O<sub>3</sub> exposed to 900°C or 1200°C Ar-6% H<sub>2</sub> for 4 h were performed. The mass change of the Ga<sub>2</sub>O<sub>3</sub> powder far exceeded that of 2.5 g samples of the PuO<sub>2</sub> powders (Fig. 12).

#### 4. Discussion

##### 4.1. Process variable effects

Test duration has an effect on TIGR. The remaining Ga concentration decays roughly exponentially. Thus, increasing exposure time produces diminishing returns. Note that test duration as we define it only incorporates the time at temperature, not the ramp-up and ramp-down time. Therefore, if there is some time-temperature equivalence, the time-temperature integral could be

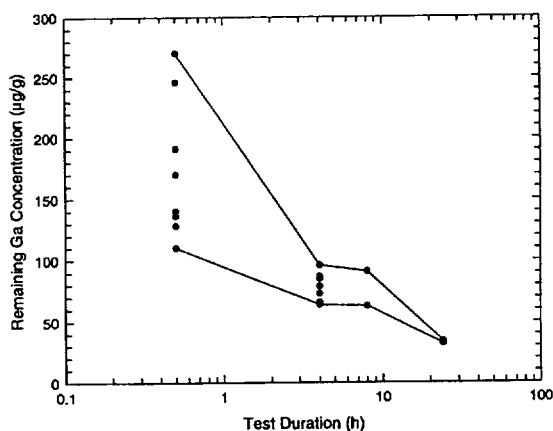


Fig. 7. Remaining Ga concentration in three-step samples as a function of test duration for 0.9 g samples at 1200°C.

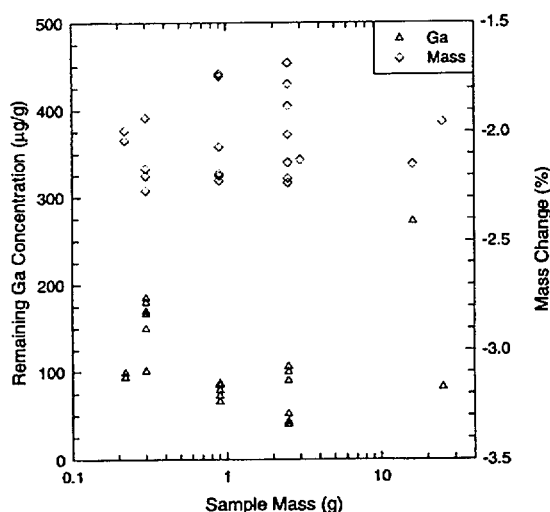


Fig. 8. Remaining Ga concentration and mass change as a function of three-step sample size. Temperature: 1200°C; duration: 4 h; gas flow velocity: 1.5 cm/s.

evaluated and added to the test duration to give a more accurate assessment of Ga removal as a function of time. However, given the scatter in the Ga concentration analyses, this refinement of the data may be considered insignificant and, thus, was not performed. Gas flow velocity had an effect on mass change but not on Ga removal. It may be speculated that the primary effect of flow rate on mass loss is attributable to an effect on PuO<sub>2</sub> reduction because Ga evolution and water desorption (LOI) are unaffected by flow rate. Sample volume had no apparent effect on Ga removal for sample masses of 0.2–25 g for the time-temperature combinations in this study.

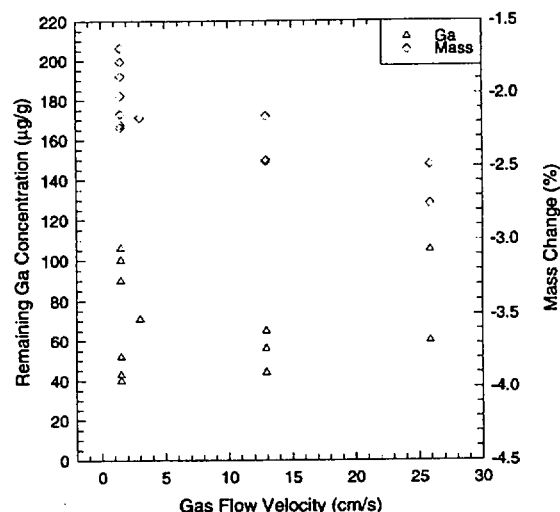


Fig. 9. Remaining Ga concentration in, and mass change of, three-step samples as a function of gas flow velocity. Temperature: 1200°C; duration: 4 h; sample mass: 2.5 g.

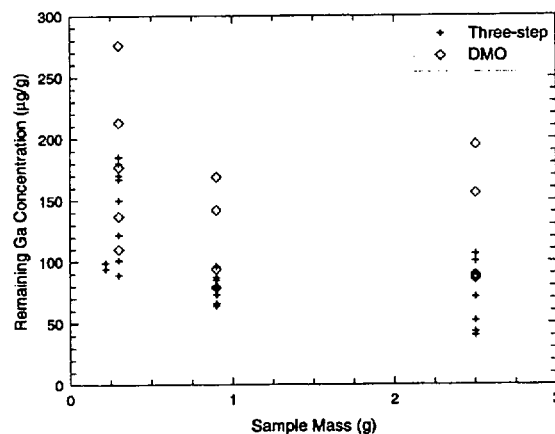


Fig. 10. Comparison of the remaining Ga concentrations within three-step and DMO powders treated at 1200°C for 4 h.

Of the process variables, temperature plays the strongest role in mass change and Ga removal. Fig. 4 shows that there is significant mass loss between 600°C and 800°C even though there is little Ga evolution at these temperatures. Thus, the majority of the mass loss at the lower temperatures is attributable to something other than Ga evolution, i.e., desorption of water [24] and PuO<sub>2</sub> reduction [25–27]. H<sub>2</sub> gas is a known reductant of PuO<sub>2</sub> [25–27]. At lower temperatures, water desorption dominates mass loss, with essentially all water desorbed at 1000°C [24]. At higher temperatures, a significant fraction of the mass loss is attributable to Ga removal. Some reduction of the PuO<sub>2</sub> occurs above

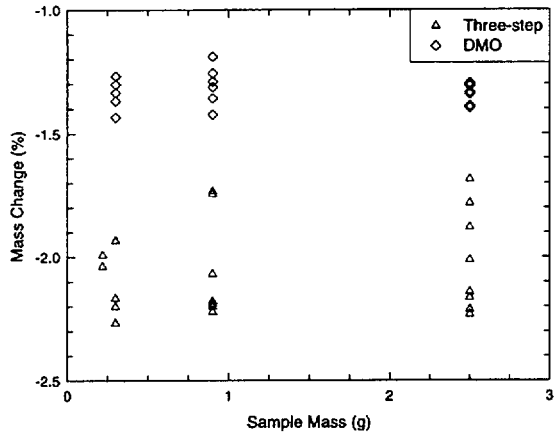


Fig. 11. Comparison of the mass change of three-step and DMO powders treated at 1200°C for 4 h in flowing Ar-6% H<sub>2</sub>

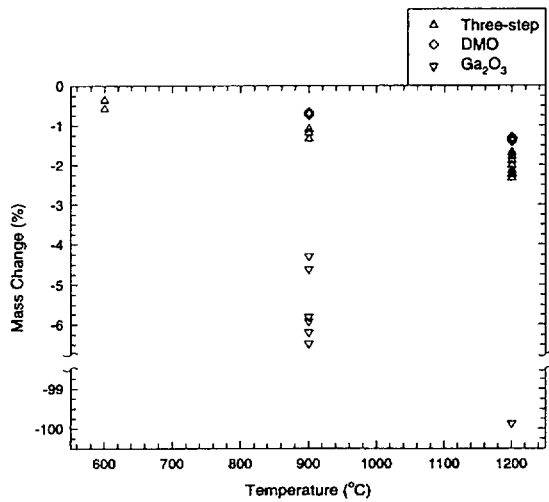


Fig. 12. Plot of mass change as a function of process temperature for different powders exposed to flowing Ar-6% H<sub>2</sub>. Test duration: 4 h; Sample mass: 2.5 g; Flow velocity: 1.5 cm/s.

1000°C because full Ga<sub>2</sub>O<sub>3</sub> loss (1.12 wt%) and H<sub>2</sub>O desorption (0.58 wt%) combined cannot account for the total mass loss of the three-step samples. Mass losses attributable to Ga removal and PuO<sub>2</sub> reduction increase with increasing exposure temperature. A maximum of approximately 4% O<sub>2</sub> loss following PuO<sub>2</sub> reduction is calculated for 1200°C tests.

Regardless of the value of other process parameters, little Ga is removed below 1000°C. Above 1000°C, significant Ga removal occurs during 4 h processing runs. At 1200°C, Ga concentrations as low as 25 ppm were attained (24 h exposure). It is unclear whether there is an ultimate limit for Ga removal or whether the residual

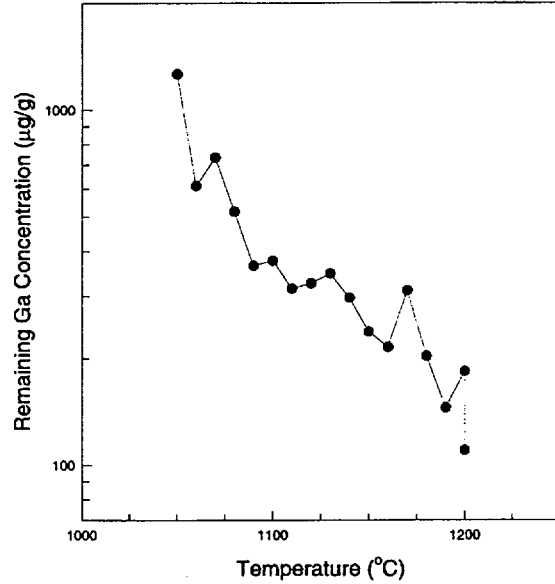


Fig. 13. Plot of remaining Ga concentration as a function of process temperature for 17.5 g DMO samples exposed for 4 h to a 1.5 cm/s gas flow velocity.

Ga concentration can continually be reduced with temperature. Tests employing fine temperature increments between 1050°C and 1200°C suggest that if an ultimate limit exists it is not approached at 1200°C (Fig. 13). Therefore, it is likely that even greater Ga removal could be obtained at higher temperatures.

#### 4.2. Comparison of TIGR from different powders: assessment of the rate limiting step for TIGR

Regardless of the method used to convert Pu-Ga metal to PuO<sub>2</sub>-Ga<sub>2</sub>O<sub>3</sub> powder, the TIGR process used in this study is effective in separating Ga<sub>2</sub>O<sub>3</sub> from PuO<sub>2</sub>. The three-step powder experienced greater mass loss due to Ga removal, given its greater starting concentration of Ga and lower final concentration. The DMO material experienced far less mass loss than the three-step powder regardless of process temperature (Fig. 12), sample size (Fig. 11), test duration (not shown), or gas flow velocity (not shown). The difference in mass loss is primarily attributable to reduced water desorption. The starting DMO powder had approximately 0.5 wt% less water adsorbed on its surface as a result of its smaller surface area. Assuming that Ga evolution, water desorption, and PuO<sub>2</sub> reduction are the only mechanisms for mass loss, the amount of reduction can be calculated. The data suggest that the three-step PuO<sub>2</sub> experienced greater reduction by the H<sub>2</sub> gas than the DMO powder, but this cannot be definitively concluded due to the scatter in the data.

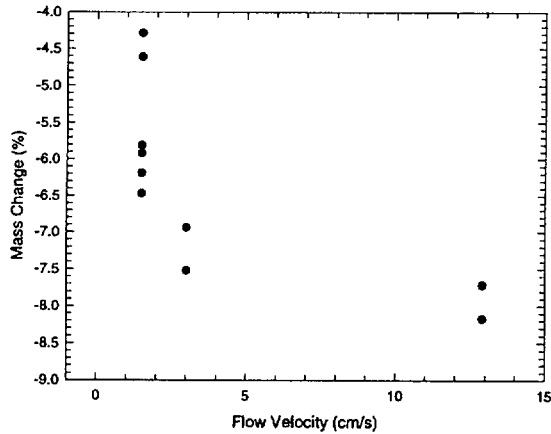


Fig. 14. Plot of mass change as a function of gas flow velocity for 2.5 g samples of commercially pure  $\text{Ga}_2\text{O}_3$  exposed at  $900^\circ\text{C}$  for 4 h.

Ga evolution from commercially pure  $\text{Ga}_2\text{O}_3$  is much greater than that from either of the  $\text{Ga}_2\text{O}_3$ - $\text{PuO}_2$  powders (Fig. 12). Moreover, for pure  $\text{Ga}_2\text{O}_3$ , increasing gas flow rate increases the rate of Ga evolution (Fig. 14). The increased evolution as compared to  $\text{PuO}_2$  and the observed dependence on flow rate indicate that Ga evolution is not reaction rate limited (Eq. (1)) but rather is limited by mass transport. Calculations indicate that in the event of mass transport limitation,  $\text{Ga}_2\text{O}$  will be the limiting species, as opposed to  $\text{H}_2$  or  $\text{H}_2\text{O}$  (Fig. 15) [28]. Thus,  $\text{Ga}_2\text{O}$  transport likely limits the  $\text{Ga}_2\text{O}$  evolution from  $\text{Ga}_2\text{O}_3$ . Given that  $\text{Ga}_2\text{O}$  evolution is not reaction rate limited for pure  $\text{Ga}_2\text{O}_3$ , evolution should not be reaction rate limited for  $\text{PuO}_2$ - $\text{Ga}_2\text{O}_3$ .

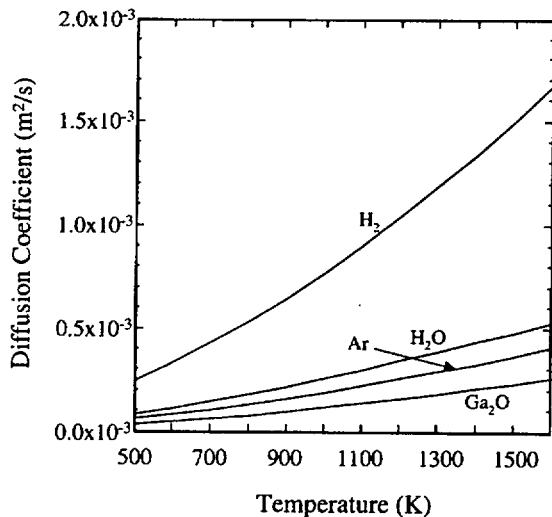


Fig. 15. Diffusion coefficients for relevant gas species as a function of temperature [28].

The fact that Ga removal from  $\text{PuO}_2$ - $\text{Ga}_2\text{O}_3$  powder is unaffected by flow rate suggests that Ga evolution is not limited by mass transport of  $\text{Ga}_2\text{O}$  away from the boat to its deposition point downstream. As Ga evolution does not appear to be either reaction rate limited or mass transport limited by transport away from the boat, the potential rate limiting steps are either mass transport within the  $\text{PuO}_2$  particles themselves, or mass transport within the interstices between the powder particles.

The lack of sample volume effect on TIGR suggests that mass transport within the interstices between the powder particles is not rate controlling. 0.3, 0.9 and 2.5 g samples were placed in identical boats. The depth of the powder was approximately 1, 3 and 7 mm for the 0.3, 0.9 and 2.5 g samples. If mass transport within the interstices was rate limiting it would be expected that larger samples would retain more Ga following processing than smaller samples. This was not observed. In order to further assess whether mass transport within the particle interstices controls TIGR, a 0.3 g sample of three-step  $\text{PuO}_2$  was spread on an alumina plate so that the powder depth was roughly one tenth of that when in the boat. Enhanced TIGR was not observed for the thinly spread sample. Therefore, although not fully conclusive, it does not appear that mass transport within the powder interstices controls Ga evolution.

Given that the larger DMO particles experience less Ga removal than the smaller three-step particles, it may be hypothesized that TIGR is controlled by mass transport within the powder particles. This hypothesis is supported by the fact that the other mechanisms discussed above do not appear to be controlling. However, it cannot be definitively concluded that the system is under solid-state mass transport control at this time. The experiments performed in this work were designed to determine the optimal processing conditions and were not optimized to determine the controlling mechanisms. Other experiments, such as those incorporating a fluidized bed, would be required to reach a definitive conclusion.

The microstructure of  $\text{PuO}_2$ - $\text{Ga}_2\text{O}_3$  may evolve during processing. Initially, a two-phase microstructure is present because  $\text{Ga}_2\text{O}_3$  has a low solubility in  $\text{PuO}_2$ , roughly 45 wppm at  $1200^\circ\text{C}$  [23]. Therefore, there is little  $\text{Ga}_2\text{O}_3$  in solution and the vast majority of the  $\text{Ga}_2\text{O}_3$  in  $\text{PuO}_2$ -1 wt%  $\text{Ga}_2\text{O}_3$  exists as second-phase particles having a  $\text{Ga}_2\text{O}_3$  activity approaching one. As shown by microprobe measurements of  $\text{CeO}_2$  surrogate material [28,29], which is an excellent surrogate for  $\text{PuO}_2$  with respect to TIGR [28–30], Ga migrates to grain boundaries during processing in Ar-6%  $\text{H}_2$ . It has been speculated that the grain boundary compound is not  $\text{Ga}_2\text{O}_3$  but the perovskite-phase  $\text{PuGaO}_3$ , based on thermodynamic predictions [23,28] and experimental evidence [31]. Note that  $\text{PuGaO}_3$  is only stable under reducing conditions.

When the Ga concentration is reduced to levels below 45 wppm, it is unclear whether the remaining Ga is primarily in solution in the PuO<sub>2</sub>, or whether it is primarily present as a grain boundary compound. The remaining Ga is almost certainly not present as the original second-phase Ga<sub>2</sub>O<sub>3</sub> particles because the activity of Ga<sub>2</sub>O<sub>3</sub> in these particles is much larger than that in the PuO<sub>2</sub> matrix. Therefore, the driving force for Ga evolution from second-phase particles is much stronger than that from solid solution. It is clear that if there is an ultimate limit for Ga removal, it is below the 45 wppm solubility of Ga<sub>2</sub>O<sub>3</sub> in PuO<sub>2</sub>, given that 25 wppm Ga remains in PuO<sub>2</sub> following processing at 1200°C for 24 h.

It is clear from the data that the most efficient TIGR from PuO<sub>2</sub> requires the highest temperature achievable, although particle sintering may diminish the benefit from increased temperature under some conditions. In addition to increasing the process temperature, some benefit can be obtained by increasing the exposure duration. However, increasing duration produces diminishing returns. Reducing the starting particle size increases the efficiency of Ga removal, however particle agglomeration during processing (Figs. 5 and 6) limits this benefit. Increasing the intrinsic mass transport at a given temperature would enhance TIGR. However, until the composition and microstructure of Ga within processed powder are better understood, the means for enhancing intrinsic mass transport are unclear. From an industrial standpoint, enhancement of intrinsic mass transport may be preferable to increased temperature, given the increasing attack of furnace materials by Ga<sub>2</sub>O with temperature [15].

## 5. Conclusions

A process for removing Ga<sub>2</sub>O<sub>3</sub> from PuO<sub>2</sub> by exposing PuO<sub>2</sub> powder to Ar–6% H<sub>2</sub> gas at elevated temperature was developed. The effects of temperature, exposure duration, gas flow velocity, and sample size on TIGR from different PuO<sub>2</sub> powders were examined. Little Ga removal was observed at process temperatures below 1000°C. Above 1000°C, Ga removal increased with increasing temperature, with as little as 25 ppm remaining in the powder following a 24 h exposure at 1200°C. Processing at 1200°C resulted in both larger particle sizes and reduced surface areas. Increasing test duration increased TIGR, albeit with diminishing returns over time. Limited benefit is obtained by processing beyond 4 h. Gas flow velocity and sample volume did not appear to significantly affect Ga evolution. It is unclear whether there is an ultimate limit for Ga removal, but it appears that TIGR at even greater temperatures could reduce the remaining Ga concentration within PuO<sub>2</sub> even further. Based on TIGR from Ga<sub>2</sub>O<sub>3</sub>, DMO PuO<sub>2</sub>, and three-step PuO<sub>2</sub>, it appears

that mass transport control within the powder particles limits Ga removal. Further study of the microstructure would be required to determine if the intrinsic mass transport could be enhanced to aid in TIGR.

## Acknowledgements

This work was supported by the Office of Fissile Materials Disposition, United States Department of Energy.

## References

- [1] L.R. Kelman, W.D. Wilkinson, F.L. Yagee, in: Resistance of materials to attack by liquid metals, Argonne National Laboratory Report # ANL-4417, Lemont, IL, 1950.
- [2] P.R. Luebbbers, W.F. Michaud, O.K. Chopra, Compatibility of ITER candidate structural materials with static gallium, Argonne National Laboratory Report # ANL-93/31, Lemont, IL, December 1993.
- [3] M.H. Kamdar, in: ASM Handbook, vol. 11, Failure Analysis and Prevention, American Society for Metals International, Metals Park, OH, 1986, p. 225.
- [4] W.D. Wilkinson, Effects of gallium on materials at elevated temperatures, Argonne National Laboratory Report # ANL-5027, Lemont, IL, 1953.
- [5] M.H. Kamdar, in: C.L. Briant and S.K. Banerji (Eds.), Treatise on Materials Science and Technology, vol. 25, Academic Press, London, 1983, p. 361.
- [6] M.H. Kamdar, Prog. Mater. Sci. 15 (1973) 289.
- [7] T.M. Regand, N.S. Stolo, Metall. Trans. A 8A (1977) 885.
- [8] M. Tanaka, H. Fukunaga, J. Soc. Mater. Sci. Jpn. 18 (1969) 411.
- [9] B.A. Benson, R.G. Hoagland, Scr. Metall. 23 (1989) 1943.
- [10] S.P. Lynch, Acta Metal. 29 (1981) 325.
- [11] C.F. Old, P. Trevena, Met. Sci. 13 (1979) 591.
- [12] J.A. Kargol, D.L. Albright, Metall. Trans. A 8A (1977) 27.
- [13] J.T. Lukowski, D.B. Kasul, L.A. Heldt, C.L. White, Scr. Metall. 24 (1990) 1959.
- [14] D.G. Kolman, Corros. Sci. 42 (2000) in press.
- [15] D.G. Kolman, T.N. Taylor, Y.S. Park, M. Stan, D.P. Butt, C.J. Maggiore, J.R. Tesmer, G.J. Havrilla, Gallium Suboxide Attack of Stainless Steel and Nickel Alloys at 800°C–1200°C, Los Alamos National Laboratory Report # LA-UR-00-0864, February 2000; submitted to Oxidation of Metals.
- [16] D.F. Wilson, J.R. DiStefano, J.P. Strizak, J.F. King, E.T. Manneschildt, Interactions of zircaloy cladding with gallium: Final Report, Oak Ridge National Laboratory Technical Report No. ORNLTM-13684, Oak Ridge, TN, September 1998.
- [17] P.H. Au-Yeung, J.T. Lukowski, L.A. Heldt, C.L. White, Scr. Metall. 24 (1990) 95.
- [18] M.K. West, Gallium interactions with zircaloy, Amarillo National Resource Center for Plutonium Technical Report No. ANRCP-1999-2, Amarillo, TX, January 1999.

- [19] R.R. Hart, J. Rennie, K. Aucoin, M. West, K. Ünl and C. Ríos-Martinez, Gallium Interactions with Zircaloy Cladding, Amarillo National Resource Center for Plutonium Report ANRCP-1998-5, Amarillo, TX, 1998.
- [20] J.M. Cleveland, in: O.J. Wick (Ed.), Plutonium Handbook, A guide to the Technology, vol. 1, American Nuclear Society, La Grange Park, IL, 1980, p. 553.
- [21] T.M. Besmann, J. Am. Ceram. Soc. 81 (1998) 3071.
- [22] D.P. Butt, Y. Park, T.N. Taylor, J Nucl Mater 264 (1999) 71.
- [23] H.R. Trellue, T. Baros, H.T. Blair, J.J. Buksa, D.P. Butt, K. Chidester, S.F. De Muth, S.L. Eaton, R. Hanrahan, G.J. Havrilla, C.A. James, D.G. Kolman, R.E. Mason, Y. Park, M. Stan, J.H. Steele Jr., S.S. Voss, T.C. Wallace Sr., C.G. Worley, Nuclear Fuels Technologies Fiscal Year 1997 Research and Development Test Results, Los Alamos National Laboratory Report # LA-UR-97-4423, Los Alamos, NM, October 1997.
- [24] J.L. Stakebake, L.M. Steward, J. Colloid Interf. Sci. 42 (1973) 328.
- [25] E.R. Gardner, T.L. Markin, R.S. Street, J. Inorg. Nucl. Chem. 27 (1965) 541.
- [26] H.E. Flotow, M. Tetenbaum, J. Chem. Phys. 74 (1981) 5269.
- [27] R.L. Deaton, G.L. Silver, Radiochem. Radioanal. Lett. 10 (1972) 277.
- [28] H.R. Trellue, D.P. Butt, S.F. De Muth, S.L. Eaton, R. Hanrahan, G.J. Havrilla, C. Haertling, C.A. James, D.G. Kolman, R.E. Mason, P. Chodak, A.D. Neuman, Y. Park, C.A. Smith, M. Stan, S.A. Talachy, J. Teague, C.G. Worley, Nuclear Fuels Technologies Fiscal Year 1998 Research and Development; Summary of Test Results, Los Alamos National Laboratory Report # LA-UR-98-5355, Los Alamos, NM, November 1998.
- [29] Y. Park, D.G. Kolman, H. Zira e, C. Haertling, D.P. Butt, Mater. Res. Soc. Symp. Proc. 556 (1999) 129.
- [30] D.G. Kolman, Y. Park, M. Stan, R.J. Hanrahan Jr., D.P. Butt, An assessment of the validity of cerium oxide as a surrogate for plutonium oxide gallium removal studies, Los Alamos National Laboratory Report # LA-UR-99-491, Los Alamos, NM, January 1999.
- [31] J.R. Schoonover, A. Saab, J.S. Bridgewater, G.J. Havrilla, C.T. Zugates, P.J. Treado, Appl. Spectrosc. 54 (2000) in press.



**GROUNDWATER MIXING ZONE  
APPLICATION  
FOR THE  
OLD F-AREA SEEPAGE BASIN (U)**

March 1997

# 81

Westinghouse Savannah River Company  
Savannah River Site  
Aiken, South Carolina 29808

---

PREPARED FOR THE U. S. DEPARTMENT OF ENERGY  
UNDER CONTRACT NO. DE-AC09-96SR18500



**GROUNDWATER MIXING ZONE  
APPLICATION  
FOR THE  
OLD F-AREA SEEPAGE BASIN (904-49G) (U)**

**Prepared By:**

**Westinghouse Savannah River Company  
Savannah River Site  
Aiken, South Carolina 29808**

**Prepared for the U.S. Department Of Energy  
Under Contract DE-AC09-96SR18500**

**GROUNDWATER MIXING ZONE APPLICATION  
FOR THE  
OLD F-AREA SEEPAGE BASIN (904-49G) (U)**

**DISCLAIMER**

This report was prepared for the United States Department of Energy under Contract No. DE-AC09-96SR18500 and is an account of work performed under that contract. Reference herein to any specific commercial product, process or service does not necessarily constitute or imply endorsement, recommendation, or favoring of same by Westinghouse Savannah River Company or by the United States Government or any agency thereof.

Printed in the United States of America

Prepared For  
U. S. Department of Energy  
and  
Westinghouse Savannah River Company

**TABLE OF CONTENTS**

<b>1.0 INTRODUCTION.....</b>	<b>1</b>
1.1 PURPOSE.....	1
1.2 GROUNDWATER MIXING ZONE APPLICATION REQUIREMENTS.....	2
1.3 UNIT DESCRIPTION.....	2
<b>2.0 GROUNDWATER DATA SUMMARY.....</b>	<b>3</b>
<b>3.0 DESCRIPTION OF MODELING.....</b>	<b>6</b>
<b>4.0 MODEL RESULTS.....</b>	<b>7</b>
<b>5.0 COMPLIANCE WELL MONITORING.....</b>	<b>9</b>
<b>6.0 UNCERTAINTIES.....</b>	<b>10</b>
<b>7.0 CONCLUSIONS.....</b>	<b>11</b>
<b>REFERENCES.....</b>	<b>13</b>

**APPENDIX A: Old F-Area Seepage Basin Modeling**

List of Tables

*Table 1. Contaminant Concentrations Exceeding MCLs from Third Quarter 1993 to Second Quarter 1996.....4*

*Table 2. Input parameters for OFASB solute transport model.....7*

*Table 3. Listing of MZCLs and MCLs for the Constituents of Concern.....8*

*Table 4. Contaminants not Modeled but Requiring Further Monitoring.....8*

*Table 5. Sampling Schedule for Plume Wells and Compliance Boundary Wells.....10*

List of Figures

*Figure 1. Simulated Vertical Groundwater Flow.....14*

*Figure 2. Concentration Trend for Gross Alpha.....15*

*Figure 3. Concentration Trend for Non-volatile Beta.....16*

*Figure 4. Concentration Trend for Iodine-129.....17*

*Figure 5. Concentration Trend for Total Lead.....18*

*Figure 6. Concentration Trend for Lead-212.....19*

*Figure 7. Concentration Trend for Manganese.....20*

*Figure 8. Concentration Trend for Nitrate as Nitrogen.....21*

*Figure 9. Concentration Trend for Potassium-40.....22*

*Figure 10. Concentration Trend for Radium-228.....23*

*Figure 11. Concentration Trend for Radium-226.....24*

*Figure 12. Concentration Trend for Strontium-90.....25*

*Figure 13. Concentration Trend for Tritium.....26*

*Figure 14. Concentration Trend for Total Uranium.....27*

*Figure 15. Concentration Trend for Uranium-234.....28*

*Figure 16. Concentration Trend for Uranium-238.....29*

*Figure 17. Initial Concentration Contours for Iodine-129.....30*

*Figure 18. Initial Concentration Contours for Nitrate.....31*

*Figure 19. Initial Concentration Contours for Strontium-90.....32*

*Figure 20. Initial Concentration Contours for Tritium.....33*

*Figure 21. Initial Concentration Contours for Total Uranium.....34*

*Figure 22. Location Modeled Compliance Boundary.....35*

*Figure 23. Iodine-129 Concentration at Compliance Boundary.....36*

*Figure 24. Nitrate Concentration at Compliance Boundary.....37*

*Figure 25. Strontium-90 Concentration at Compliance Boundary.....38*

*Figure 26. Tritium Concentration at Compliance Boundary.....39*

*Figure 27. Total Uranium Concentration at Compliance Boundary.....40*

*Figure 28. Locations of Plume Wells, Intermediate Wells, and Compliance Boundary Wells.....41*

## 1.0 INTRODUCTION

### 1.1 Purpose

This document provides the technical justification and basis for the groundwater mixing zone (GWMZ) application in support of the Old F-Area Seepage Basin (OFASB) at the Savannah River Site (SRS). This document is being prepared pursuant to the South Carolina Water Classifications and Standards (R.61-68 and R.61-69). The Corrective Measures Study/Feasibility Study (CMS/FS) (WSRC 1996a) and the Statement of Basis/Proposed Plan (WSRC 1996b) have been submitted and approved by the South Carolina Department of Health and Environmental Control (SCDHEC) and the Environmental Protection Agency (EPA). The Record of Decision (ROD) document has been submitted to SCDHEC and EPA. The selected remedy in the ROD addresses the contaminated soils in the OFASB that pose the principal threat to human health and the environment. The remedial action objective (RAO) for the groundwater beneath the OFASB is that, through natural attenuation, the concentrations of the contaminants in the groundwater will decrease to levels at or below the remedial goal options (RGOs) specified for the contaminants of interest. The RGOs are the Maximum Contaminant Levels (MCLs) or risk-based concentrations (RBCs), where MCLs are not available.

The selected remedial action for the surface unit consists of stabilizing the contaminated soil within the basin, filling the basin with clean soil, and capping the basin. Although groundwater concentrations beneath the unit have exceeded MCLs in previous sampling events, the concentrations of contaminants have not been increasing over time. The remedial actions selected for the surface unit will reduce the potential for further contamination by stabilizing the contaminants and by significantly reducing infiltration through the contaminated soil. In addition, through institutional controls the selected remedy will control potential human exposure to contaminants during the time period when the groundwater mixing zone is in effect. During this time, radiological and chemical degradation, dilution, and sorption to soil particles in the aquifer should be sufficient to provide passive aquifer restoration within a period of 2 to 115 years, depending on the contaminant.

Mixing Zone Concentration Limits (MZCLs) are established for those contaminants that exceeded MCLs during the sampling events reported in the Resource Conservation and Recovery Act (RCRA) Facility Investigation/Remedial Investigation (RFI/RI) (WSRC 1995a) and which continue to exceed MCLs in subsequent sampling events. Additionally, this application outlines a long-term monitoring program utilizing the existing monitoring well network, as well as a series of monitoring wells to be installed at the compliance boundary and at a location between the OFASB and the compliance boundary.

### **1.2 Groundwater Mixing Zone Application Requirements**

This GWMZ application is being prepared in accordance with the *Ground-Water Mixing Zone Guidance Document* issued by SCDHEC (1994). A satisfactory GWMZ application must meet the four criteria identified in the guidance document. These criteria are listed below:

- (1) reasonable measures have been taken or binding commitments are made to minimize the addition of contaminants to groundwater and/or control the migration of contaminants in groundwater.
- (2) the groundwater in question is confined to a shallow geologic unit that has little or no potential of being an Underground Source of Drinking Water, and discharges or will discharge to surface waters without contravening the surface water standard as set forth in this regulation.
- (3) the contaminants in question occur on the property of the applicant, and there is minimum possibility for ground-water withdrawals (present or future) to create drawdown such that contaminants would flow off-site.
- (4) the contaminants or combination of contaminants in question are not dangerously toxic, mobile, or persistent.

This document provides discussion and results of groundwater modeling that addresses each of these criteria.

### **1.3 Unit Description**

A complete unit description and unit history can be found in the OFASB CMS/FS Report (WSRC 1996a). This section provides a brief unit description of the features that are relevant to the GWMZ application.

The OFASB is located near the geographic center of SRS, approximately 600 feet north of F Area and one mile east of Road C, in an area which has been recommended for industrial use by the SRS Citizen's Advisory Board (CAB). The OFASB is located at the top of a gentle slope at an elevation of 285 feet above mean sea level (msl). Surface drainage is to the north toward Upper Three Runs (UTR) Creek. The topography between the OFASB and the wetland area near UTR Creek slopes sharply.

The water table is approximately 75 feet below ground surface in the area of the OFASB. Groundwater flow for the water table is north toward Upper Three Runs Creek with a horizontal hydraulic gradient of 0.02. Estimates of hydraulic conductivity for the water

table obtained from several groundwater flow models were from 0.66 to 4.25 feet/day. Total porosity of the sediments range approximately from 0.35 to 0.60. Effective porosity values range approximately from 0.20 to 0.40 (WSRC 1996a).

## 2.0 Groundwater Data Summary

Groundwater monitoring data indicate that release of radiological substances to groundwater from the OFASB has occurred. Groundwater data was obtained from eight wells located in the vicinity of the OFASB (FNB wells). Five of the FNB wells are screened in the water table (Aquifer IIB) and three are screened in the Gordon Aquifer (IIA). Data from the Gordon Aquifer (IIA) was not considered in this GWMZ application, because, it is highly unlikely that the source of the contamination in the Gordon Aquifer (IIA) is the OFASB. Particle tracking performed in the flow model illustrates that infiltration through the OFASB would discharge to the water table and disperse in three dimensions. The horizontal dispersion is much larger than the vertical dispersion. No vertical migration through the Gordon Confining Unit (Confining Unit IIA-IIB) is predicted until just before the water table discharges to Upper Three Runs (UTR) Creek (see Figure 1).

Data obtained from the third quarter of 1993 (3Q93) through the second quarter of 1994 (2Q94) indicated that the maximum detected concentration of eight contaminants exceeded the corresponding MCLs (WSRC 1996b). The Baseline Risk Assessment (BRA) (WSRC 1995b) also identified contaminants of concern (COCs) using a risk-based approach. COCs, contaminants that resulted in a risk of greater than  $1E-6$  or a hazard quotient (HQ) greater than 0.1 (for use scenarios exceeding a hazard index of 1.0), were also considered for inclusion in this GWMZ application. Where no MCL was available, the maximum concentration of the COCs was compared to EPA Region III Risk Based Concentrations (RBCs). Table 1 provides the maximum detected concentrations and the corresponding MCLs or RBCs.

The MCLs provided for the beta emitters in Table 1 result in a dose rate of 4 mrem/year assuming an ingestion rate of two liters per day and dose conversion factors published in the International Council for Radiation Protection (ICRP) Publication 2 (1959). MCLs have been proposed for beta emitters that are based on the derived limits (in ICRP Publication 30) that incorporate considerable advances in the state of knowledge of radionuclide dosimetry and biological transport in humans achieved since 1959 (EPA 1988). These proposed MCLs are anticipated to become effective in the near future. This GWMZ Application should be revised to include any future changes in the MCLs.

Table 1. Contaminant Concentrations Exceeding MCLs from Third Quarter 1993 to Second Quarter 1996

Contaminants	Maximum Detected Concentration (3Q93 to 2Q94) Included in RFI/RI	Maximum Detected Concentration (3Q94 to 2Q96) Since RFI/RI	MCL	RBC
<b>With Primary Drinking Water MCLs</b>				
Iodine-129 (pCi/L)	43.9	47.7	1	
Nitrate (mg/L)	78.1	20.9	10	
Radium-226 (pCi/L)	19.4	8.6	5**	
Radium-228 (pCi/L)	132.7	4.34	5**	
Strontium-90 (pCi/L)	146	99.6	8	
Tritium (pCi/ml)	336	216	20	
<b>Without MCLs (risk based)</b>				
Lead-212 (pCi/L)	37	26.7	NA	NA
Manganese (µg/L)	461	352	NA	840
Potassium-40 (pCi/L)	236	BDL	NA	NA
Uranium-234 (pCi/L)	42.6	36.5	NA	NA
Uranium-238 (pCi/L)	51.9	37.7	NA	NA
<b>With Only Proposed MCLs/Standards</b>				
Lead (µg/L)	20.4	3.6	15	
Uranium (total) (µg/L)	82.6	NA	20*	
<b>Indicator Parameters</b>				
Gross Alpha (pCi/L)	127	104	15	
Non-Volatile Beta (pCi/L)	502	413	Total Effective Dose 4 mrem/year	

\*MCL to be considered in EPA's Proposed Rule, 1991.

\*\*MCL is for total radium (radium-226 and radium-228 combined)

NA - not available, BDL - below detection limit

Shaded rows identify the contaminants for which MZCLs were calculated

Groundwater data collected subsequent to the RFI/RI (3Q94 to 2Q96) are also shown in Table 1. During this time, the maximum concentration of lead has dropped below the MCL. Therefore, contaminant plume modeling was not performed for lead.

The maximum concentration of radium-228 has dropped considerably since the sampling events reported in the RFI/RI. When combined with the radium-226 concentrations, the total radium MCL of 5 pCi/L is exceeded. However, radium-226 is naturally occurring and is usually found in groundwater where it is the result of geological conditions. EPA has proposed an individual MCL of 20 pCi/L for both radium-226 and radium-228. When combined, the maximum concentrations of total radium measured from 3Q94 to 2Q96 fall below EPA's proposed standard. Because radium is naturally occurring and the MCL of 20 pCi/L is likely to become effective within the time period that would represent the minimum travel time from the OFASB to the compliance boundary, neither radium-226 nor radium-228 are included in the modeling.

Potassium-40 is a naturally occurring radionuclide that was not produced by SRS operations. Lead-212 has a half life of 10.6 hours and is a distal daughter product of thorium-232, a naturally occurring radionuclide. The presence of these naturally occurring isotopes is not considered to be the result of OFASB operation. Therefore, potassium-40 and lead-212 were not considered as contaminants of interest for this GWMZ application.

Uranium-234 and uranium-238 are two isotopes of uranium. The transport properties of these isotopes are identical to those of total uranium. Because total uranium was reported as exceeding a proposed MCL, total uranium was modeled and compliance will be measured against the proposed MCL. The specific isotopes, uranium-234 and uranium-238, were not modeled.

Although manganese was considered a COC in the BRA, the maximum concentration of manganese is below the RBC. Manganese was not modeled because compliance with the RBC is already achieved. The reference dose (Rfd) has been updated from 5E-3 to 1.43E-5 mg/kg/day since the publication of the BRA which accounts for the discrepancy in the hazard quotient as compared to the RBC.

Gross alpha and non-volatile beta are indicator parameters and, although MCLs are generally assigned to these parameters, they are not suitable for a mixing zone calculation. Because these parameters serve as a catch-all for a large number of species, there is not a way to determine physical properties for the parameters.

Concentration trends for the contaminants listed in Table 1 are provided on Figures 2-16. It should be noted that values reported as being below the detection limit are not included in the trend plots. There is no data for total uranium in the FNB wells after 4Q94.

Based on the discussion above, the final list of contaminants for which a mixing zone is proposed is as follows: iodine-129, nitrate, strontium-90, tritium, and total uranium.

Concentration contour maps for many contaminants were provided in the RFI/RI (WSRC 1994) and were based on the maximum concentrations detected from 3Q93 to 2Q94. These concentration contour maps have been regenerated for the contaminants included in the model (Figures 17-21) for purposes of estimating the total mass of the plume. In drawing the concentration contours for strontium-90 and total uranium, maximum concentrations from 3Q93 to 2Q94 were used. However, for the more mobile contaminants, nitrate and tritium, maximum values from data collected during 1995 were used to provide a more accurate depiction of current conditions. The maximum detected concentration of iodine-129 reported in the 3Q93 to 2Q94 has been re-evaluated by the Environmental Monitoring Section (EMS) and has been qualified as a rejected value due to laboratory reporting error. For iodine-129, the highest detected concentration reported from 1993 was used in drawing the contour.

### 3.0 Description of Modeling

Groundwater modeling was used to predict contaminant concentrations at the compliance boundary, which is down-gradient and within the path of groundwater flow. Because the plume concentrations have not been increasing and the selected remedial action for the surface unit includes stabilizing and capping the residual contamination left in the soil, groundwater concentrations are expected to decrease to acceptable standards through natural attenuation. A groundwater flow and transport model was used to adequately demonstrate this expected decrease in concentrations.

Groundwater flow and contaminant migration were simulated using a transient three-dimensional, finite element computer code. The code, called Flow And Contaminant Transport (FACT) (Hamm, et al. 1995), has been designed to simulate isothermal groundwater flow, moisture movement, and solute transport in variably saturated and fully saturated subsurface media. The code is designed specifically to handle complex multilayer and/or heterogeneous aquifer systems in an efficient manner and accommodates a wide range of boundary conditions. An analytical model was not chosen for application to the conditions at the OFASB, because a one-dimensional flow field assumption is not reasonable for the water table conditions between the OFASB and the UTR Creek. The water table moving from the OFASB to UTR Creek drops sharply in elevation and passes beneath the "tan clay" just past the basin.

Contaminant retardation due to geochemical effects was modeled using a constant dispersion coefficient ( $K_d$ ) and conservative values. The initial plume configuration and concentration levels are defined from the concentration contour maps shown Figures 17-21. The vertical extent of contamination was assumed to be 33 feet below the water table (near the bottom of the screen zones in the monitoring wells and approximately half the aquifer thickness). Candidate compliance boundary wells were placed perpendicular to groundwater flow about 1600 feet upgradient of the Upper Three Runs Creek (Figure 22).

The screen zones of these compliance boundary wells are 30 feet in length, nearly fully penetrating, and are designed to capture the core of the plume. Plume migration was simulated from the present time through break-through at the compliance boundary. Table 2 summarizes transport model inputs. A complete discussion of the model and assumptions and sensitivities is provided in Appendix A.

**Table 2. Input parameters for OFASB solute transport model.**

Parameter	Value
Soil-solute distribution coeff. ( $K_d$ )	Tritium 0.001 ml/g Uranium 4 ml/g Strontium-90 3 ml/g Iodine-129 3.6 ml/g Nitrate 0.01 ml/g
Radioactive half-life	Tritium 12.3 yr Uranium infinite (assumed) Strontium-90 28.1 yr Iodine-129 infinite (assumed) Nitrate NA
Dispersivity	Longitudinal 30 ft Transverse horizontal 5 ft Transverse vertical 0.1 ft
Effective porosity	0.30
Bulk density	1.6 g/ml
Horizontal conductivity	UTR aquifer unit; "upper" zone 8.0 ft/d avg. UTR aquifer unit; "lower" zone 8.7 ft/d avg. Gordon aquifer unit 40 ft/d avg.
Vertical conductivity	UTR aquifer unit; "tan clay" zone 0.005 ft/d avg. Gordon confining unit $1.0 \times 10^{-5}$ ft/d avg.
Average recharge	14 in/yr

#### 4.0 Model Results

The recommended compliance boundary, based on the modeling, is depicted in Figure 22. This boundary location was selected because it is in the direct path of the groundwater flow from the basin, above the seepline and near the terminus of the predicted plumes.

As part of the modeling effort, five candidate wells were modeled at the compliance boundary. Groundwater modeling demonstrates that, using the concentration contours depicted in Figures 17-21 as the initial model conditions, concentrations in these five compliance boundary wells will not exceed MCLs for four of the five contaminants modeled. The model indicates that the maximum concentration of iodine-129 in one

compliance boundary well (2d) will reach a value equal to approximately 1.1 pCi/L, which is 0.1 pCi/L above the MCL, in approximately 180 years. The maximum predicted concentrations of iodine-129 in all the compliance boundary wells are less than the proposed MCL of 21 pCi/L, which is anticipated to become effective prior to the peak occurrence in the compliance well.

Plots of the contaminant concentrations in the compliance boundary wells vs. time are provided in Figures 23 - 27 for each of the contaminants modeled. The plots demonstrate that the bulk of the contaminant plume travels through hypothetical wells 2c and 2d.

The maximum concentrations of each contaminant were used in developing the initial conditions for the modeling effort. Because the modeling results are based on the maximum concentrations, and because data indicates that the plume concentrations are not increasing with time, the groundwater concentration limits (MZCLs) are set at the maximum observed concentrations. A listing of the MZCLs and the MCLs is provided in Table 3. Additional contaminants that were not modeled because they are considered naturally occurring, the concentrations are currently below MCLs, or are indicator parameters are listed in Table 4. These additional contaminants and indicator parameters will be monitored, as described in Section 5.0 of this application, to ensure that the concentration in the plume wells remains below MCLs.

**Table 3. Listing of MZCLs and MCLs for the Constituents of Concern**

Contaminant	MZCL	MCL
Iodine-129 (pCi/L)	48	1
Nitrate (mg/L)	20.9	10
Strontium-90 (pCi/L)	146	8
Tritium (pCi/mL)	216	20
Uranium (total) (µg/L)	83	20*

\*EPA Proposed Rule, 1991

**Table 4. Contaminants not Modeled but Requiring Further Monitoring**

Contaminant	MZCL	MCL
Lead (µg/L)	NC	15
Radium-228, -226	NC	5
Gross alpha	NC	15
Non-volatile beta	NC	Total effective Dose 4 mrem/year

NC - not calculated

There is no potential for the contaminant plume from the OFASB to migrate off SRS at concentrations exceeding MCLs. Passive aquifer restoration will be achieved within a

period of 2 to 115 years depending upon the contaminant and assuming that the proposed MCLs will become effective within this time frame. The FACT model was used to plot the maximum point concentration of each contaminant as a function of time (see Appendix A, Figure A-34). Of the five contaminants modeled, nitrate is predicted to be the first to achieve compliance with the MCLs within a time period of 2 years. Using the current MCL of 1 pCi/L, restoration of the iodine-129 plume will require 320 years. However, it is anticipated that the proposed MCL of 20 pCi/L will become effective in the near future, in which case restoration of the iodine-129 plume would require approximately 20 years. Considering that the proposed MCLs will become effective in the near future, the total uranium plume requires the longest time, 115 years, for restoration to below MCLs.

## 5.0 Compliance Well Monitoring

Compliance with the MZCLs will be demonstrated by sampling and analyzing groundwater from the existing monitoring wells within the plume. Monitoring wells FNB-2, FNB-3, and FNB-5 are located within the plume and have exhibited the highest concentrations of the contaminants of concern. The existing plume wells will be monitored on a semi-annual basis for the contaminants in Table 3 (and radionuclide indicator parameters) to ensure that the contaminants of concern do not exceed the MZCLs. If an MZCL is exceeded during a semi-annual event, all of the plume wells will be re-sampled within 30 days to validate this exceedence. In the event that the MZCL is exceeded again, SRS will submit a plan for corrective action to SCDHEC and EPA within 90 days of the receipt of the confirmatory data. The need for continued monitoring of the plume wells will be re-evaluated once the concentrations in the plume wells fall below MCLs and at least every 5 years as part of the ROD review.

The three plume wells will also be monitored for the constituents in Table 4. Although data collected from 3Q94 to 2Q96 indicate that the maximum concentration of lead is below the MCL, additional monitoring may be required to demonstrate compliance. Radium-226 and radium-228 will also be sampled and compared to the appropriate MCL for radium. Sampling for lead, radium-226, and radium-228 will continue on a semi-annual basis until compliance with the MCLs is satisfactorily demonstrated to SCDHEC and EPA. Indicator parameters listed in Table 4 will continue to be monitored in the plume wells semi-annually for the duration of the plume well monitoring schedule. If the lead and radium-228 concentrations exceed MCLs, these constituents will be evaluated for inclusion in the contaminant transport model.

Four monitoring wells will be installed near the downflow plume boundary, termed the compliance boundary wells. The approximate location of these wells is shown on Figure 28. These locations were chosen because they cover and exceed the predicted capture zone of candidate compliance boundary wells used in the modeling and were recommended by SCDHEC. The four compliance boundary wells will be installed with 30 foot screens, straddling the mid-point of the water table, to ensure that the contaminant

plume is captured. These wells will be sampled semi-annually for the contaminants in Table 3 (and radionuclide indicator parameters) to ensure that the maximum concentration does not exceed MCLs. Similar to the plume wells, if an exceedence of an MCL is observed in the compliance boundary wells, the wells will be re-sampled within 30 days. In the event that the MCL is exceeded again, SRS will submit a plan for corrective action to SCDHEC and EPA within 90 days of the receipt of the confirmatory data. The sampling schedule for the plume wells and compliance boundary wells is summarized in Table 5. This sampling schedule will be re-evaluated as part of the five year ROD review.

In addition to the four compliance boundary wells, three intermediate wells will be installed between the OFASB and the compliance boundary to validate the model predictions at the request of SCDHEC. The approximate location of these wells is shown on Figure 28. These intermediate wells will be monitored semi-annually for the contaminants listed in Table 3 and contaminant concentrations will be compared to model predictions. The model predictions for contaminant concentrations in the intermediate wells will be provided to SCDHEC and EPA in post-ROD documentation. If contaminant concentrations exceed model predictions, the model will be re-calibrated with the new data and the effects of the increased concentrations on the compliance boundary wells will be determined. If the recalibrated model indicates that the MCLs will be exceeded at the compliance boundary, then SRS will submit a plan for corrective action to SCDHEC and EPA within 90 days of the determination.

**Table 5. Sampling Schedule for Plume Wells and Compliance Boundary Wells**

Well Identification	Constituents to be Analyzed	Comparison Criteria	Sampling Frequency	Reporting Frequency
Plume wells - FNB-2 - FNB-3 - FNB-5	Constituents listed in Tables 3 and 4	MZCLs	semi-annually (subject to review after plume well concentrations fall below MCLs and at least every 5 years)	annually
Compliance wells (4 wells to be installed)	Constituents listed in Table 3 (including gross alpha and non-volatile beta)	MCL	semi-annually (subject to review every 5 years)	annually
Intermediate wells (3 wells to be installed)	Constituents listed in Table 3 (including gross alpha and non-volatile beta)	Model predictions	semi-annually (subject to review every 5 years)	annually

## 6.0 Uncertainties

A detailed discussion of modeling uncertainties is provided in Appendix A. Although uncertainties have been minimized by using monitoring well, geologic and hydrogeologic

data collected over the entire General Separations Area (GSA) as inputs into the groundwater model, data gaps still exist. No groundwater data has been collected from the area beyond a distance of approximately 600 feet from the basin to UTR Creek to confirm the absence of contamination.

Another source of uncertainty lies with the potential for past and present up-gradient sources of tritium contamination in the groundwater influencing OFASB plume wells and compliance boundary wells. Tritium contamination exists in the groundwater upgradient from the OFASB (from the general vicinity of F-Area laboratories) (WSRC 1993) and is likely the source of existing tritium concentrations observed in the wetland down-gradient of the OFASB. Although data from F-Area wells demonstrates the presence of tritium up-gradient of the OFASB, there is insufficient information to determine the extent of mixing of this plume with plumes from the OFASB. Therefore, the installation of additional wells immediately up-gradient of the OFASB is being considered as part of an action which will be separate from the GWMZ request.

## 7.0 Conclusions

An examination of groundwater monitoring data from existing plume wells at the OFASB illustrates that contaminant concentrations are not increasing over time. Because the selected remedy for the unit soils will include stabilizing and capping the contaminated soil, no further migration of contaminants to the groundwater is expected once the remedy has been completed. The selected remedy was identified in the Statement of Basis/Proposed Plan and is part of the ROD for the OFASB. Additional information on the remedy may be found in these documents.

The groundwater contamination from the OFASB is limited to the water table aquifer, which is not currently used as a drinking water source. It is unlikely that the water table aquifer will be used for drinking water in the future, especially for a residential setting. The selected remedy includes institutional controls on future land use at this unit, as described in the Statement of Basis/Proposed Plan and ROD. Residential use will be prohibited and access controls will ensure that these restrictions will be maintained. Although there is a potential for small amounts of the contaminants to migrate vertically through the Gordon Confining Unit (IIA-IIB), the impact to the Gordon Aquifer (IIA) is minimal because both the Gordon Aquifer (IIA) and Upper Three Runs Aquifer Unit (IIB) groundwater discharges to UTR Creek only a short distance after such migration could be expected. This is illustrated in Figure 1 and by the vertical plume maps provided in Appendix A.

As illustrated through groundwater modeling, the contaminant plume is contained within an area immediately adjacent to the OFASB. There is no potential for the contaminants

from the OFASB to migrate off SRS at concentrations exceeding MCLs. Plume maps generated as a result of the groundwater modeling (see Appendix A) show no increase in the area (or volume) of contamination that exceeds the MCLs.

The results from the modeling demonstrate that concentrations of four of the five contaminants will meet existing MCLs at the compliance boundary, with only a slight exceedence of the iodine-129 MCL in one compliance boundary well. It is anticipated that the MCL for iodine-129 will be revised from 1 pCi/L to 21 pCi/L before the iodine-129 plume reaches the compliance boundary. Additionally, the model predicted that contaminant concentrations will decrease over time in each of the plume wells (FNB wells -2, -3, and -5) to below MCLs, as discussed in Appendix A. The maximum time predicted for the plume wells to fall below the MCL was estimated to be 90 years for iodine-129 (using the MCL of 1 pCi/L). The maximum concentrations in the entire plume will fall below MCLs within a time period of 2 to 115 years, depending on the contaminant and assuming that the proposed MCL for iodine-129 will become effective in the near future.

A groundwater monitoring program will be implemented that will demonstrate compliance with the MCLs at the compliance boundary and compliance with the MZCLs at the plume wells. Details of the monitoring well installations, monitoring schedule, and recommended actions to be taken if the compliance boundary wells are shown to be out of compliance will be provided in post-ROD documentation.

## References

- EPA (Environmental Protection Agency) 1988. "Limiting Values of Radionuclide Intake and Air Concentration and Dose Conversion Factors for Inhalation, Submersion and Ingestion," *Federal Guidance Report No. 11*, EPA-520/1-88-020, September 1988.
- Hamm, L. L., S. E. Aleman, W. F. Jones, G. P. Flach, J. S. Haselow, P. S. Huyakorn, S. Panday and T. Birdie, 1995, *FACT: Subsurface Flow and Contaminant Transport Documentation and User's Guide*, WSRC-TR-95-223, in preparation.
- SCDHEC (South Carolina Department of Health and Environmental Control) 1994. *Groundwater Mixing Zone Guidance Document*, March 1994.
- WSRC (Westinghouse Savannah River Company) 1993. *Final Report of the WSRC Source Assessment Task Team: Potential Sources for Observed Contamination in Well FCA 9DR (U)*, WSRC-RP-93-045, July 16, 1993.
- WSRC (Westinghouse Savannah River Company) 1995a. *RCRA Facility Investigation/Remedial Investigation Report for the Old F-Area Seepage Basin (904-49G)(U)*, Rev. 1, WSRC-RP-94-942, June 1995.
- WSRC (Westinghouse Savannah River Company) 1995b. *Baseline Risk Assessment for the Old F-Area Seepage Basin (904-49G)(U)*, Rev. 1, WSRC-RP-94-1174, June 1995.
- WSRC (Westinghouse Savannah River Company) 1996a. *Corrective Measures Study/Feasibility Study for the Old F-Area Seepage Basin (904-49G)(U)*, Rev. 1, WSRC-RP-95-385, February 1996.
- WSRC (Westinghouse Savannah River Company) 1996b. *Statement of Basis/Proposed Plan for the Old F-Area Seepage Basin (904-49G)(U)*, Rev. 1, WSRC-RP-95-1557, June 1996.

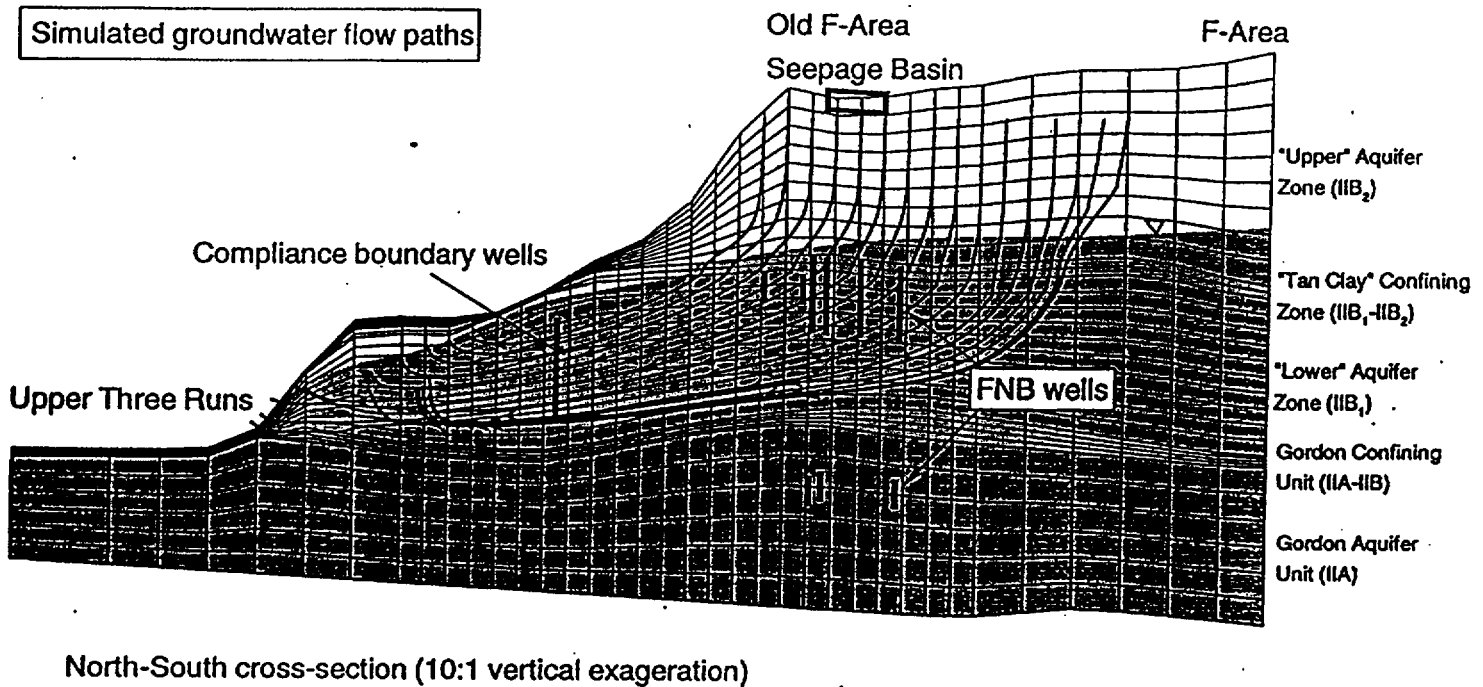


Figure 1. Simulated Vertical Groundwater Flow

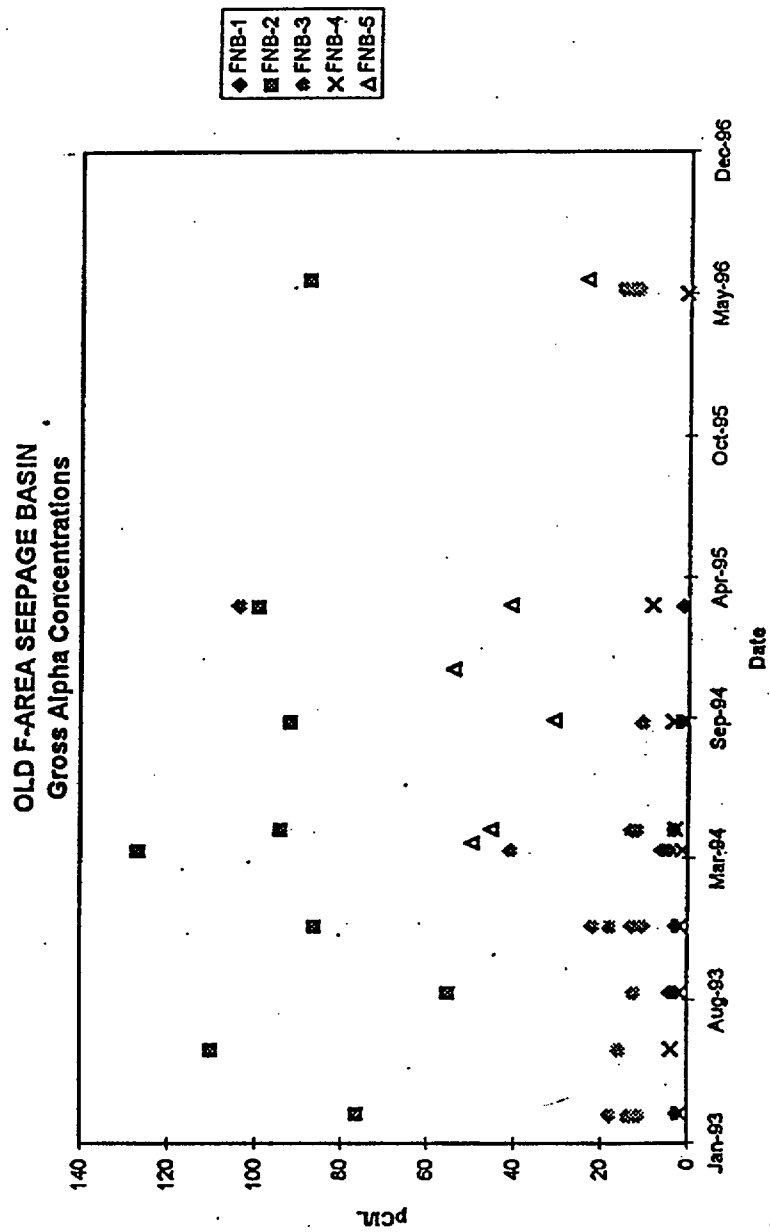


Figure 2. Concentration Trend for Gross Alpha

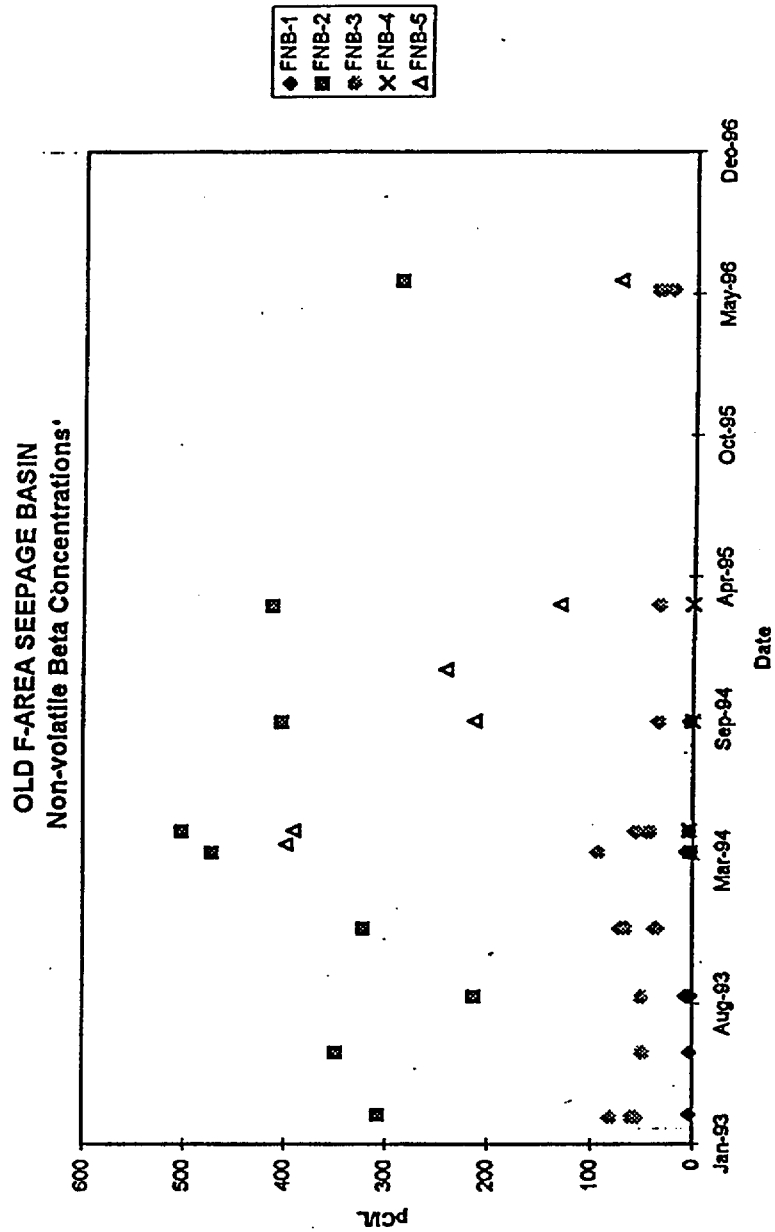


Figure 3. Concentration Trend for Non-volatile Beta

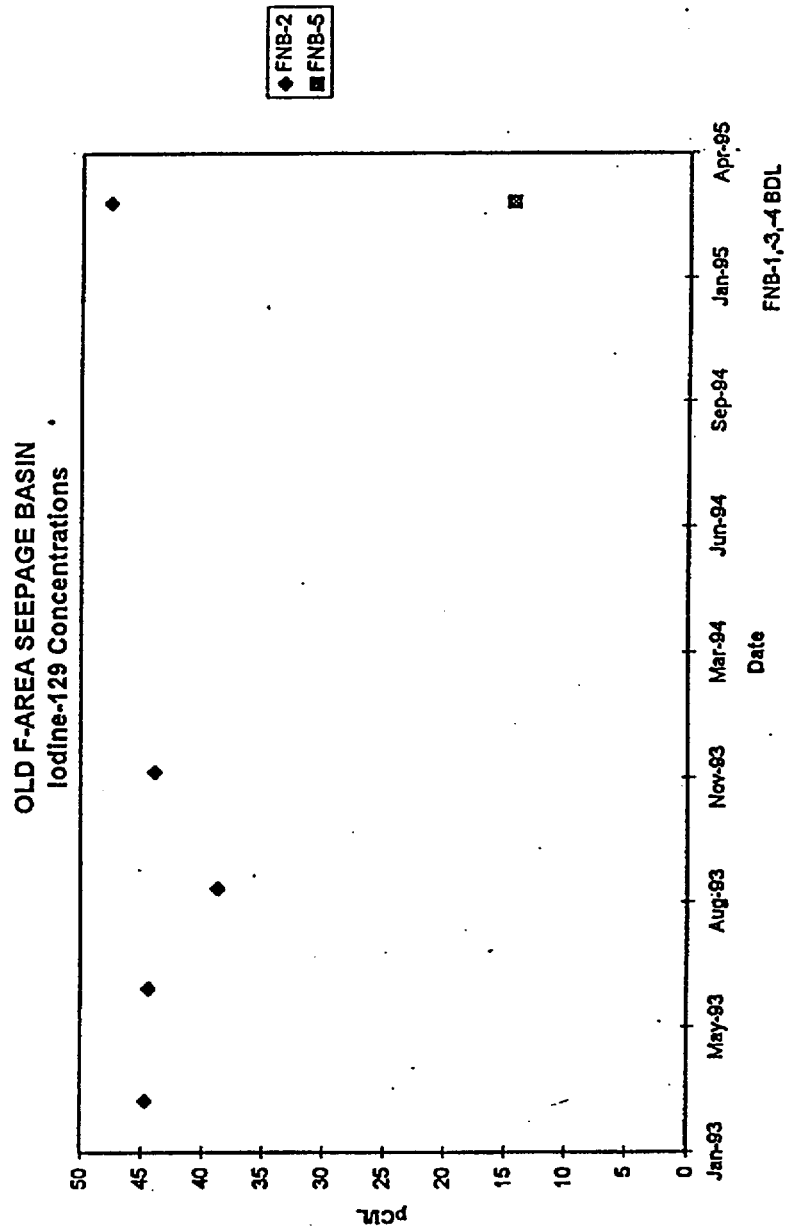


Figure 4. Concentration Trend for Iodine-129

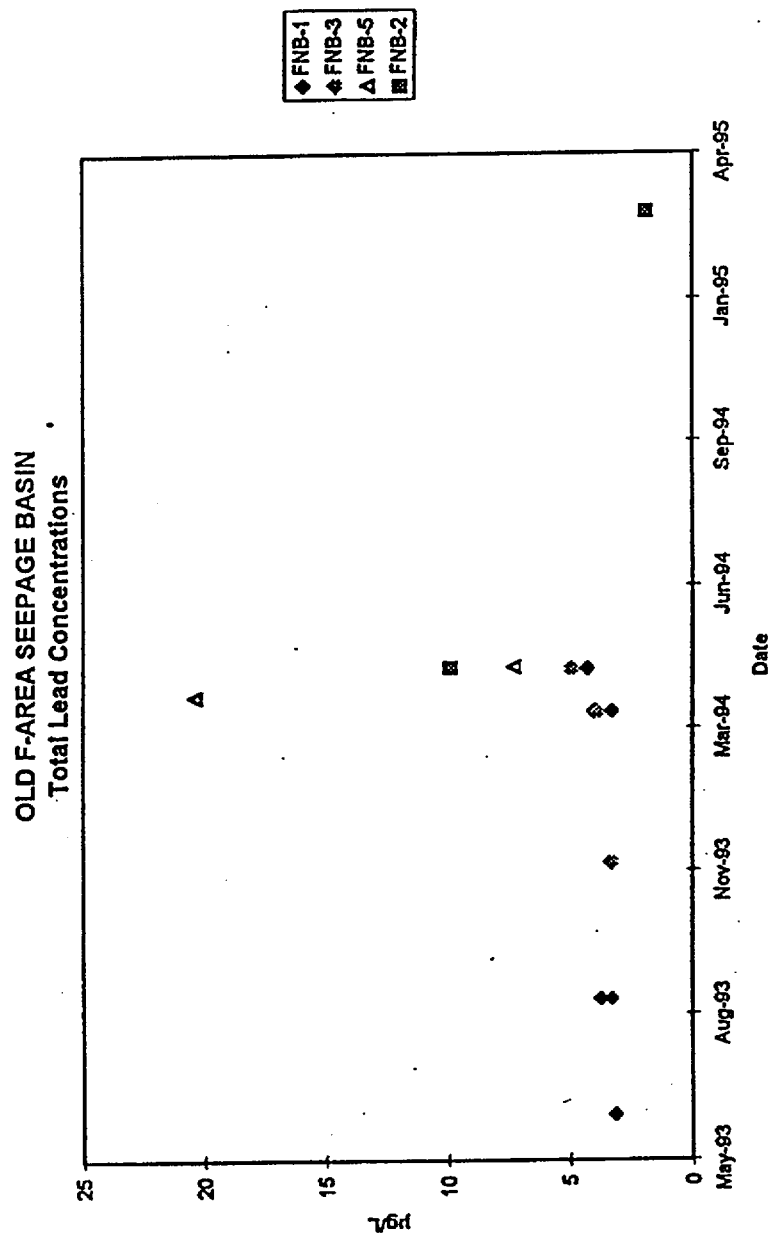


Figure 5. Concentration Trend for Total Lead

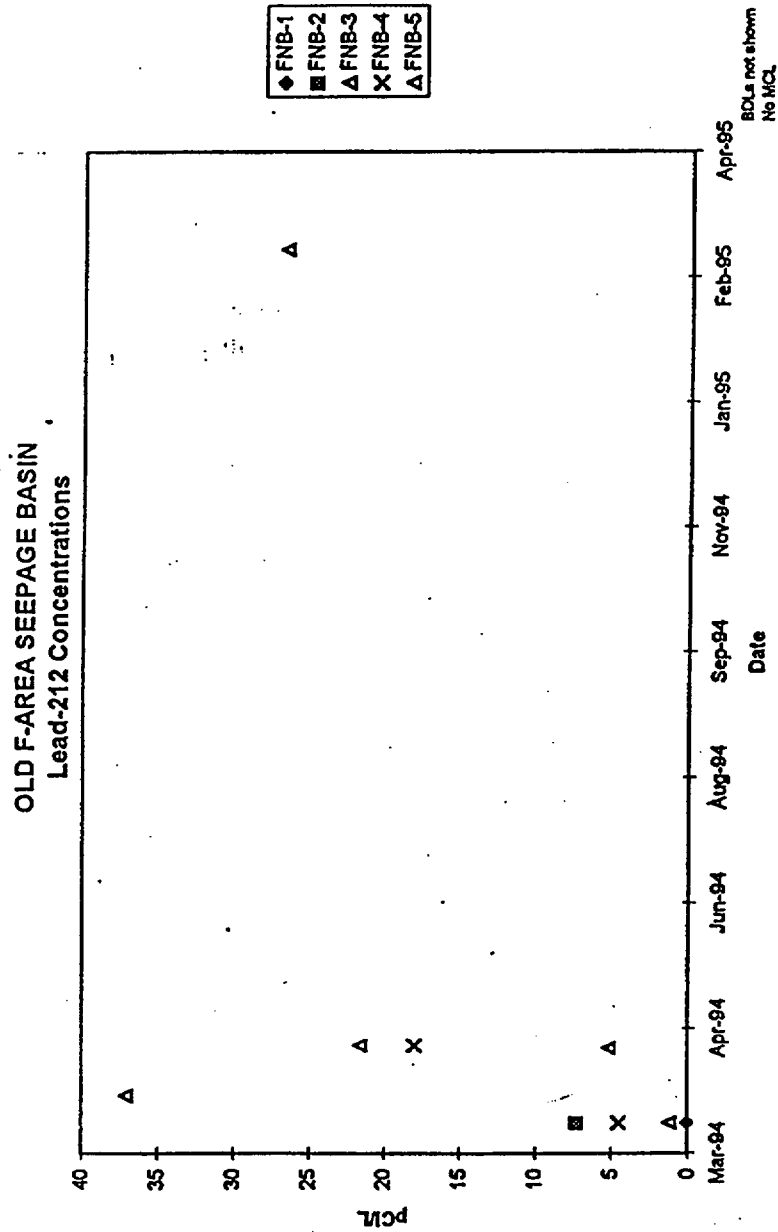


Figure 6. Concentration Trend for Lead-212

at least 1 detect Chart 15

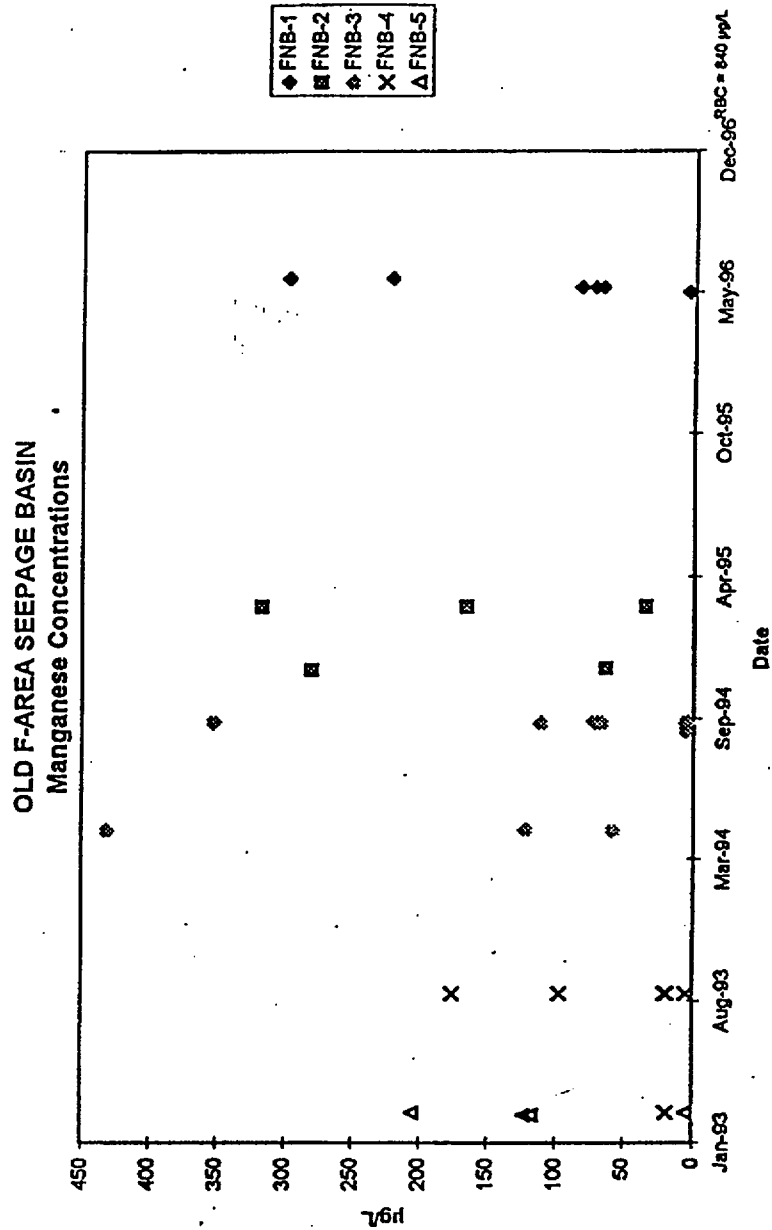


Figure 7. Concentration Trend for Manganese



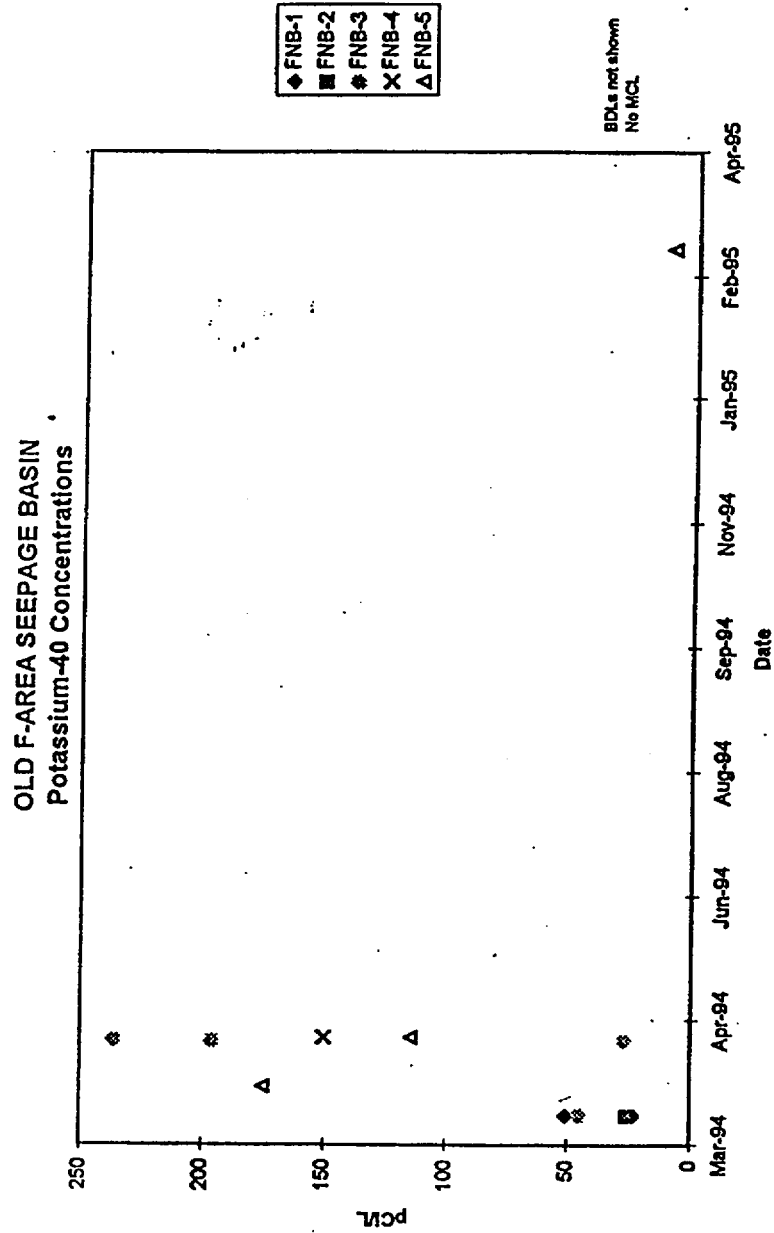


Figure 9. Concentration Trend for Potassium-40

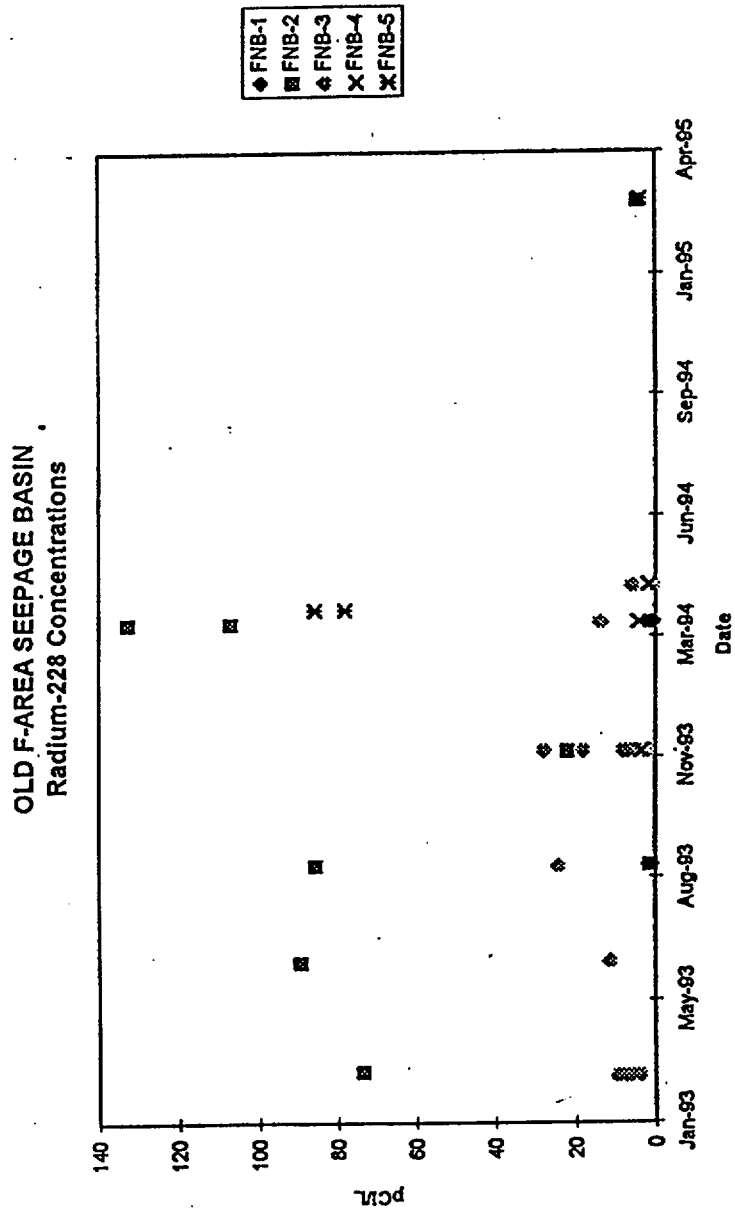


Figure 10. Concentration Trend for Radium-228

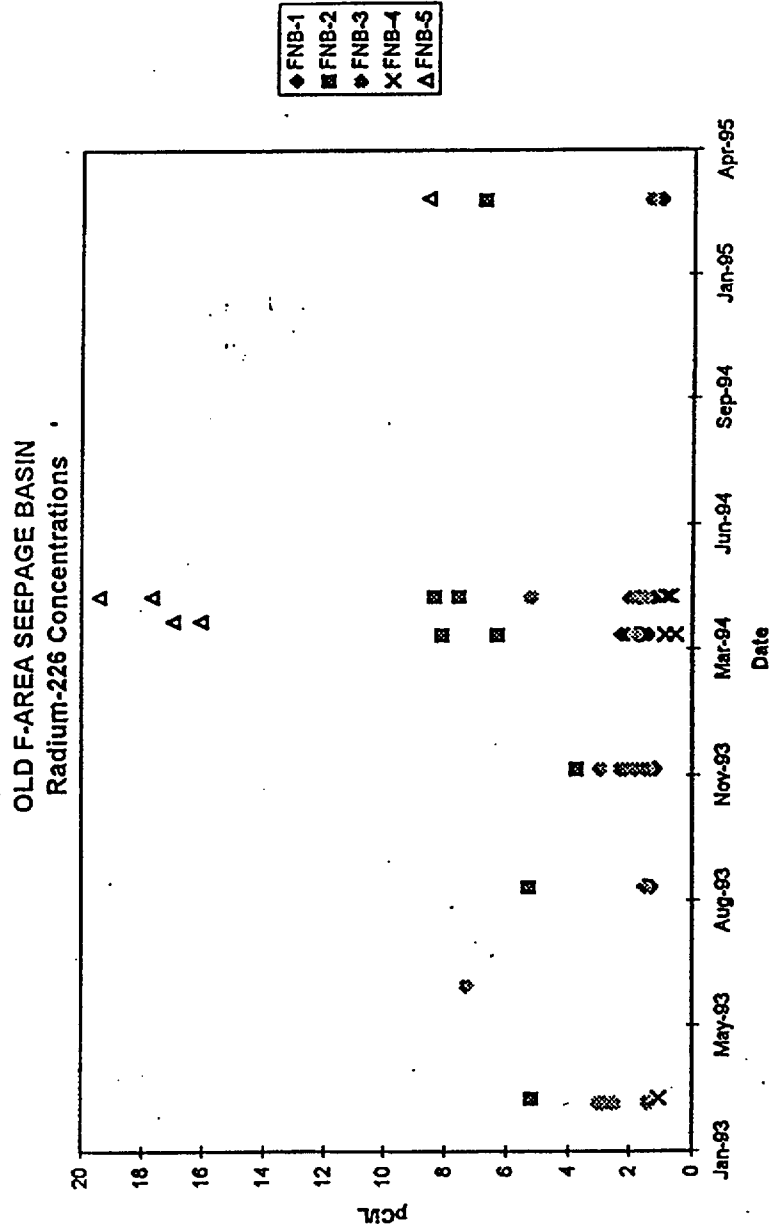


Figure 11. Concentration Trend for Radium-226

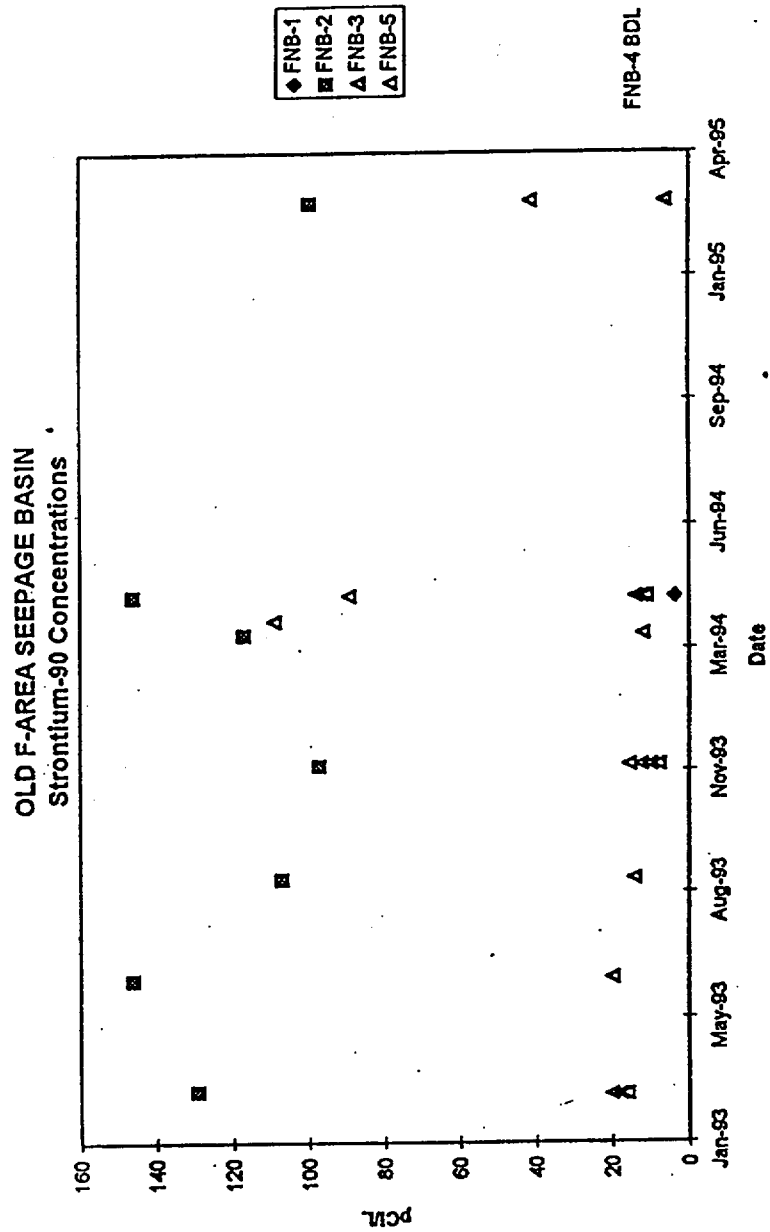


Figure 12. Concentration Trend for Strontium-90

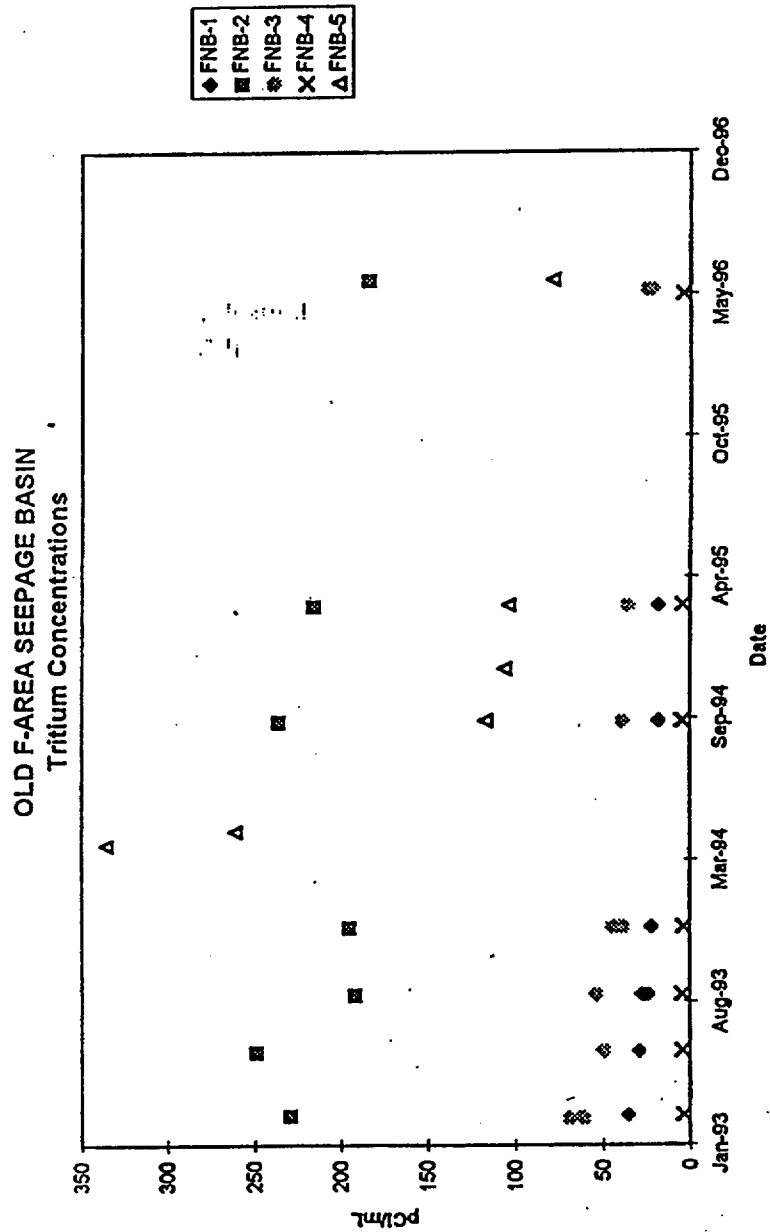


Figure 13. Concentration Trend for Tritium

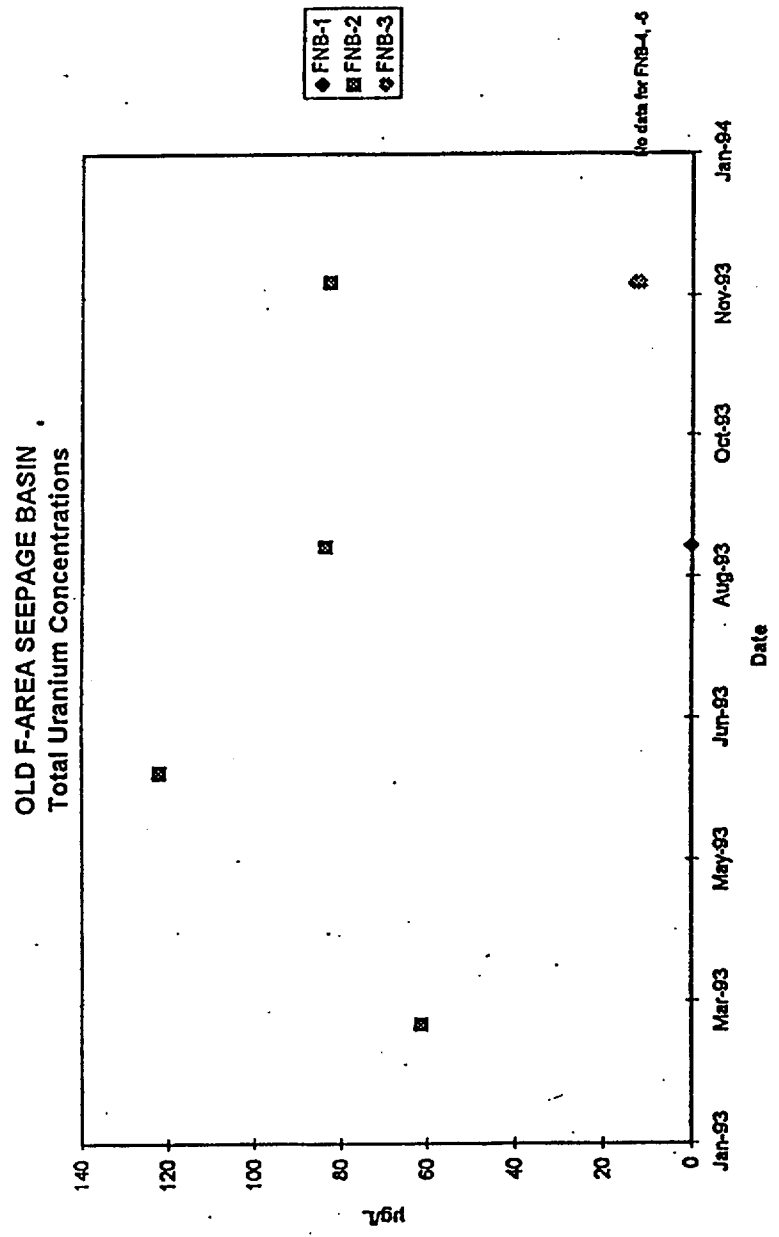


Figure 14. Concentration Trend for Total Uranium

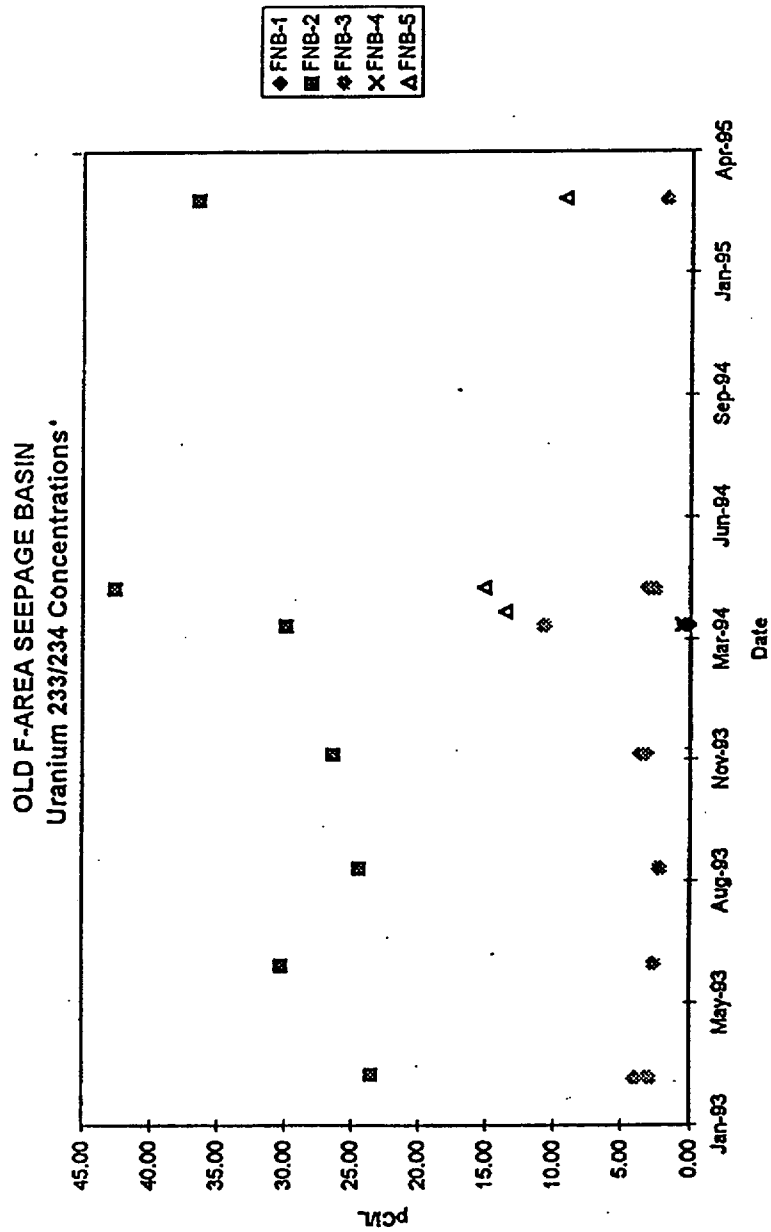


Figure 15. Concentration Trend for Uranium-234

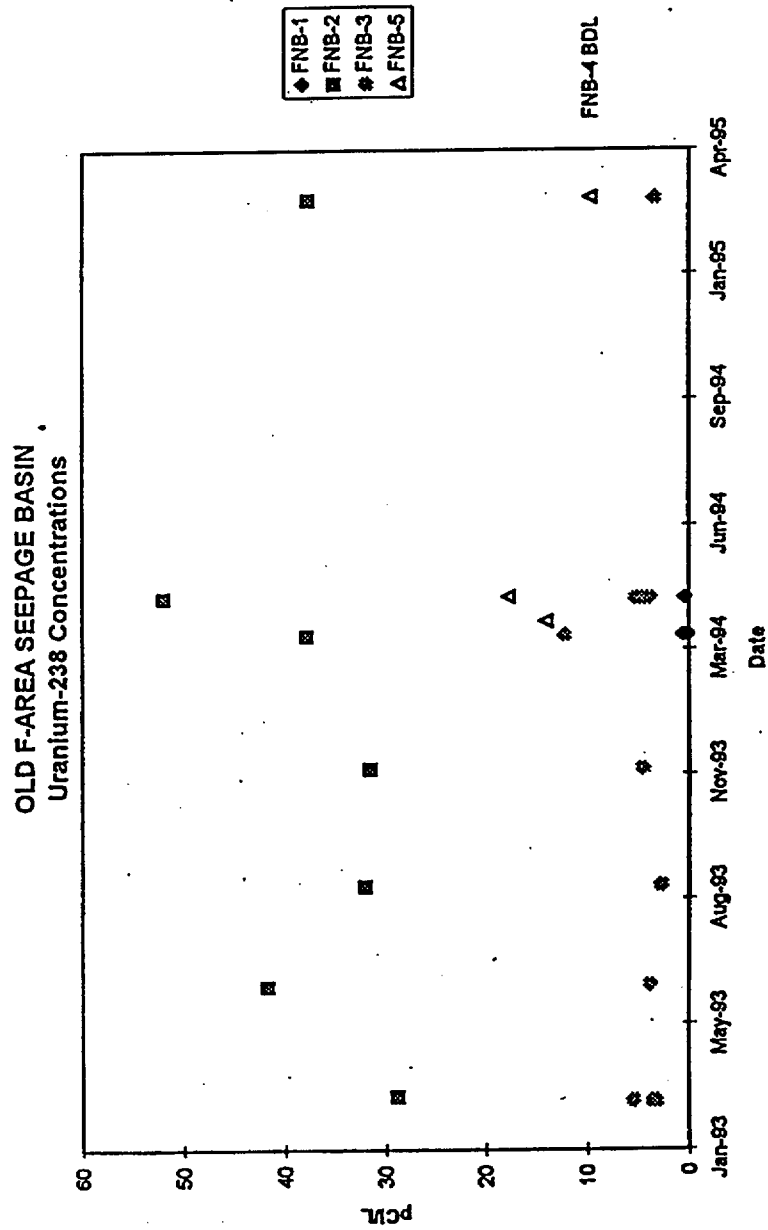


Figure 16. Concentration Trend for Uranium-238



Groundwater Mixing Zone Application  
for the Old F-Area Seepage Basin

WSRC-RP-97-39  
Rev. 1

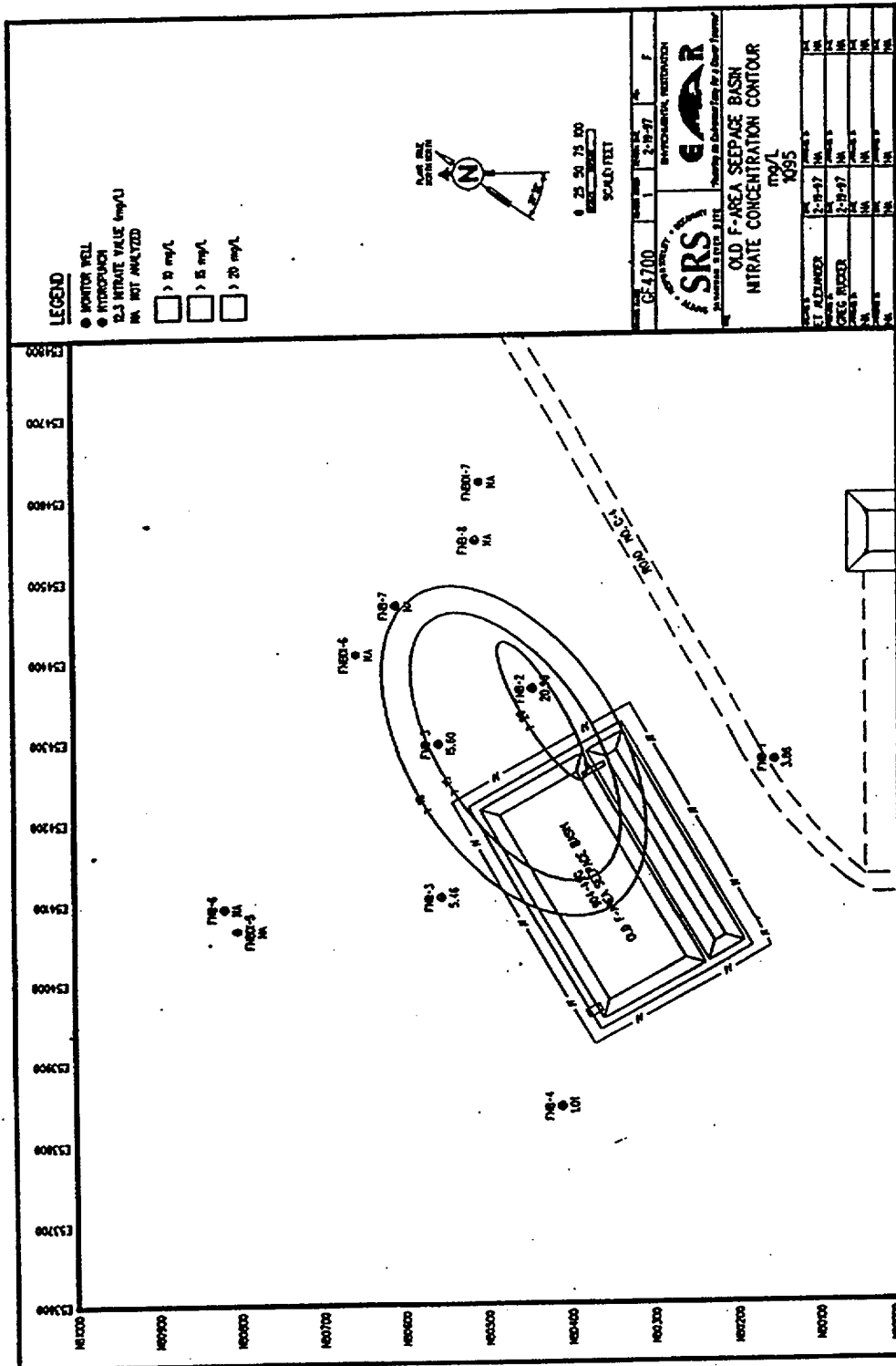


Figure 18. Initial Concentration Contours for Nitrate

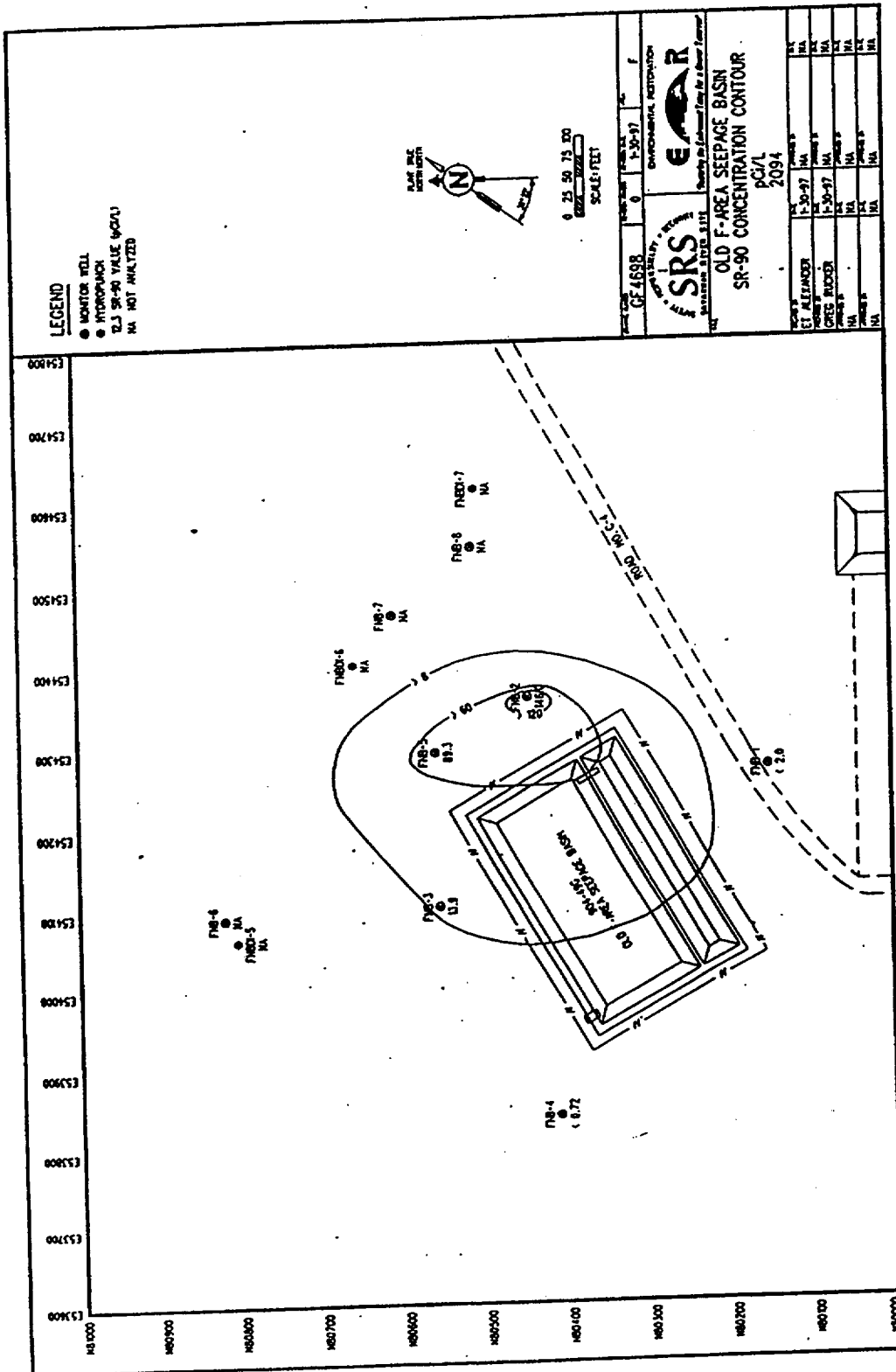


Figure 19. Initial Concentration Contours for Strontium-90

Groundwater Mixing Zone Application  
for the Old F-Area Seepage Basin

WSRC-RP-97-39  
Rev. 1

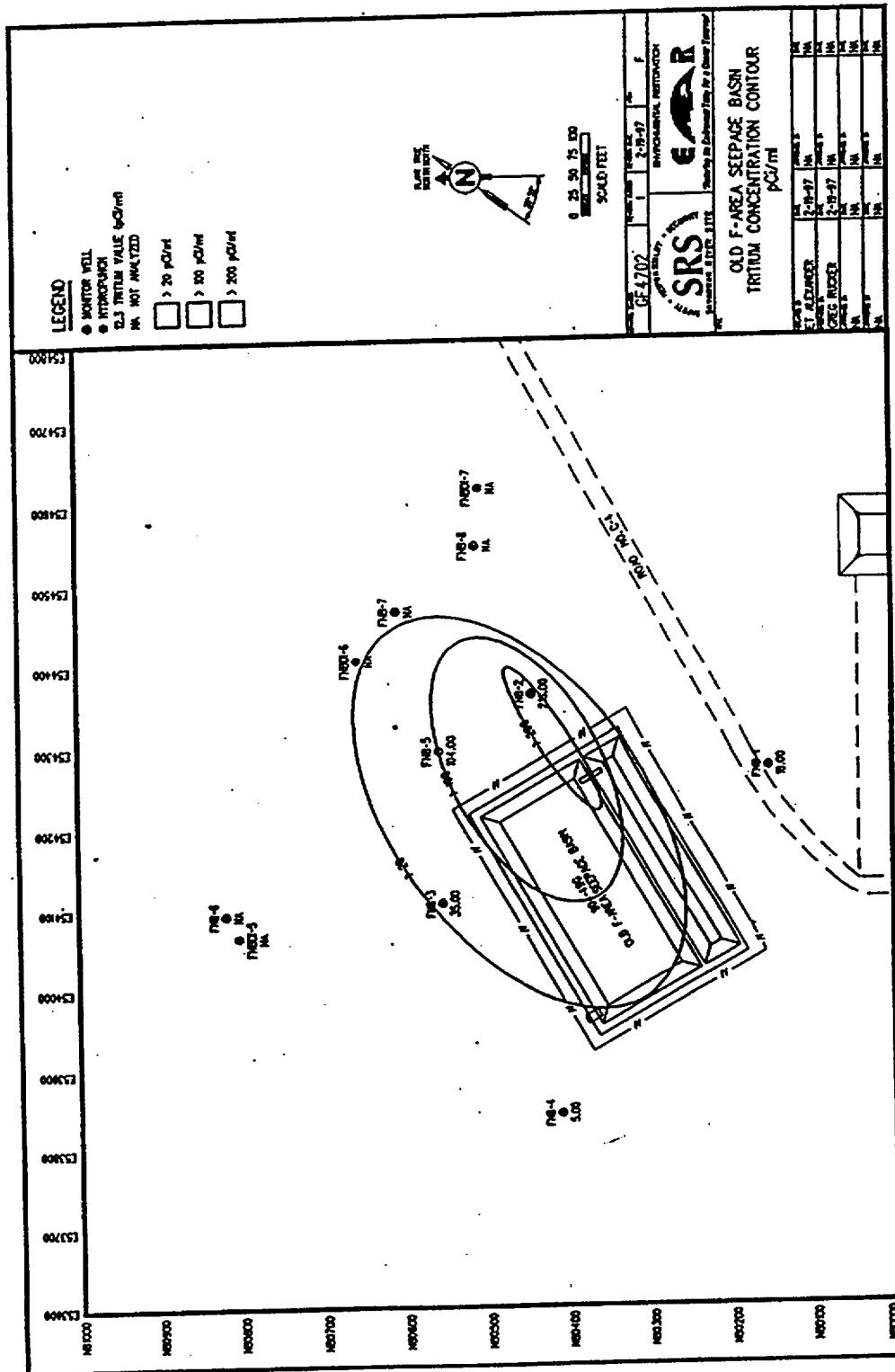


Figure 20. Initial Concentration Contours for Tritium



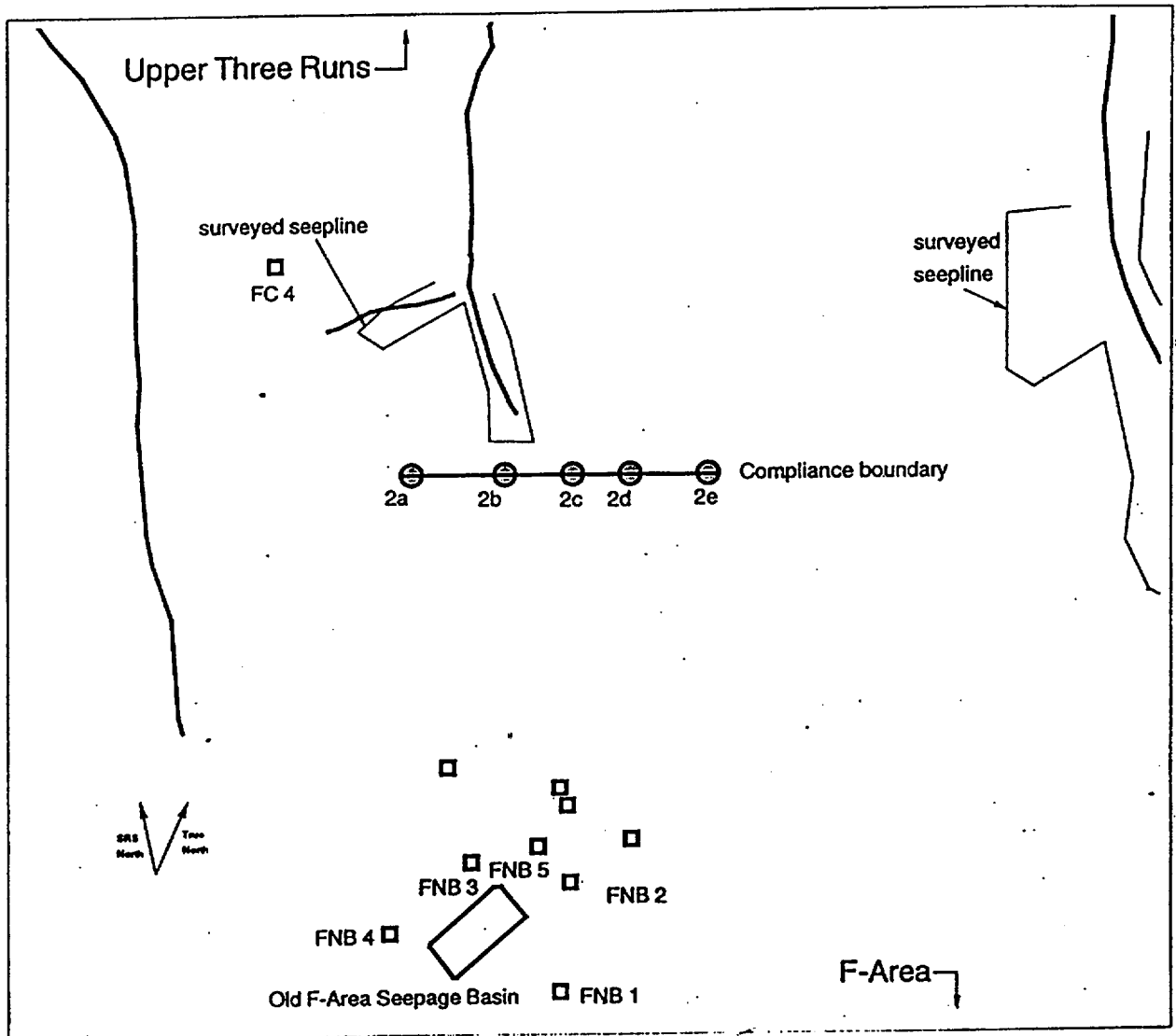


Figure 22. Location Modeled Compliance Boundary

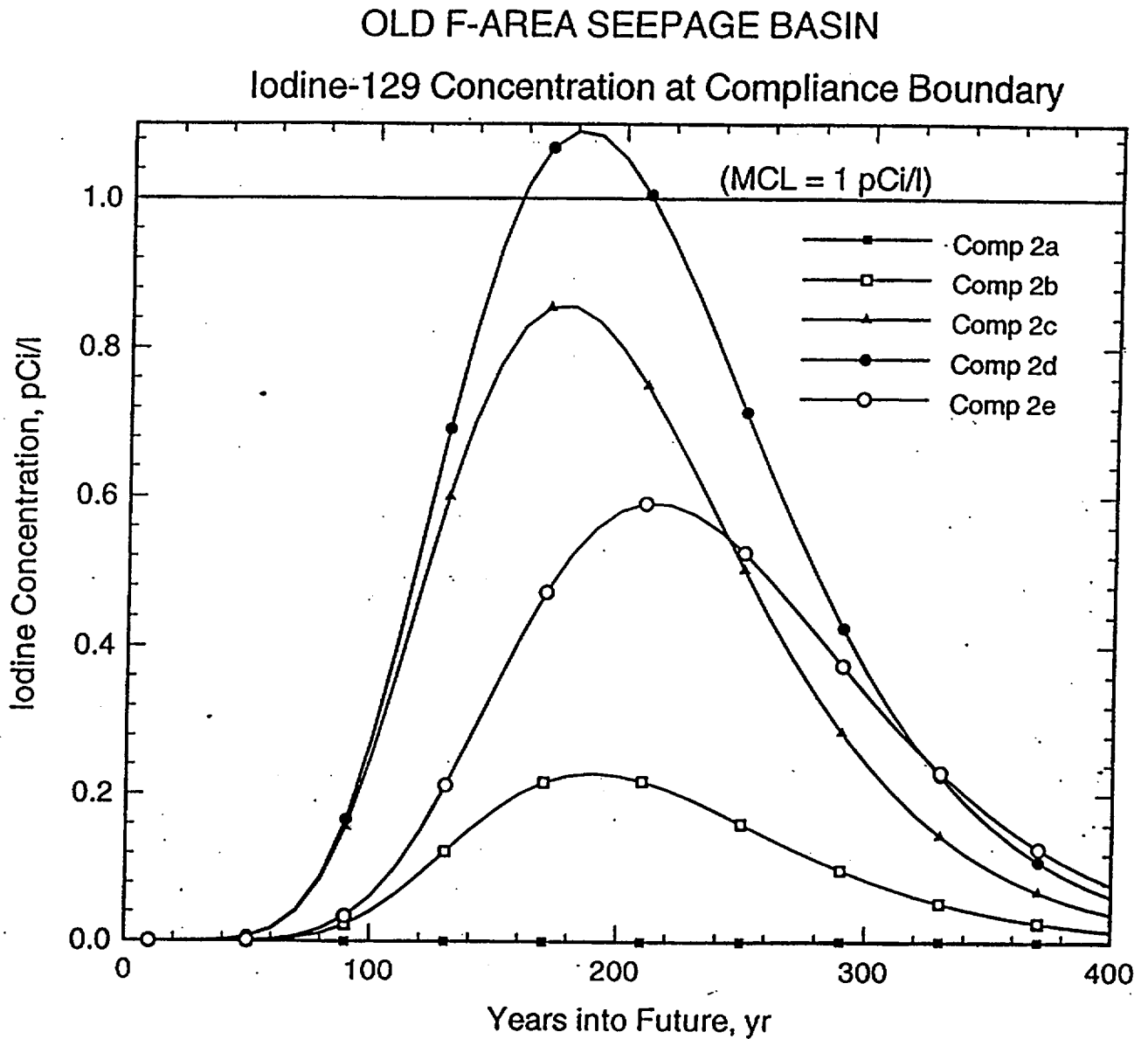


Figure 23. Iodine-129 Concentration at Compliance Boundary

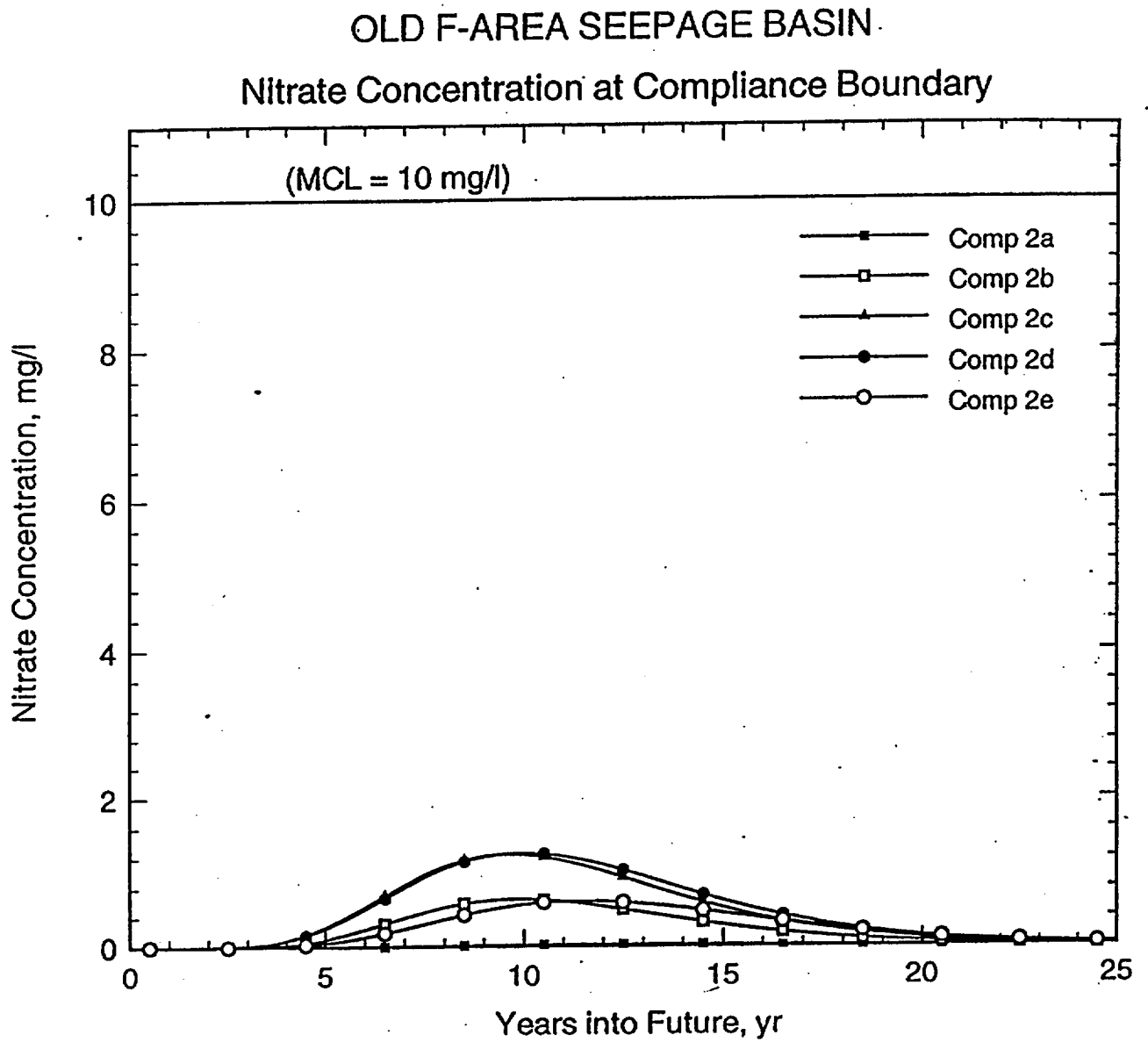


Figure 24. Nitrate Concentration at Compliance Boundary

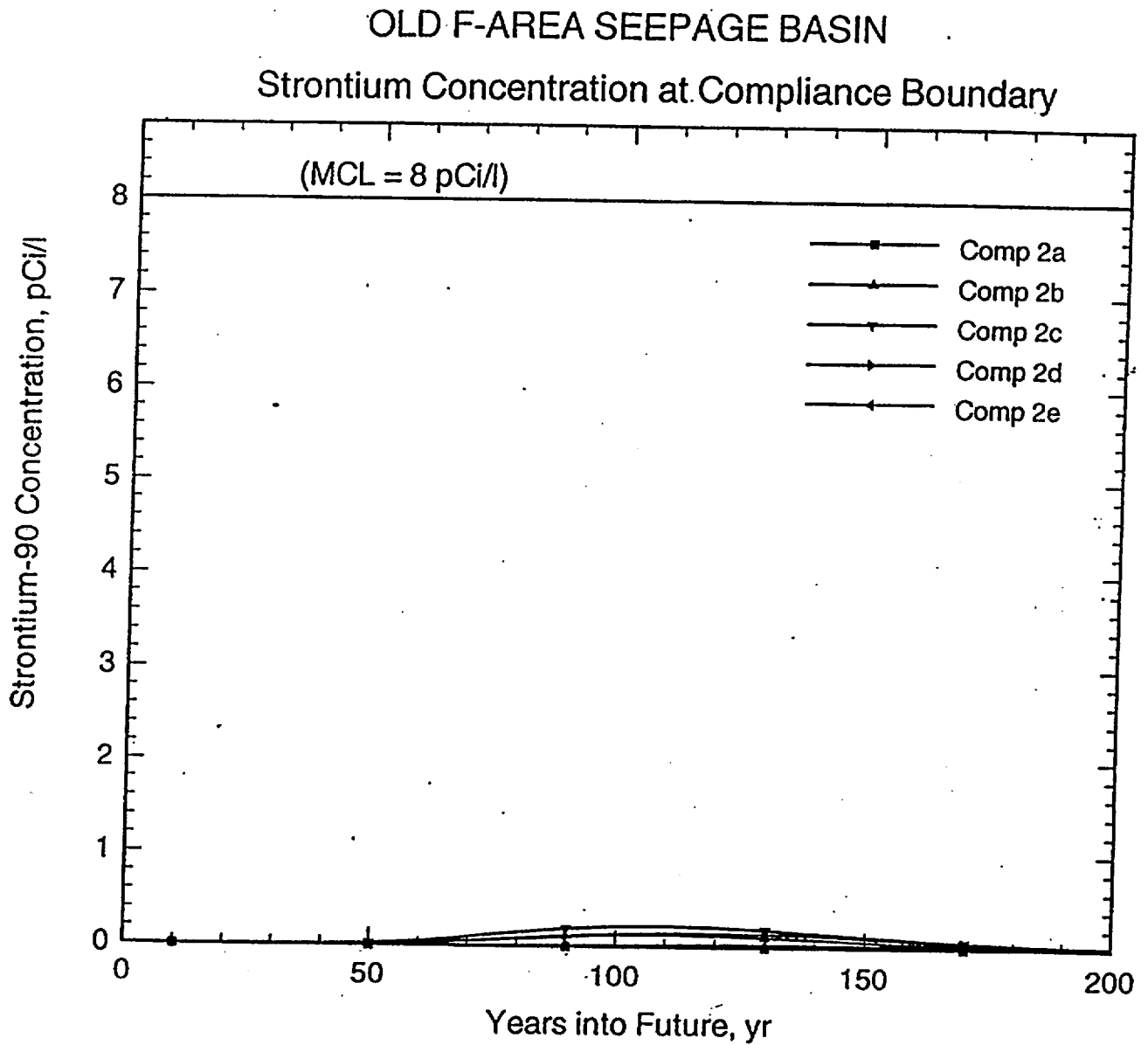


Figure 25. Strontium-90 Concentration at Compliance Boundary

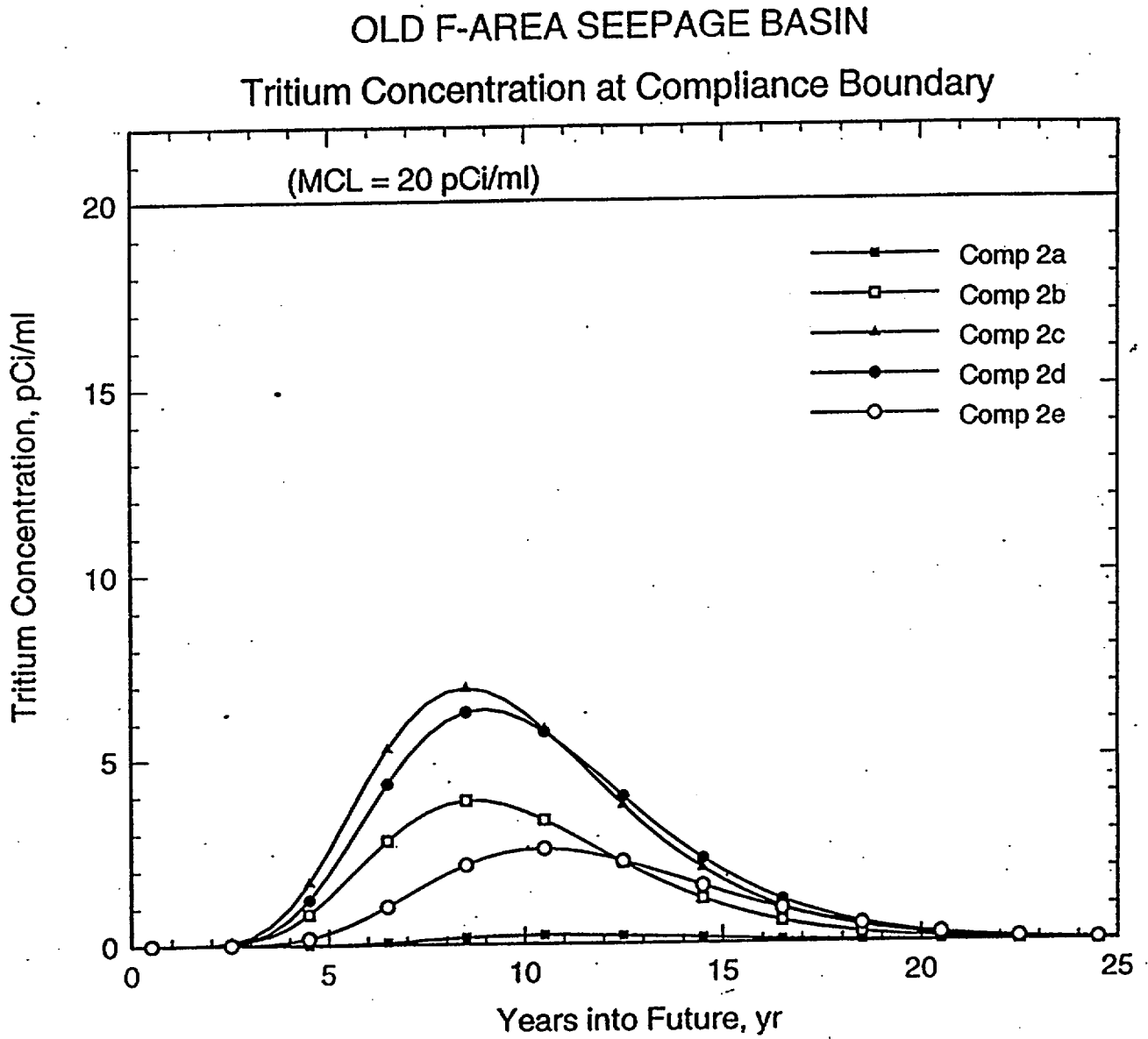


Figure 26. Tritium Concentration at Compliance Boundary

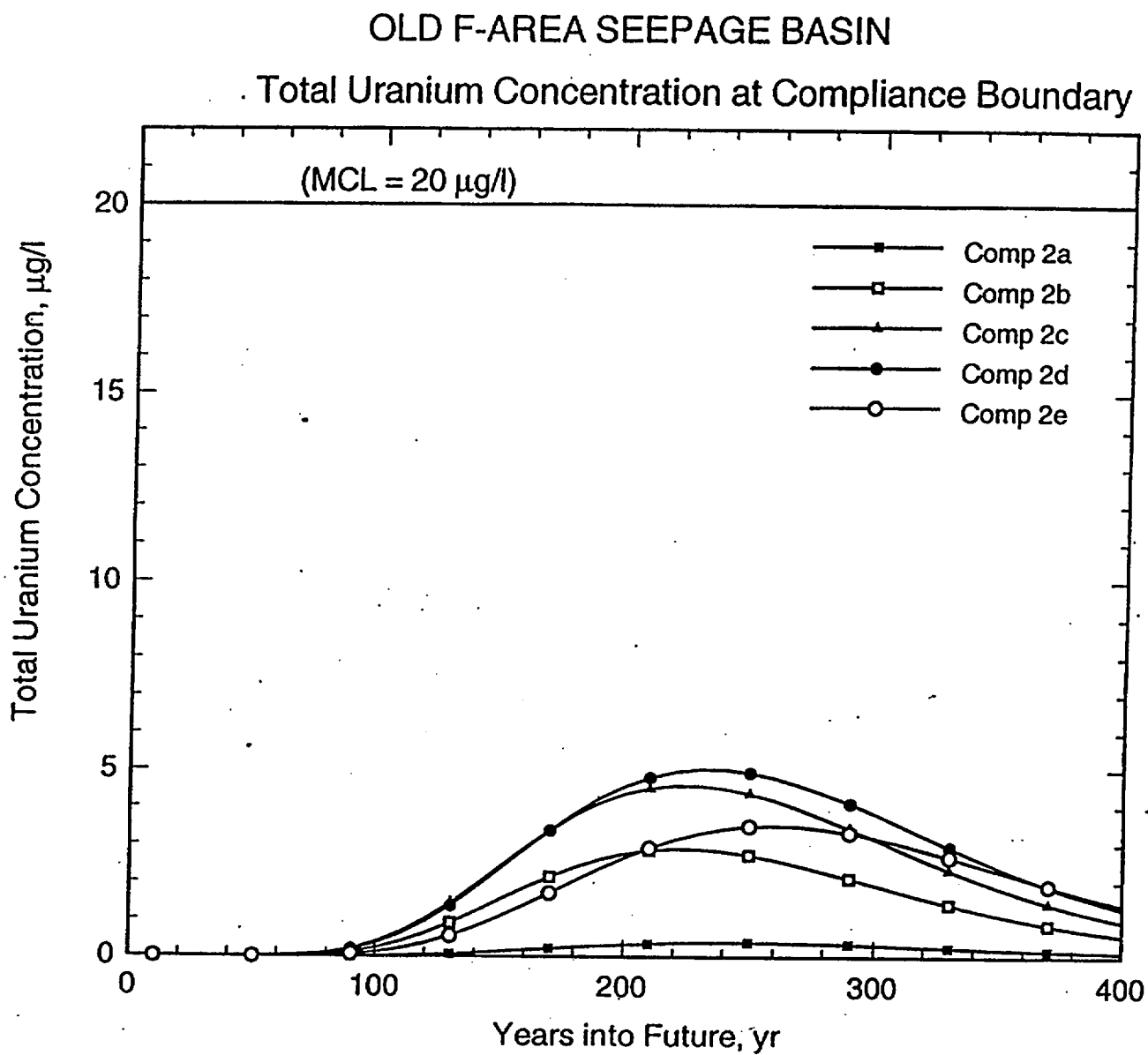


Figure 27. Total Uranium Concentration at Compliance Boundary

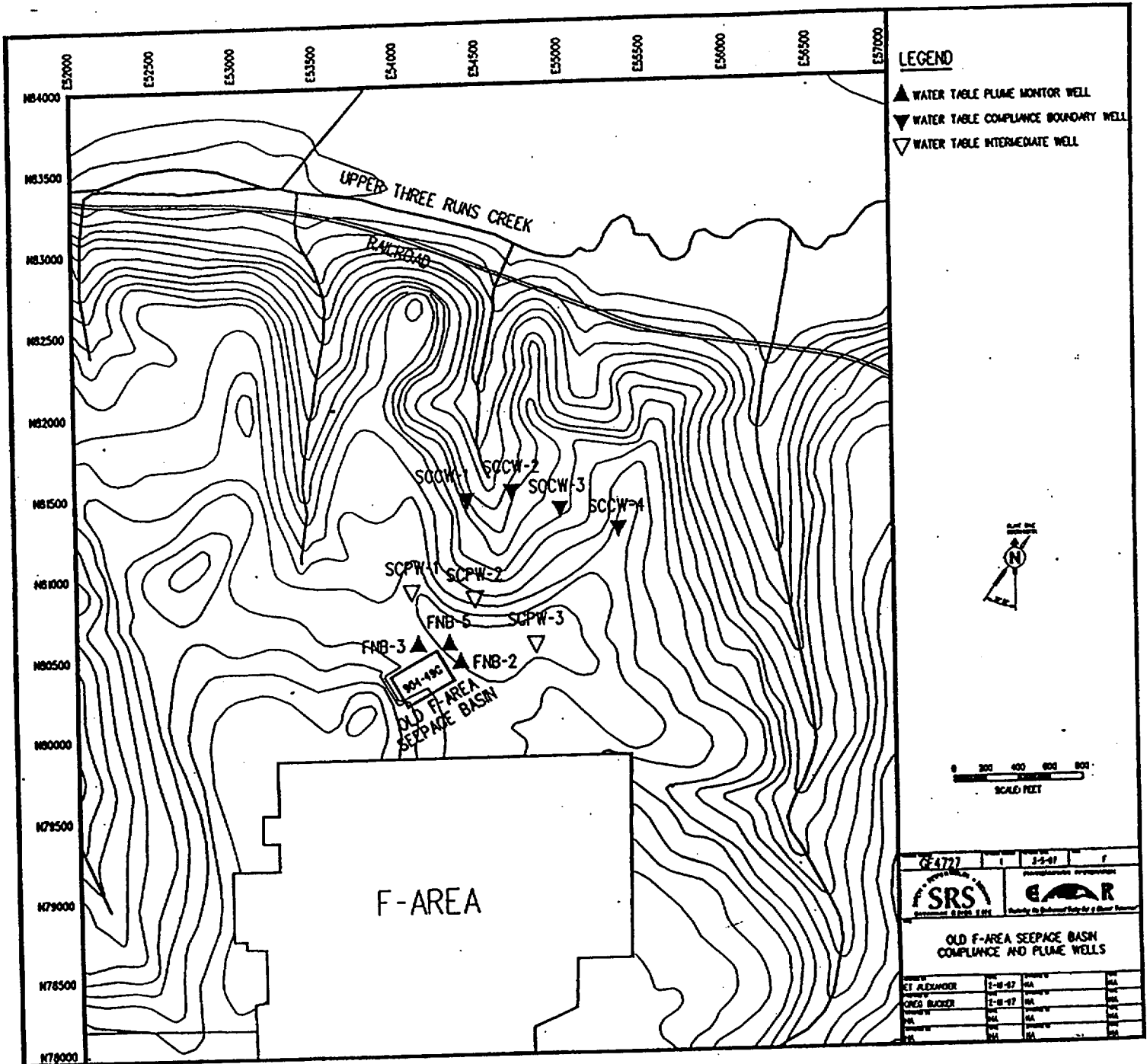


Figure 28. Locations of Plume Wells, Intermediate Wells, and Compliance Boundary Wells

**APPENDIX A**  
**OLD F-AREA SEEPAGE BASIN MODELING**

**(Pages A1 through A47)**

## Flow Model Discussion

Migration of tritium, nitrate, iodine-129, strontium-90, and total uranium from the Old F-Area Seepage Basin (OFASB) to Upper Three Runs was simulated using a three-dimensional, finite-element, fine-scale groundwater flow and solute contaminant transport model. The simulations were produced using an in-house code called FACT (Flow And Contaminant Transport). Version 2.-FB of the code has been verification and validation tested and a draft code manual is undergoing technical review (Hamm, et al., 1995). The model boundaries cover the distance extending from about 1600' south (up-gradient) of the OFASB to Upper Three Runs, and several thousand feet east and west (Figure A-1). Vertically, the model extends from ground surface to the bottom of the Gordon Aquifer Unit (Aquifer Unit IIA) (Figure A-2). Predicted contaminant plumes are well within these boundaries.

The OFASB groundwater flow model was created by refining a larger scale flow model covering the entire General Separations Area (GSA). The GSA model simulates groundwater flow between Fourmile Branch on the south and Upper Three Runs on the north, and between F-area on the west to McQueen Branch on the east. The vertical extent is from ground surface to the bottom of the Gordon Aquifer (Aquifer Unit IIA). The areal resolution of the larger scale GSA model is 200' square. The vertical resolution varies depending on hydrogeologic unit and terrain/stratigraphic variations. The GSA model representation of the "upper" aquifer zone of Upper Three Runs aquifer (aquifer zone IIB<sub>2</sub>) is comprised of 9 finite-elements in the vertical direction. The vadose zone is included in the model. The "lower" aquifer zone (aquifer zone IIB<sub>1</sub>) contains 5 finite-elements while the "tan clay" confining zone (confining zone IIB<sub>1</sub>-IIB<sub>2</sub>) separating the aquifer zones is modeled with 2 vertical elements. The Gordon confining unit (confining unit IIA-IIB) and Gordon aquifer unit (aquifer unit IIA) each contain 2 elements. Hydraulic conductivity values in the GSA model are based on pumping and slug test data, laboratory permeability measurements, and lithologic data. The conductivity field is non-uniform within hydrogeologic units and reflects variations present in the characterization data. The model was calibrated to achieve adequate agreement between measured and simulated values of hydraulic head, recharge and baseflow to area streams.

The groundwater flow model for the OFASB was created by extracting a subset of the GSA model and refining the areal and vertical mesh. The refined areal grid resolution varies from 100' around the basin to 200' in peripheral areas (Figure A-1). Figure A-2 illustrates the hydrostratigraphic nomenclature utilized herein and the number of vertical finite-elements for each hydrostratigraphic zone or unit. The "upper" aquifer zone of Upper Three Runs aquifer (aquifer zone IIB<sub>2</sub>) contains 9 vertical finite-elements and includes the vadose zone. The "lower" aquifer zone (aquifer zone IIB<sub>1</sub>) contains 10 vertical elements while the "tan clay" confining zone (confining zone IIB<sub>1</sub>-IIB<sub>2</sub>) separating the aquifer zones is modeled with 2 elements. The Gordon confining unit (confining unit IIA-IIB) contains 4 vertical elements and the Gordon aquifer unit (aquifer Unit IIA) has 6 elements. Hydraulic heads from the GSA model are used to define head boundary conditions along the perimeter of the OFASB model. Table A-1 summarizes

Starting with an initial dissolved plume, contaminant transport simulations were performed assuming no additional source terms (i.e., vadose zone or up-gradient source). This assumption is consistent with the selected remedy for the source unit. Contaminant migration was simulated using FACT and the fine-scale mesh and results from the OFASB flow model. Contaminant retardation due to geochemical effects was modeled using a constant  $K_d$  approach and conservative values. The initial plume configuration and concentration levels are defined from the plan view maps shown in the main text and assuming that the contamination extends from the water table to 33' below the water table (near the bottom of the screen zones in the monitoring wells and approximately half the aquifer thickness). Candidate compliance boundary wells were placed perpendicular to groundwater flow about 1600' upgradient of Upper Three Runs (Figure A-1). The screen zones of these compliance wells are 40' in length (nearly fully penetrating) and are designed to capture the core of the plume. Plume migration was simulated from present through at least maximum concentration break-through at the assumed compliance boundary. Table A-2 summarizes transport model inputs.

The  $K_d$  values for each contaminant were chosen based on site groundwater and soil conditions (Table A-2). A detailed discussion of the geochemical analysis behind the values given in Table A-2 is provided following the results section of this appendix. In summary,  $K_d$  values were derived from site specific studies wherever possible. Otherwise, published scientific literature pertinent to OFASB conditions were used. In addition, knowledge of contaminant behavior at F- and H-Area Seepage Basins was valuable for estimating  $K_d$  values for the geochemical model of OFASB groundwater.

It is recognized that the constant  $K_d$  approach is simplistic because of the complex nature of geochemical interactions. However, by choosing  $K_d$  values that relate to site conditions and are somewhat conservative, a model is achieved that projects the minimum reasonable retardation. Tritium, nitrate, iodine-129, and strontium-90 are the contaminants that can be most realistically modeled in a best-estimate sense using this approach. The transport behavior of these contaminants in Savannah River Site groundwater is dominated by adsorption rather than solubility or ion exchange. Further simplifying their transport is the fact that they do not generally form strong complexes with the major ions in solution. Uranium is more difficult to model in a best-estimate sense because of its natural abundance in Savannah River Site sediments and its complicated chemistry. Uranium is subject to solubility constraints, adsorption, multiple valence states, and complexation that additionally complicate modeling efforts. The uncertainty in uranium  $K_d$  is higher compared to the other contaminants as indicated in Table A-2. However, 4 ml/g is considered a conservative estimate.

## Tritium

The tritium inventory in the initial plume is about 4 Curies (Ci). Tritium is essentially unretarded (retardation coefficient,  $R = 1.005$ ). Therefore, the center of mass of the initial plume is expected to reach the compliance boundary in about 10 years. With a radioactive half-life of 12.3 years (Table A-2), half the plume activity will decay in transit. Wells FNB 2, 3, and 5 are currently above the 20 pCi/ml MCL for tritium. In the assumed absence of a source term, these 3 wells are predicted to fall below 20 pCi/ml in approximately two to four years (Figure A-5). Figure A-6 illustrates tritium break-through at the CBWs. A maximum value of 7.0 pCi/ml (which is well below the MCL) is predicted to occur in CBW 2c after 8.5 years. From that point on there is a steady decline in tritium values at CBW 2c with values below 1 pCi/ml within 20 years. Figures A-7 and A-8 illustrate plan and cross-sectional views of the plume at 2, 4, 6, and 8 years into the future. The eight year future prediction of tritium on the two illustrations corresponds approximately with the maximum tritium value of 7 pCi/ml predicted at the CBW 2c (Figures A-7 and A-8). The MCL of 20 pCi/ml for tritium is predicted never to be exceeded at the compliance boundary.

## Nitrate

The nitrate inventory in the initial plume is about 460 kg. Like tritium, nitrate is essentially unretarded (retardation coefficient,  $R = 1.05$ ) and the plume center of mass is expected to reach the compliance boundary in about 10 years. Wells FNB 2 and 5 are currently above the 10 mg/l MCL for nitrate. In the assumed absence of a source term, these 2 wells are predicted to fall below the MCL in approximately 1 - 2 years (Figure A-9). Figure A-10 illustrates nitrate break-through at the compliance boundary wells. A maximum value of 1.2 mg/l (which is well below the MCL) is predicted to occur in CBW 2c and 2d after 10 years. In approximately 20 years it is predicted that only a trace of nitrate will be present at the CBWs. Figures A-11 and A-12 illustrate plan and cross-sectional views of the plume at 2, 4, 6, and 8 years into the future. The MCL of 10 mg/l for nitrate is predicted never to be exceeded at the compliance boundary.

## Iodine-129

The iodine-129 inventory in the initial plume is about 0.006 Ci. The retardation factor (R) for iodine-129 is 20 based on the  $K_d$  value given in Table A-2. The center of mass of the plume is therefore expected to reach the compliance boundary in about 200 years. Radioactive decay is neglected because the half-life of iodine-129 is large compared to the transport times. Wells FNB 2 and 5 are currently above the 1 pCi/l MCL for iodine-129. In the assumed absence of a source term, the plume wells are predicted to fall below the MCL within 90 to 100 years (Figure A-13). Figure A-14 illustrates iodine-129 break-through at the compliance boundary wells. A maximum value of 1.1 pCi/l is predicted to occur in CBW 2d after 180 years. From that point on there is a steady decline in iodine-129 values at CBW 2d. Figures A-15 and A-16 illustrate plan and cross-sectional views of the plume at 50, 100, 200, and 300 years into the future. CBW 2d is the only

**Table A-3: Dispersivity values considered in sensitivity analysis**

Case	Longitudinal dispersivity (ft)	Transverse horizontal dispersivity (ft)	Transverse vertical dispersivity (ft)	Comments
1	10	1	0.1	Minimum values that are numerically feasible (Peclet number = 10)
(nominal)	30	5	0.1	Nominal setting
2	100	10	1	Intermediate setting
3	280	28	2.8	Longitudinal value is 10% total travel length

Case 1 produces the minimum amount of plume dispersion or dilution that can be numerically simulated for the resolution of the OFASB mesh (100 ft). This case was run for all 5 contaminants. Case 3 corresponds to the rule of thumb that longitudinal dispersivity should be about 10% of plume length. This case is considered a conservative upper limit because smaller values should be used early in the transient while the plume is small. Also, numerical dispersion creates additional plume dilution. A larger dispersivity causes more plume dilution, but also transports contamination to the compliance boundary faster before radioactive decay further reduces plume strength. These competing effects are important for tritium and strontium-90, for which radioactive decay are considered, so case 3 was run for both. Total uranium, iodine-129 and nitrate are modeled as having no decay, so case 3 would only result in a lower concentration at the compliance boundary and was not run. Case 2 is an intermediate setting run only for tritium and strontium-90.

For the porosity sensitivity analysis the low and high end member cases were analyzed. An effective porosity of 20% was considered for all 5 contaminants because this setting increases the pore velocity and decreases groundwater travel time. An effective porosity of 40% was also considered for total uranium, iodine-129 and nitrate. Strontium-90 was not considered because its nominal break-through curves is so far below MCL that changing porosity would not challenge the bottom-line outcome. Tritium was not considered because it is unretarded and has a short half-life. Increasing effective porosity for tritium would only result in a lower break-through concentration.

A  $K_d$  value of 1 ml/g was considered for iodine-129 for the purpose of testing model sensitivity to  $K_d$ . This is the maximum value reported for typical aquifer conditions by Looney et al. (1987). Typical aquifer conditions generally include a pH significantly higher than that at the OFASB (i.e. pH=5 rather than pH=4 in OFASB core of plume). Thus, the maximum value reported by Looney et al. (1987) may be a reasonable minimum value for the OFASB. The nominal  $K_d$  values for uranium, strontium-90, tritium, and nitrate already represent realistic lower bounds.

influences the surface chemistry of the aquifer minerals. The estimates of  $K_d$  values presented here attempt to account for these factors by reviewing studies that were performed under conditions pertinent to the OFASB.

Groundwater chemistry data for the five monitoring wells at the OFASB were obtained from GIMS for the time period of first quarter 1994 through first quarter 1995. Table A-4 shows the average pH and average concentrations of  $\text{Cl}^-$  and  $\text{SO}_4^{2-}$  in groundwater from these wells. The groundwater in the contaminant plume is acidic (pH=3.98-4.15). As suggested in Looney et al. (1987) this will result in greater mobility for contaminants in cationic forms than would be predicted by the  $K_d$  values reported in that document. Likewise, the transport of constituents in anionic species may be more attenuated under these acidic conditions. The groundwater chemistry suggests that the only constituent whose transport may be complicated by complexing is uranium. The dominant species of U(VI) will be  $\text{UO}_2^{+2}$  unless dissolved phosphate is elevated in the groundwater. At phosphate concentrations greater than 0.1 mg/l anionic phosphate complexes may dominate the uranium speciation (Langmuir, 1978) altering the transport behavior of uranium.

**Table A-4: pH,  $\text{Cl}^-$  and  $\text{SO}_4^{2-}$  concentrations in groundwater monitoring wells FNB-1, FNB-2, FNB-3, FNB-4, and FNB-5.**

	FNB-1	FNB-2	FNB-3	FNB-4	FNB-5
pH	5.10	3.98	4.91	4.95	4.15
$\text{Cl}^-$ (mg/l)	2.70	2.46	2.57	2.13	2.16
$\text{SO}_4^{2-}$ (mg/l)	<1	<1.11	<1	<1	<1.01

The dominant sorptive surfaces present in the soils of the OFASB are likely to be kaolinite and ferric iron oxyhydroxides (e.g. goethite). These minerals are common in the subsurface soils throughout the SRS area. Moreover, Ryan (1982) reported that the clay fractions of soil samples from the adjacent Mixed Waste Management Facility were dominated by kaolinite with traces of smectite and "fairly consistent percentages of iron on the clays".

Table A-5 shows the recommended  $K_d$  values for the five selected constituents at a groundwater pH of 4. Following Table A-5 is a discussion of each constituent that summarizes the literature reviewed and the choice of recommended values. The general method of choosing  $K_d$  values was that site specific studies took precedence over non-SRS studies.

## Strontium-90

The work of Prout (1958) and Hoeffner (1985) demonstrate that strontium-90 transport is very sensitive to pH. The  $K_d$  value chosen here (3 ml/g) is from the  $K_d$  versus pH curve Hoeffner (1985) produced from batch sorption experiments.

## Uranium (Total)

The uranium isotopes U-234, U-235, and U-238 behave the same during transport by groundwater. Ferric iron oxyhydroxides are among the strongest natural sorbents of uranium (Langmuir, 1978). Uranium sorption onto ferric iron oxyhydroxides is dependent on pH and weakens as pH drops below 5. Studies by Hsi and Langmuir (1985) and Waite et al. (1994) indicate that sorption decreases dramatically between pH of 4 and 5 depending on the concentration of uranium used, the amount of solid phase, and the nature of the solid phase. This suggests that in the pH range of OFASB groundwaters the  $K_d$  value should be significantly less than that reported for more neutral pH by Looney et al. (1987). The  $K_d$  value of 4 ml/g reported here is consistent with the studies referenced above.

The measurement of uranium transport in groundwater at SRS is complicated by the abundance of natural uranium in the aquifer sediments. The sandy aquifers contain uranium-bearing minerals such as apatite, monazite, crandallite, and sphene. These minerals can contain uranium in concentrations that exceed 100 ppm and are soluble in acidic solutions. Thus, when an acidic plume migrates through these sands it will dissolve uranium-bearing minerals, increasing the concentration of uranium in the groundwater. In some cases reprecipitation of less soluble phases may then remove uranium from the groundwater as a co-precipitate. However, until further studies reveal the nature of these reactions in Savannah River Site sediments, modeling of uranium transport will remain tenuous. The most valid approach is to use a conservative  $K_d$  value as a bounding condition so that the minimum reasonable retardation is achieved. This is the approach taken in this model.

## Flow Model Calibration Results

For model calibration purposes, a contour plot of all available hydraulic head data from Upper Three Runs aquifer (IIB<sub>1</sub> and IIB<sub>2</sub>) was prepared as shown in Figure A-31. Data from monitoring wells, seepage surveys and cone penetrometer investigations were used to construct the map. OFASB model results for hydraulic head in the "lower" aquifer zone (IIB<sub>1</sub>) are presented in Figure A-32. The simulated water table is shown in Figure A-33. Because Figure A-31 is based on data from both aquifer zones (above and below the "tan clay"), the model results presented in Figures A-32 and 33 should bracket the measured data. Overall, the agreement between the measured and simulated heads is good. Detailed head calibration results for OFASB model are presented below.

## References

- Allard, B., B. Torstenfelt, K. Anderson, and J. Rydberg, 1980, Possible retention of iodine in the ground, in *Scientific Basis for Nuclear Waste Management*, V. 2, C.J.M. Northrup, Jr. (ed.), Plenum Press, p. 673-680.
- Bellini, G., M.E. Sumner, D.E. Radcliffe, and N.P. Qafoku, 1996, Anion transport through columns of highly weathered acid soil: Adsorption and retardation, *Soil Science Society of America Journal*, v. 60, p. 132-137.
- Hamm, L. L., S. E. Aleman, W. F. Jones, G. P. Flach, J. S. Haselow, P. S. Huyakorn, S. Panday and T. Birdie, 1995, FACT: Subsurface flow and contaminant transport documentation and user's guide, WSRC-TR-95-223, in prep.
- Haselow, J. S., M. Harris, B. B. Looney, N. V. Halverson, and J. B. Gladden, 1990, Analysis of soil and water at the Four Mile Creek seep line near the F and H area of SRS (U), WSRC-RP-90-0591.
- Hoeffner, S.L., 1985, Factors that influence the pH in the SRP Burial Ground, DPST-85-243, E.I du Pont de Nemours & Co., Savannah River Laboratory, Aiken, SC.
- Hsi, C.D. and D. Langmuir, 1985, Adsorption of uranyl onto ferric oxyhydroxides: Applications of the surface complexation site-binding model, *Geochimica et Cosmochimica Acta*, v. 49, p. 1931-1941.
- Langmuir, D., 1978, Uranium solution-mineral equilibria at low temperatures with applications with applications to sedimentary ore deposits, *Geochimica et Cosmochimica Acta*, v. 42, p. 547-569.
- Li, Y.C., A.K. Alva, D.V. Calvert, and D.J. Banks, 1995, Adsorption and transport of nitrate and bromide in a spodosol, *Soil Science*, v. 160, p. 400-404.
- Looney, B. B., M. W. Grant, and C. M. King, 1987, Estimation of geochemical parameters for assessing subsurface transport at the Savannah River Plant; DPST-85-904.
- Prout, W. E., 1959, Adsorption of fission products by Savannah River Plant soil, DP-394, E. I. du Pont de Nemours and Company, Aiken, SC.
- Ryan, J.P., 1982, Batch and column strontium distribution coefficients with water-saturated soil strata from the Savannah River Plant Burial Ground, in *Environmental Migration of Long-lived Radionuclides*, International Atomic Energy Agency, Vienna.
- Waite, T.D., J.A. Davis, T.E. Payne, G.A. Waychunas, and N. Xu, 1994, Uranium (VI) adsorption to ferrihydrite: Application of a surface complexation model, *Geochimica et Cosmochimica Acta*, v. 58, p. 5465-5478.
- WSRC (Westinghouse Savannah River Company) 1995. RCRA Facility Investigation/Remedial Investigation Report for the Old F-Area Seepage Basin (904-49G)(U), Rev. 1, WSRC-RP-94-942, June 1995.

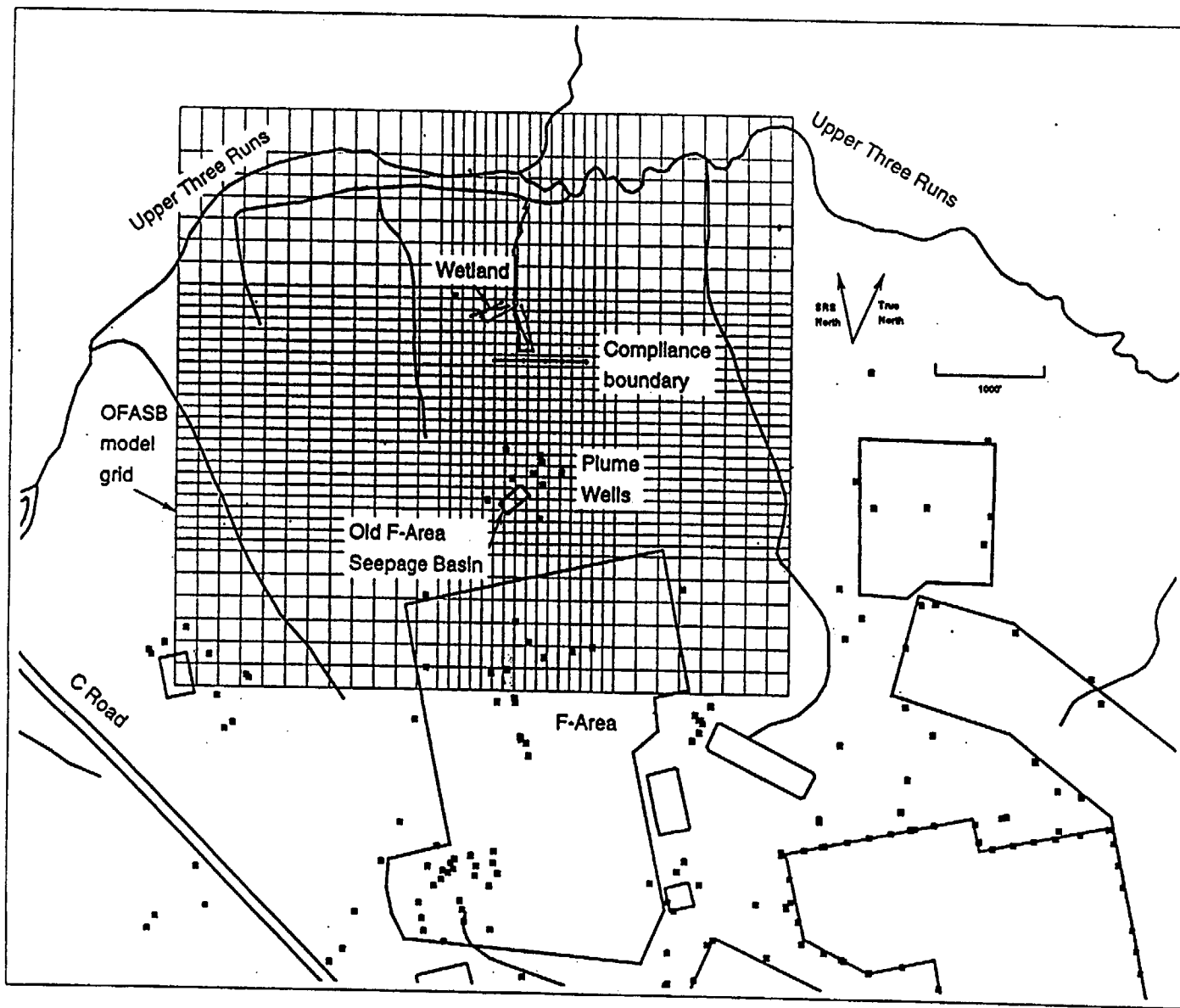


Figure A-1: Location map of the Old F Area Seepage Basin with monitoring wells, compliance boundary, and model grid.

Simulated groundwater flow paths starting from top and bottom of FNB well screens

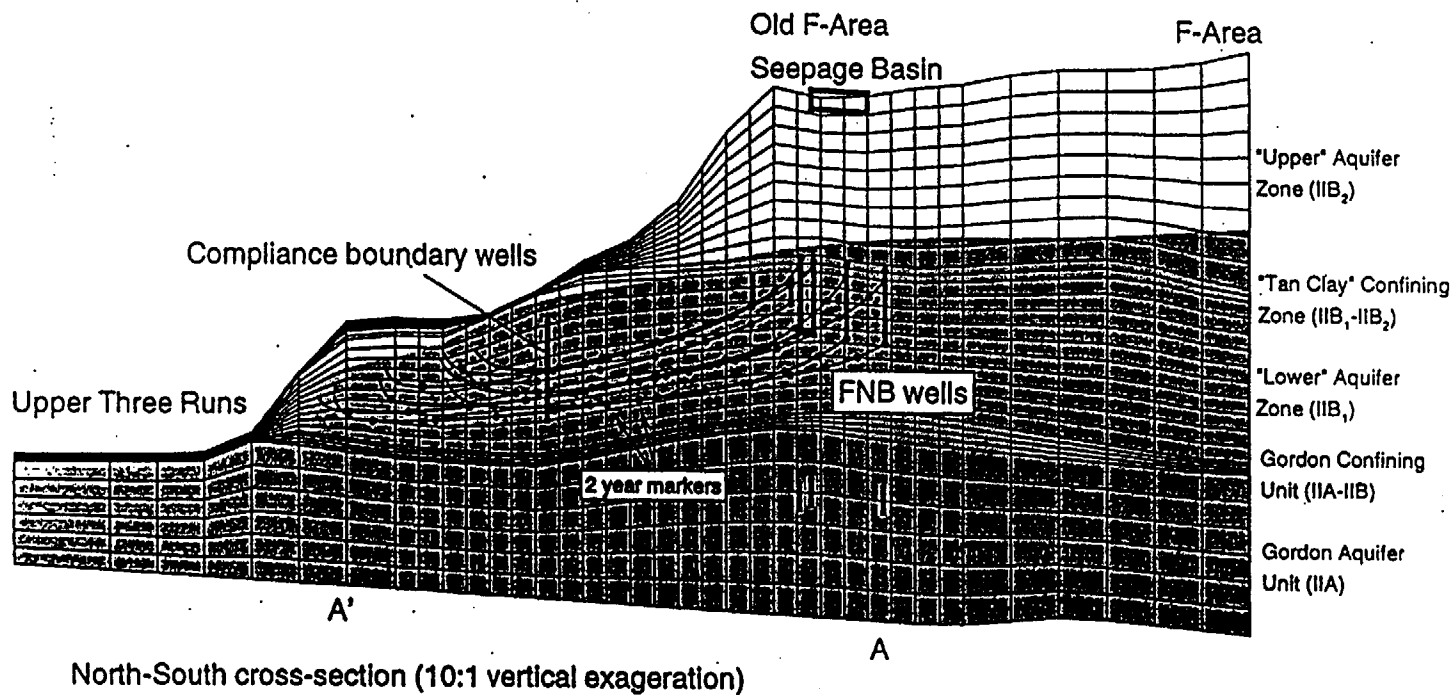


Figure A-2: Simulated vertical groundwater flow paths starting from top and bottom of FNB well screens. Hydrostratigraphic nomenclature used for vertical model grid illustrated above.

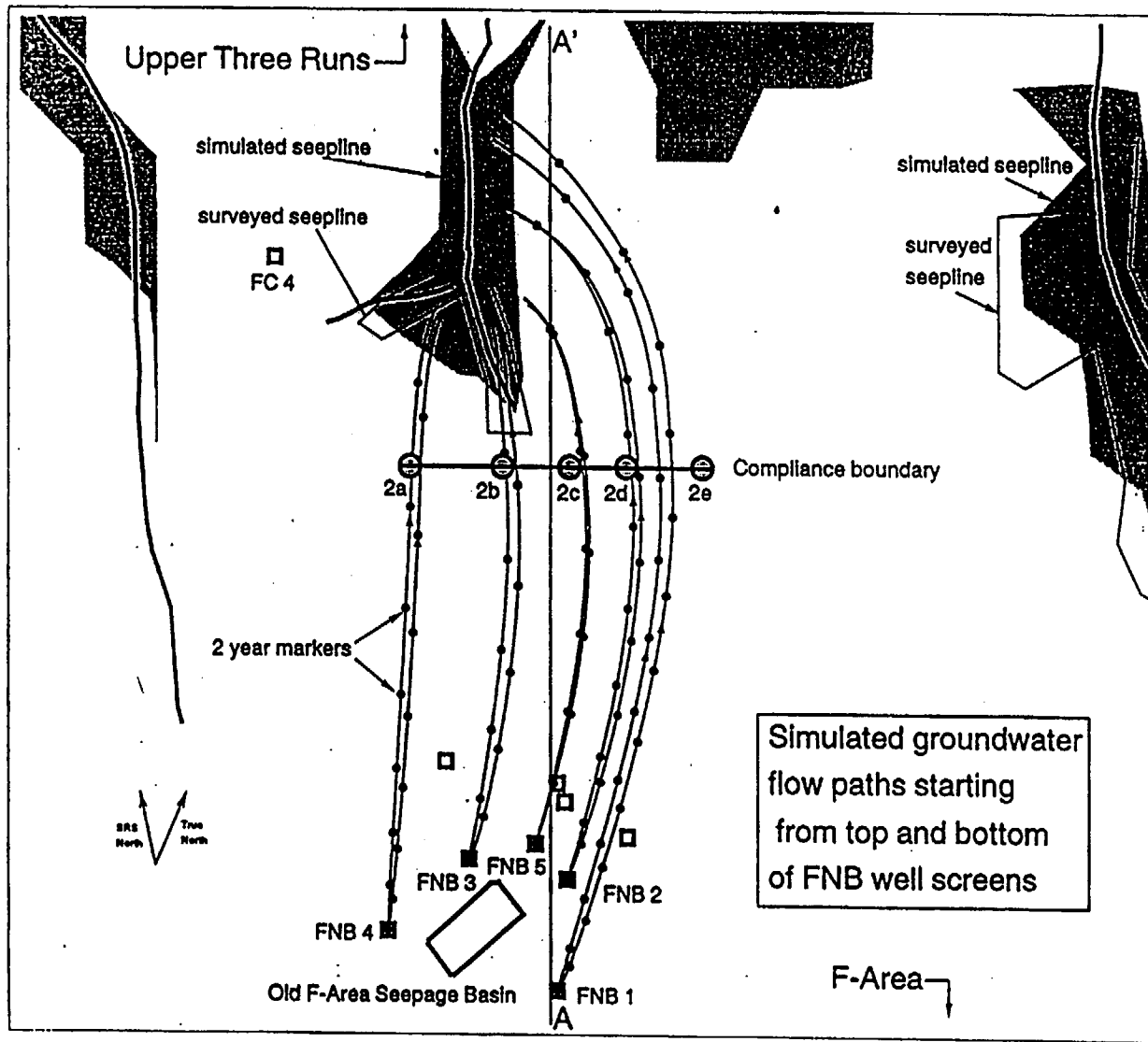


Figure A-3: Simulated groundwater flow paths starting from top and bottom of FNB well screens with 2 year markers in the vicinity of the Old F Area Seepage Basin. Compliance boundary with simulated seep line and surveyed seep line shown.

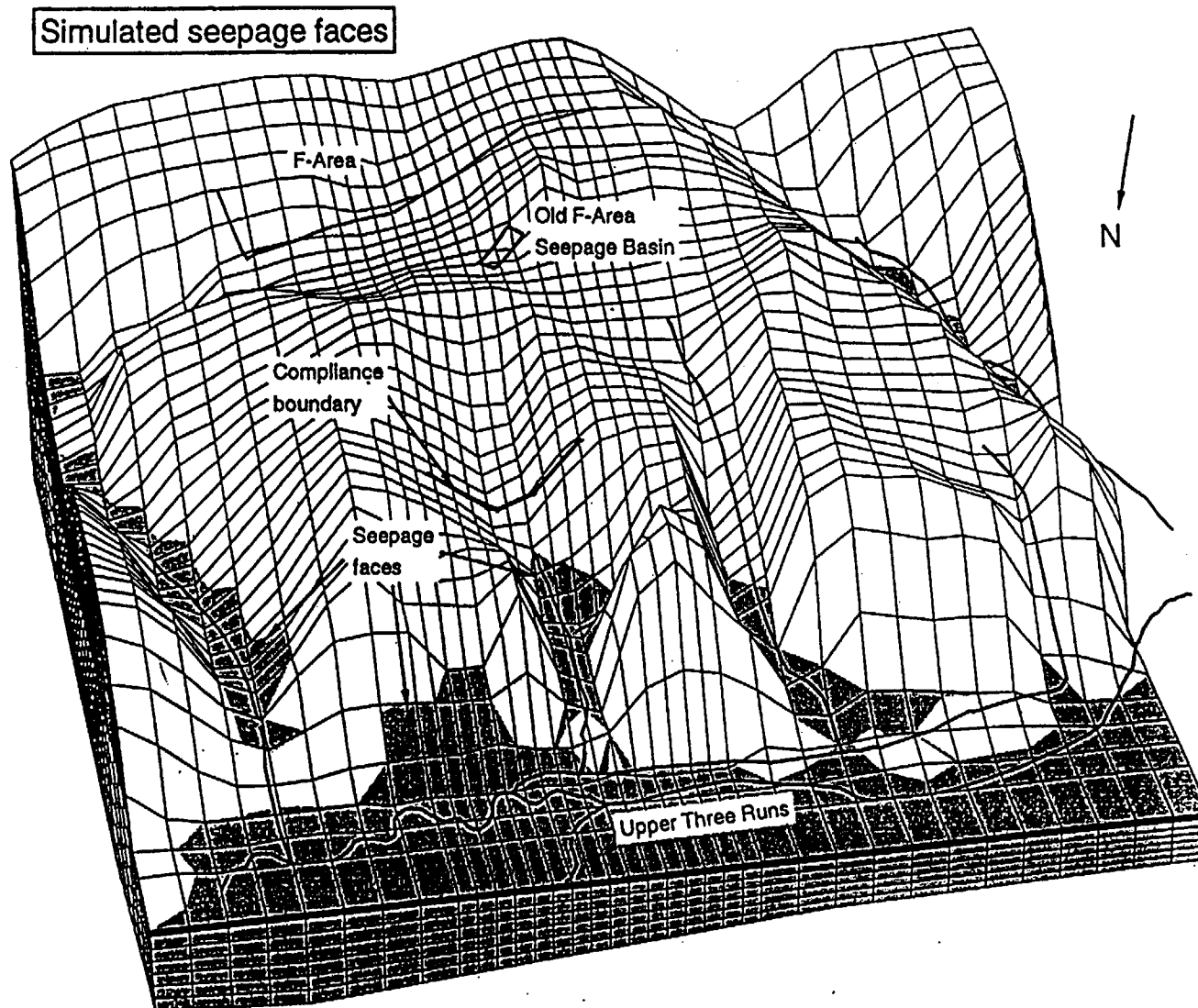


Figure A-4: Simulated three-dimensional predicted saturated zones and seepage faces.

# OLD F-AREA SEEPAGE BASIN

## Tritium Concentration at Plume Boundary

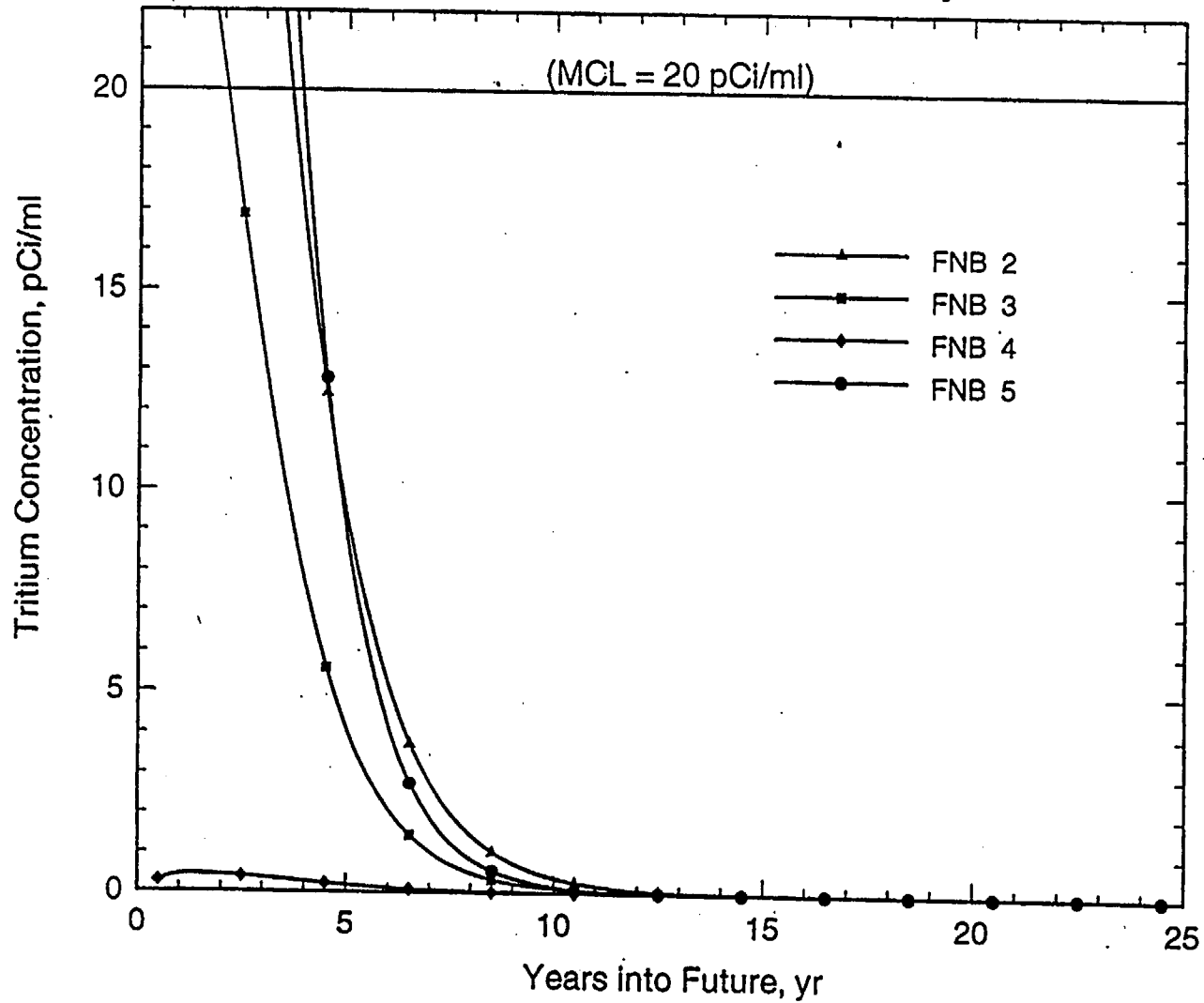


Figure A-5: Predicted tritium concentration at FNB Point of Compliance wells.

# OLD F-AREA SEEPAGE BASIN

## Tritium Concentration at Compliance Boundary

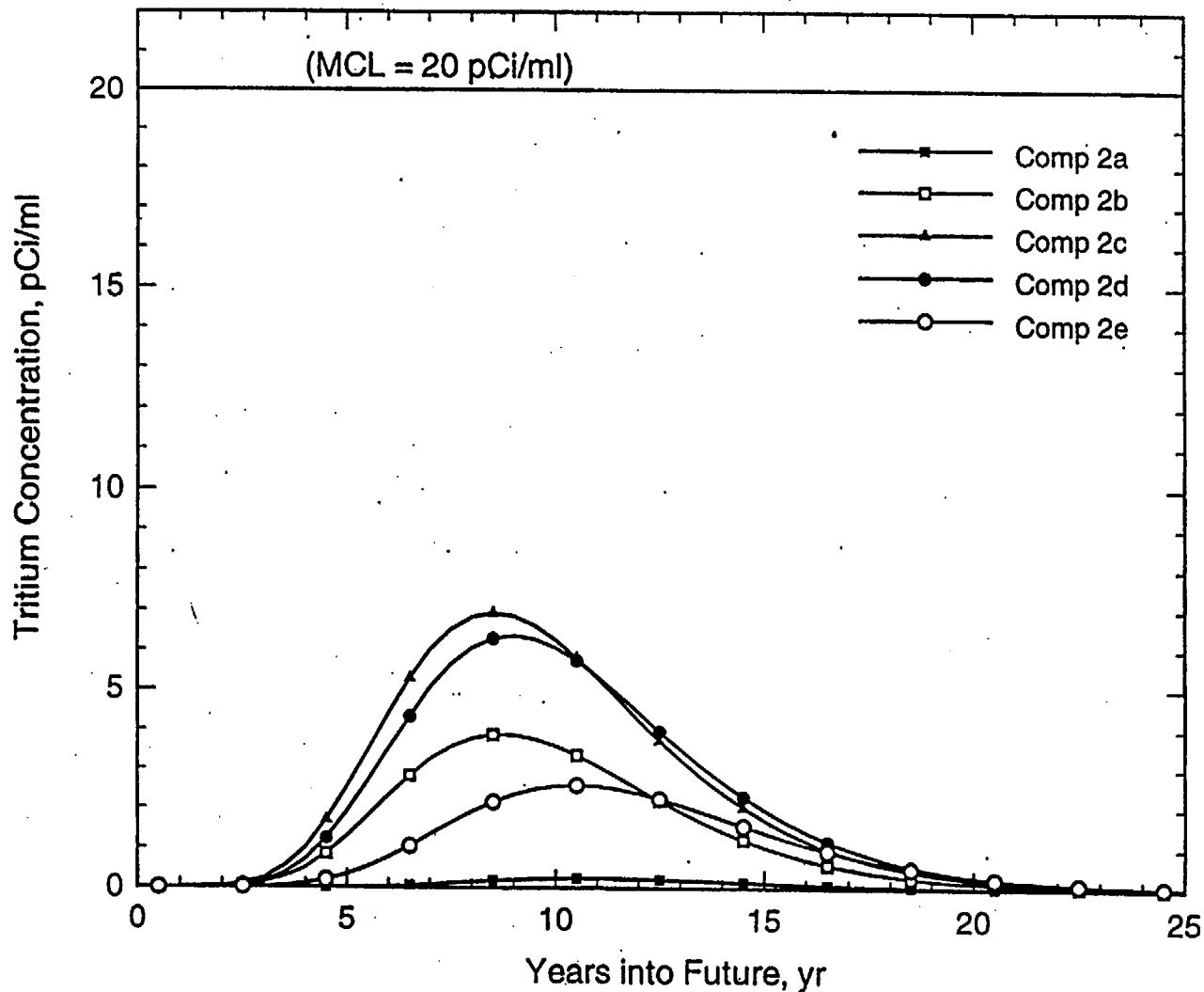


Figure A-6: Predicted tritium concentration at Compliance Boundary.

# Tritium Plume (pCi/ml) in Upper Three Runs Aquifer Unit (IIB<sub>1</sub>)

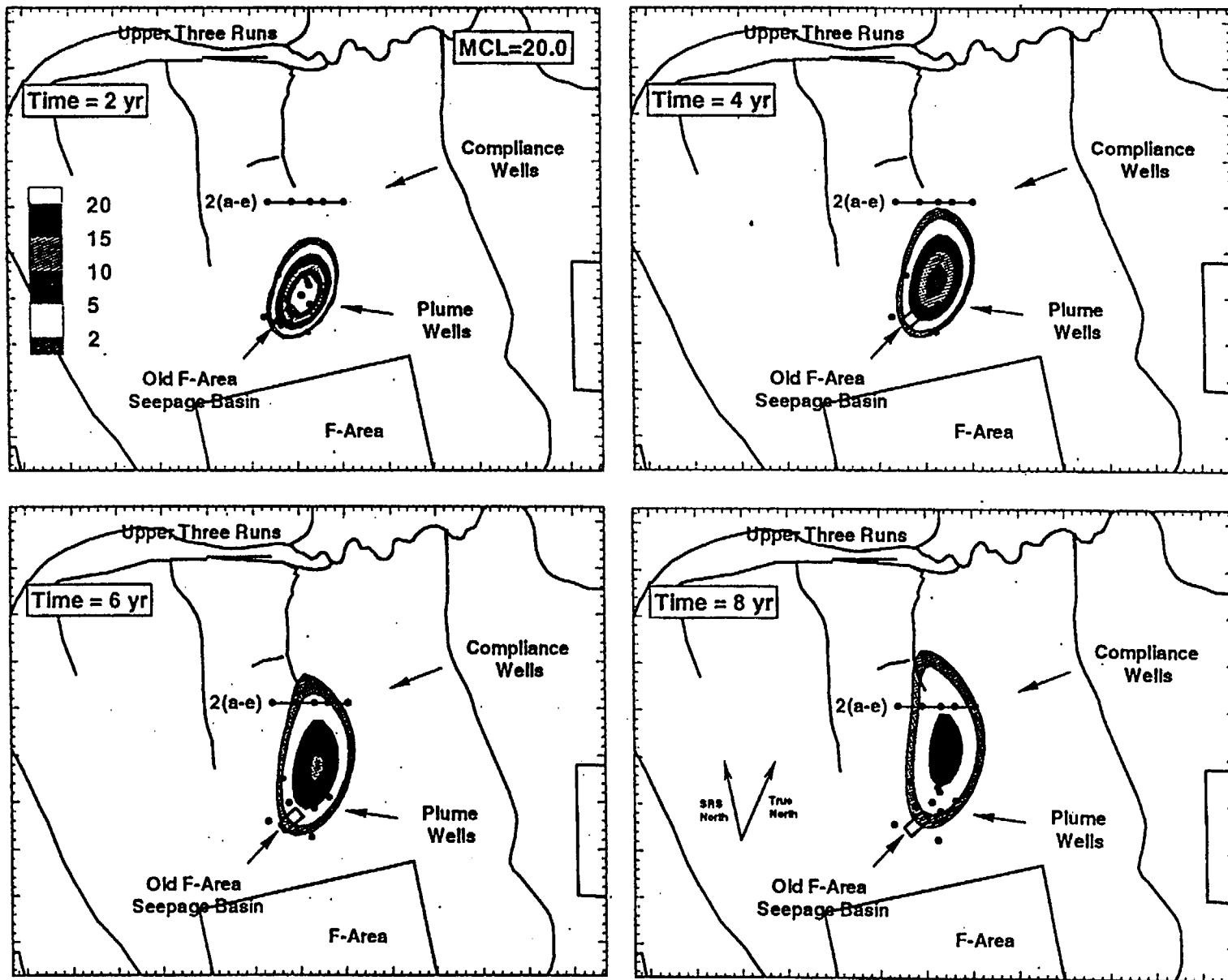


Figure A-7: Predicted tritium plume conditions in two, four, six, and eight years (areal view).

# Tritium Plume (pCi/ml) in Upper Three Runs Aquifer Unit (IIB<sub>2</sub>&IIB<sub>1</sub>)

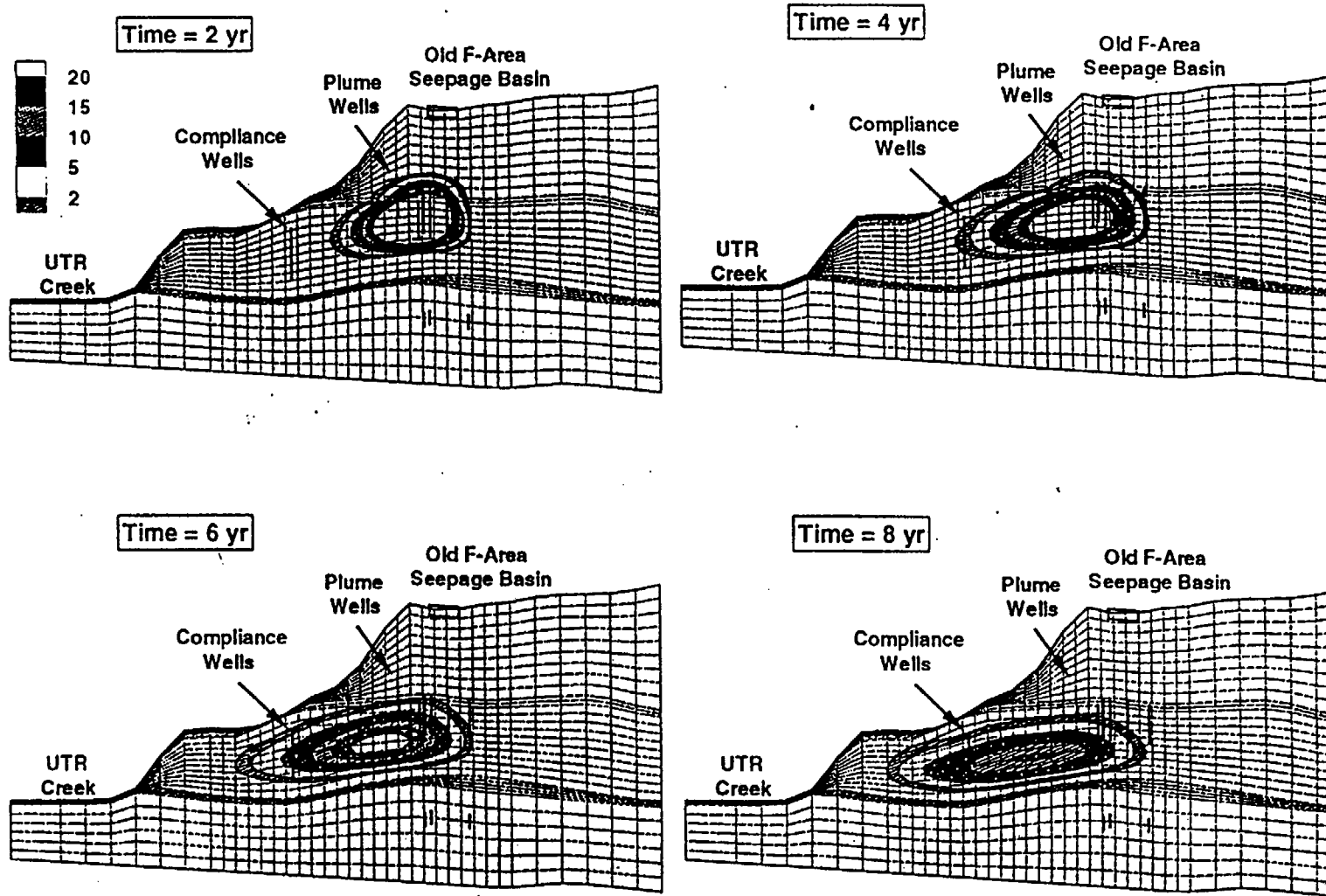


Figure A-8: Predicted tritium plume conditions in two, four, six, and eight years (cross-sectional view).

OLD F-AREA SEEPAGE BASIN  
Nitrate Concentration at Plume Boundary

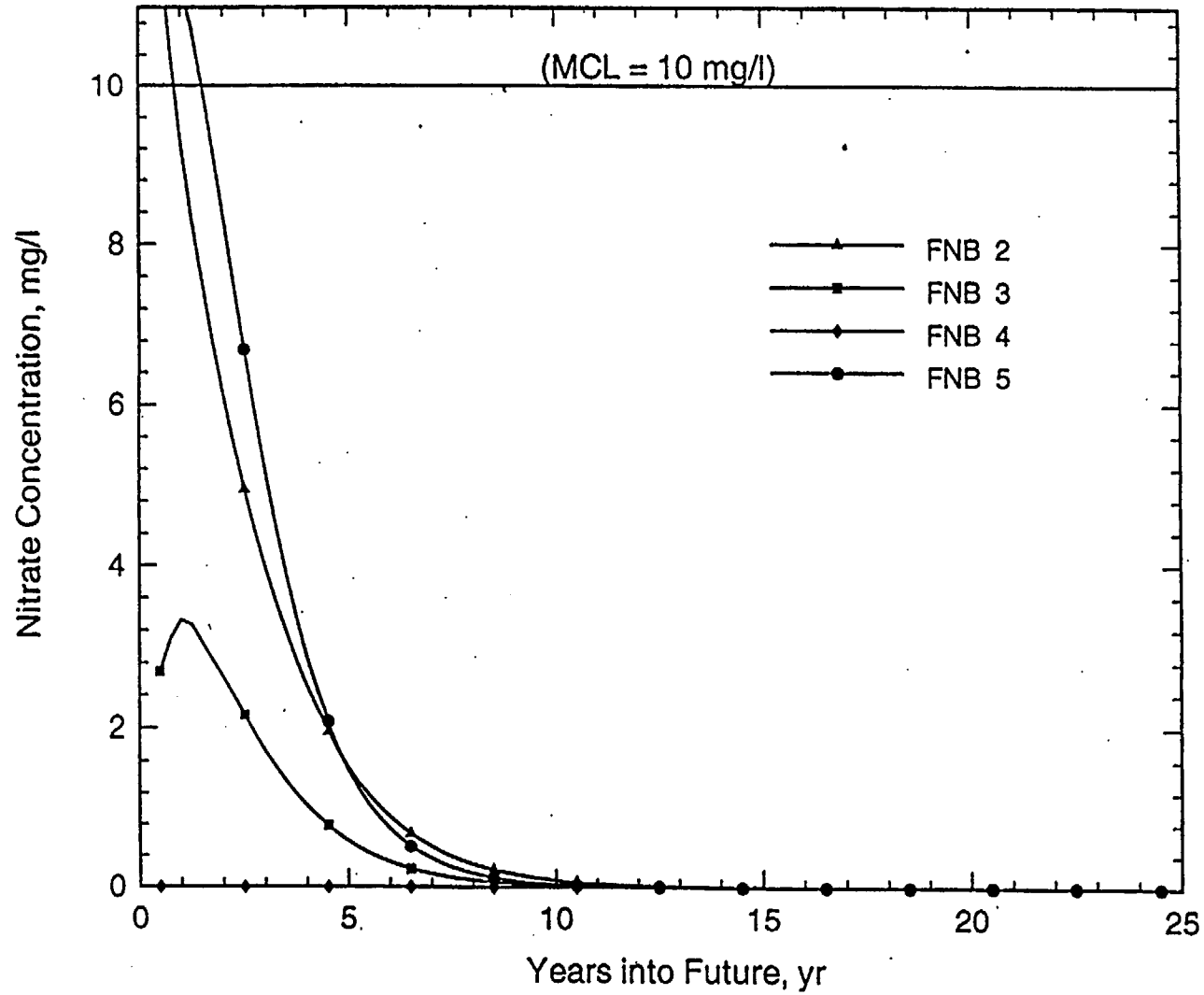


Figure A-9 Predicted nitrate concentration at FNB Point of Compliance wells.  
A-22

# OLD F-AREA SEEPAGE BASIN

## Nitrate Concentration at Compliance Boundary

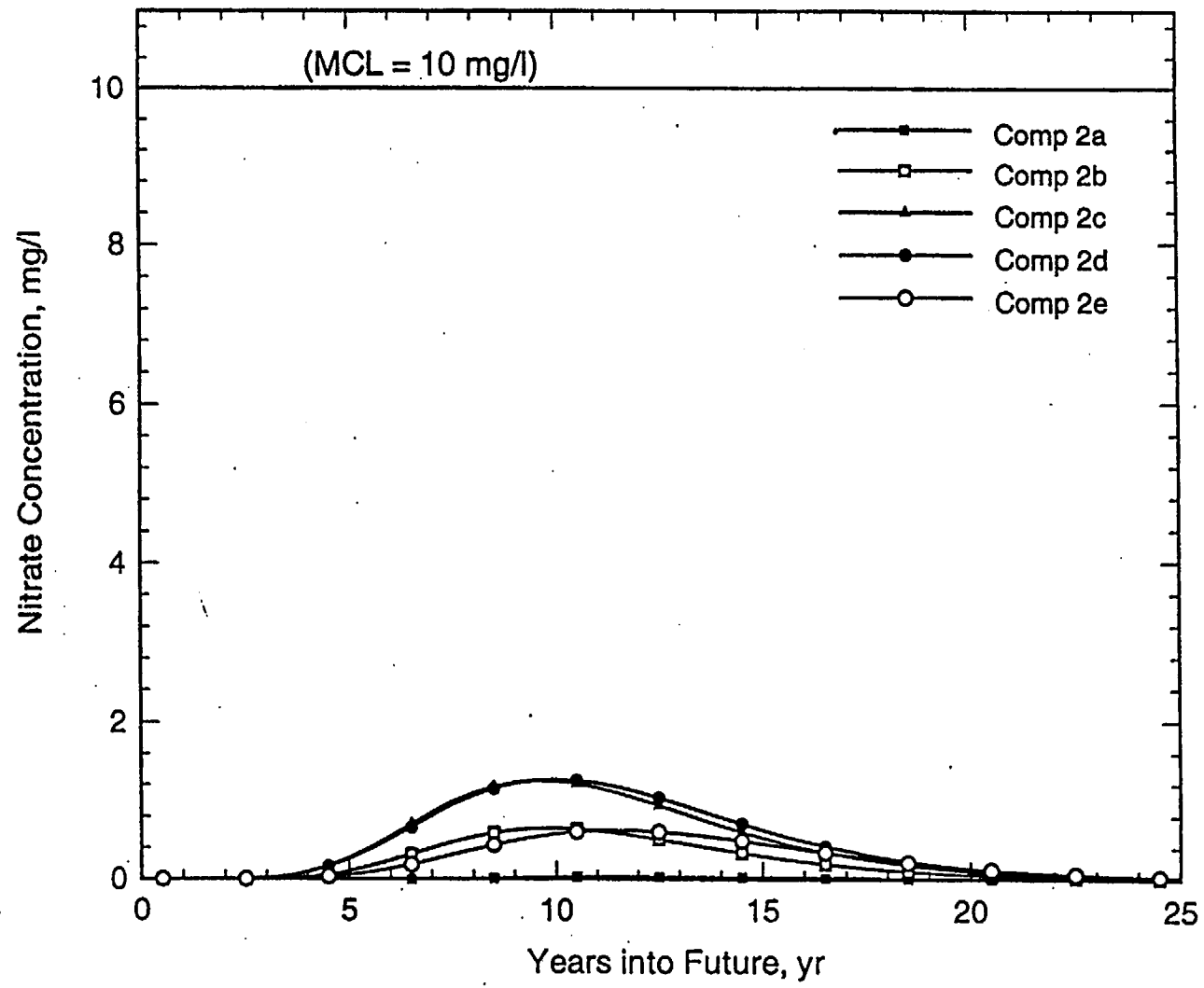


Figure A-10 Predicted nitrate concentration at Compliance Boundary.

# Nitrate Plume (mg/l) in Upper Three Runs Aquifer Unit (IIB<sub>1</sub>)

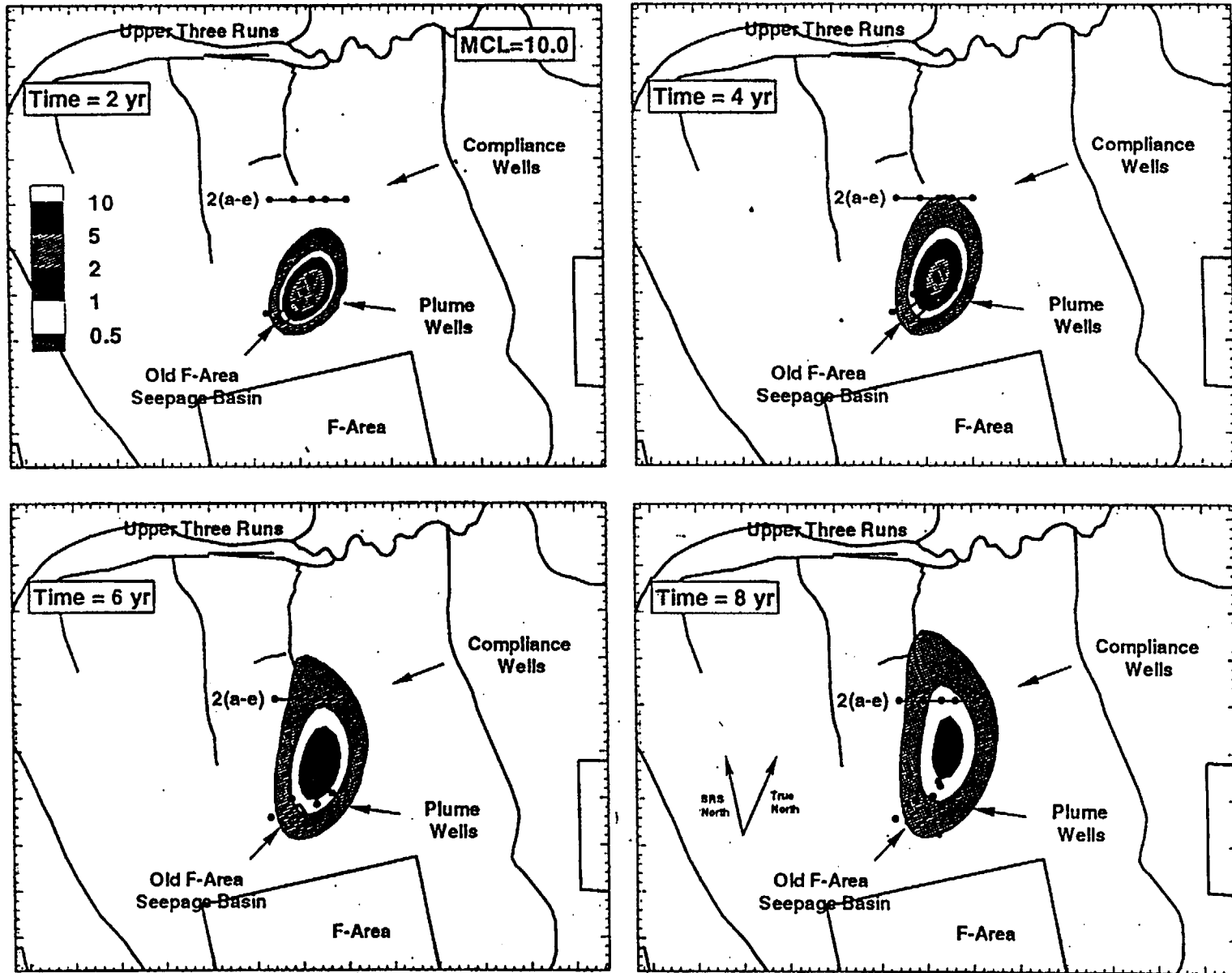


Figure A-11 Predicted nitrate plume conditions in two, four, six, and eight years (areal view).

# Nitrate Plume (mg/l) in Upper Three Runs Aquifer Unit (IIB<sub>2</sub>&IIB<sub>1</sub>)

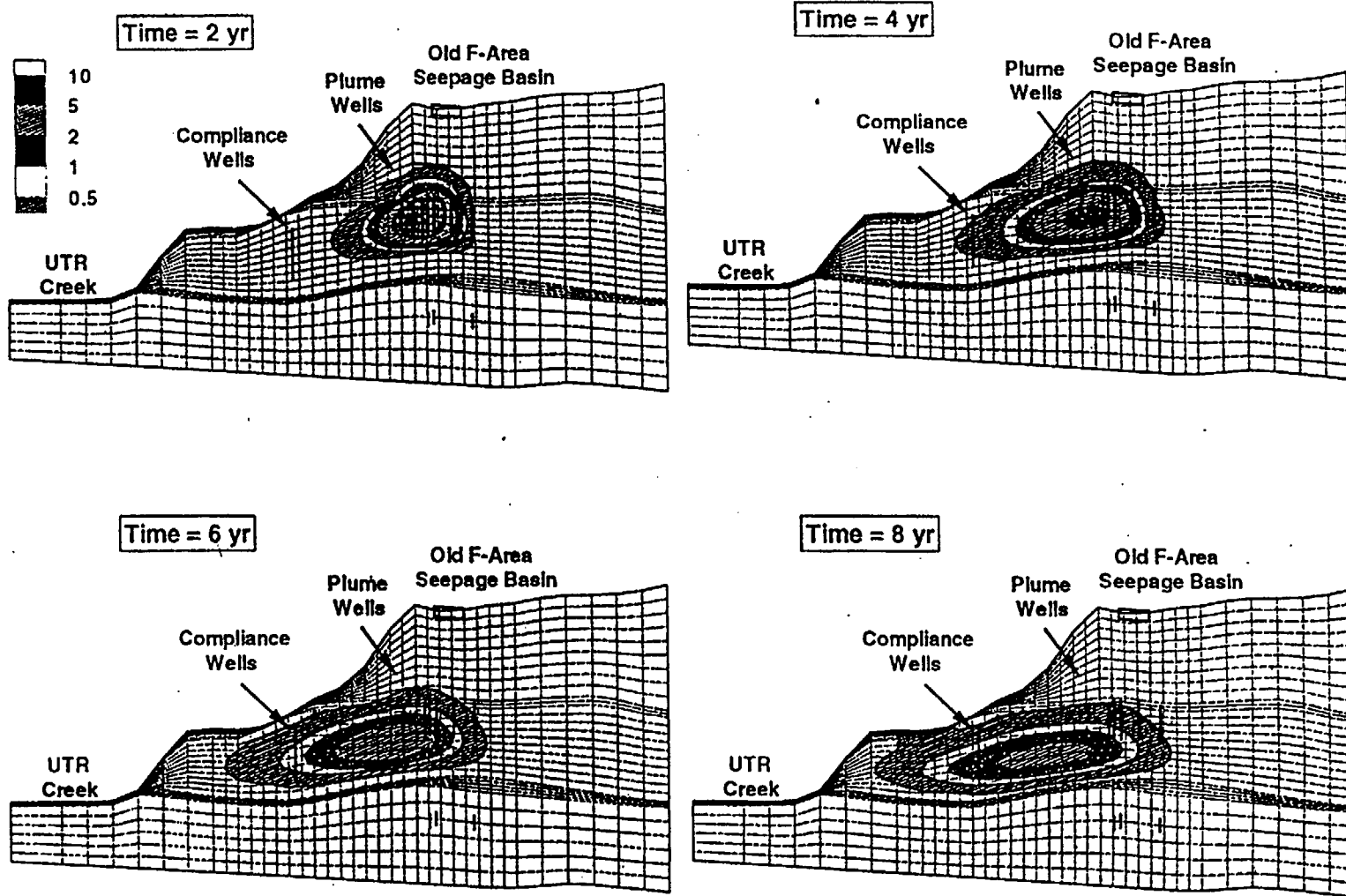


Figure A-12 Predicted nitrate plume conditions in eight years (cross-sectional view).

# OLD F-AREA SEEPAGE BASIN

## Iodine-129 Concentration at Plume Boundary

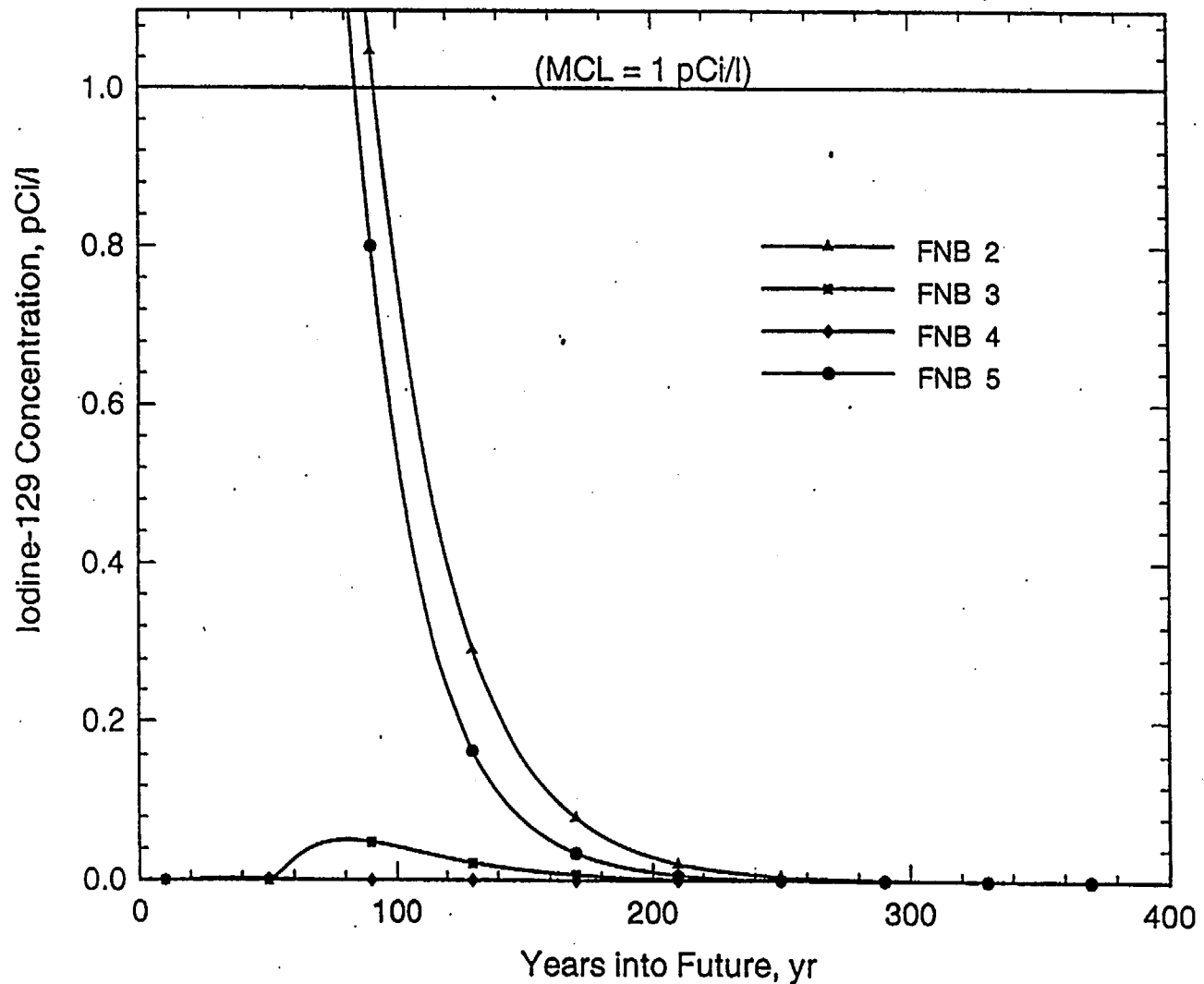


Figure A-13 Predicted iodine-129 concentration at FNB Point of Compliance wells.

OLD F-AREA SEEPAGE BASIN  
Iodine-129 Concentration at Compliance Boundary

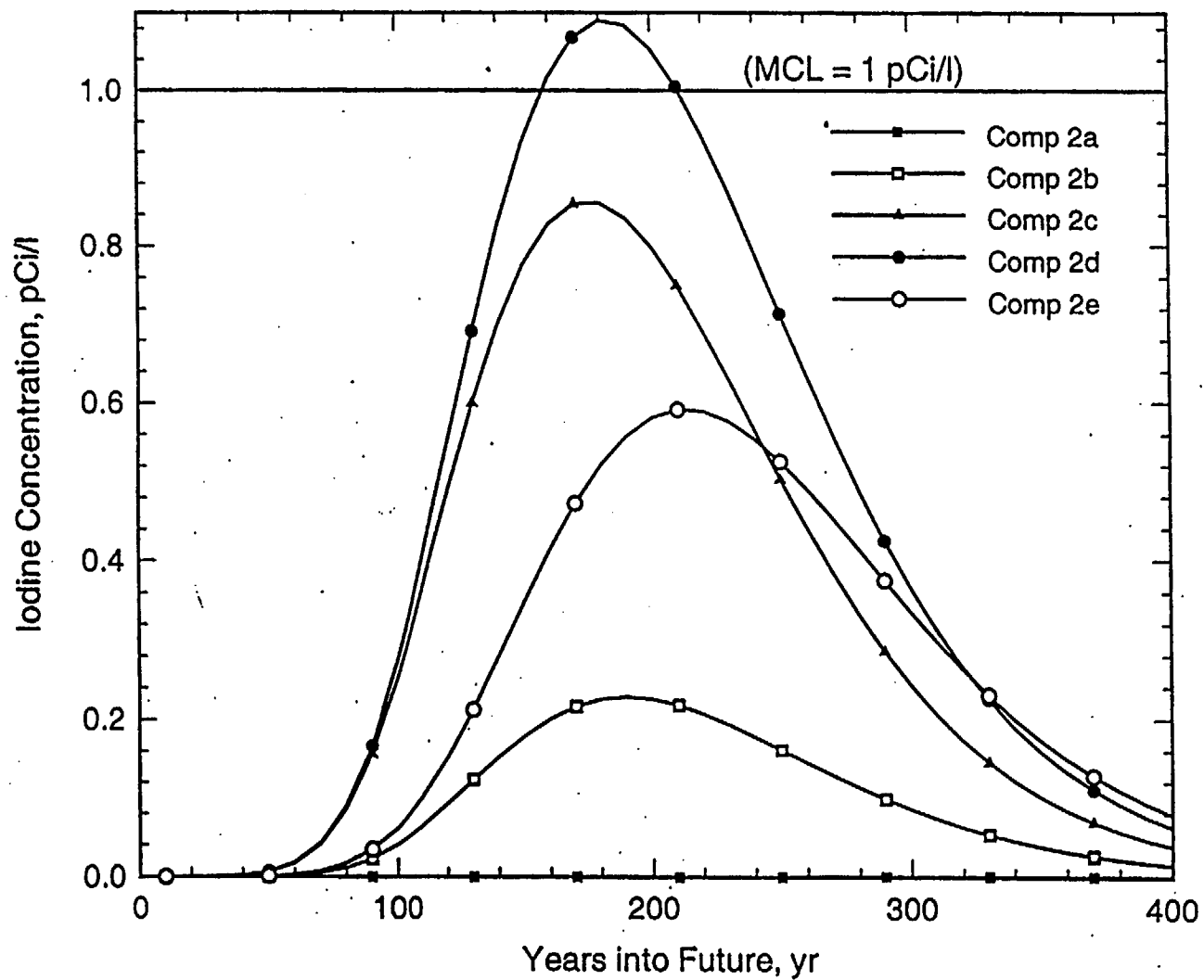


Figure A-14 Predicted iodine-129 concentration at Compliance Boundary.

# Iodine-129 Plume (pCi/l) in Upper Three Runs Aquifer Unit (IIB<sub>1</sub>)

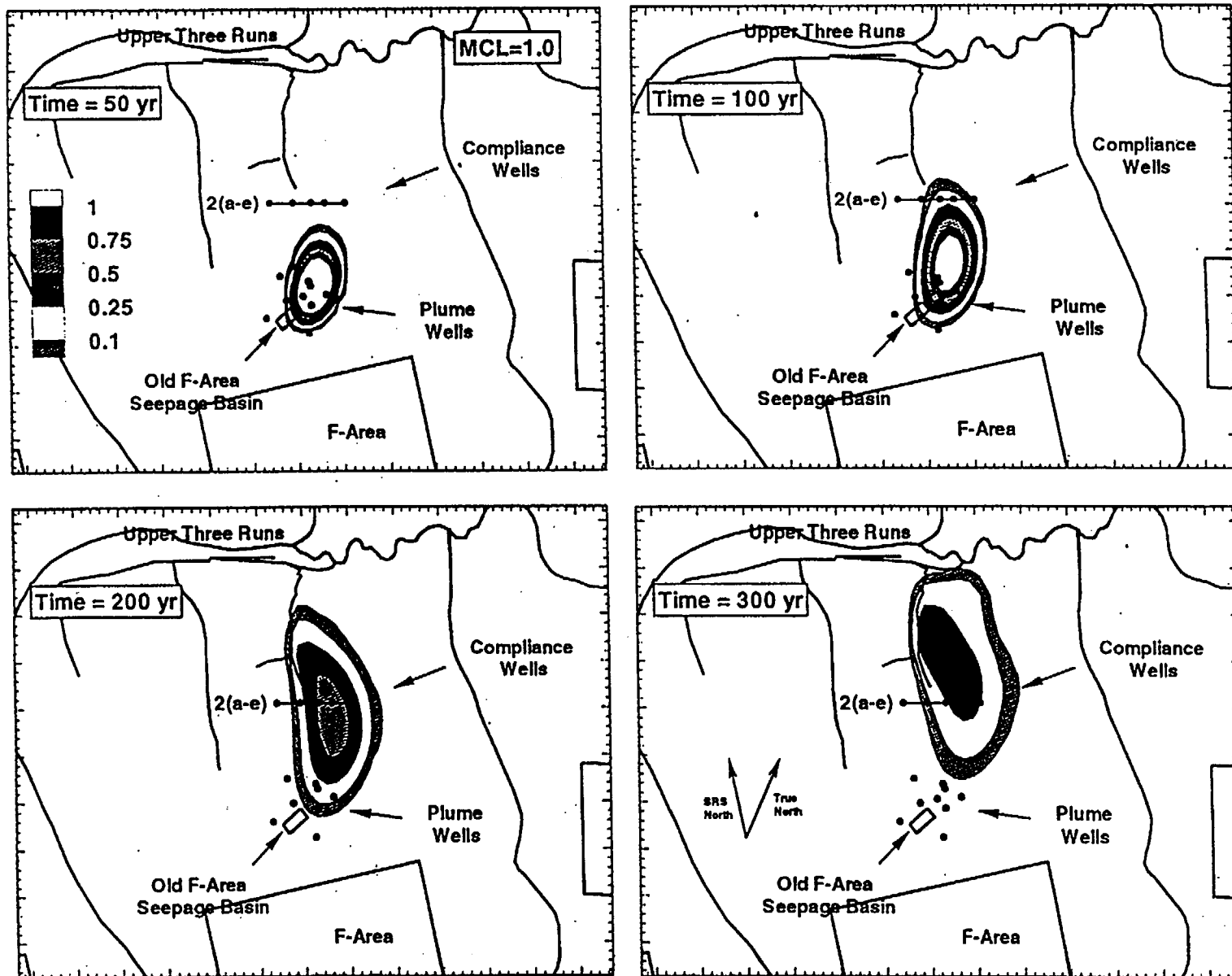


Figure A-15 Predicted iodine-129 plume conditions in 50, 100, 200, and 300 years (areal view).

# Iodine-129 Plume (pCi/l) in Upper Three Runs Aquifer Unit (IIB<sub>2</sub> & IIB<sub>1</sub>)

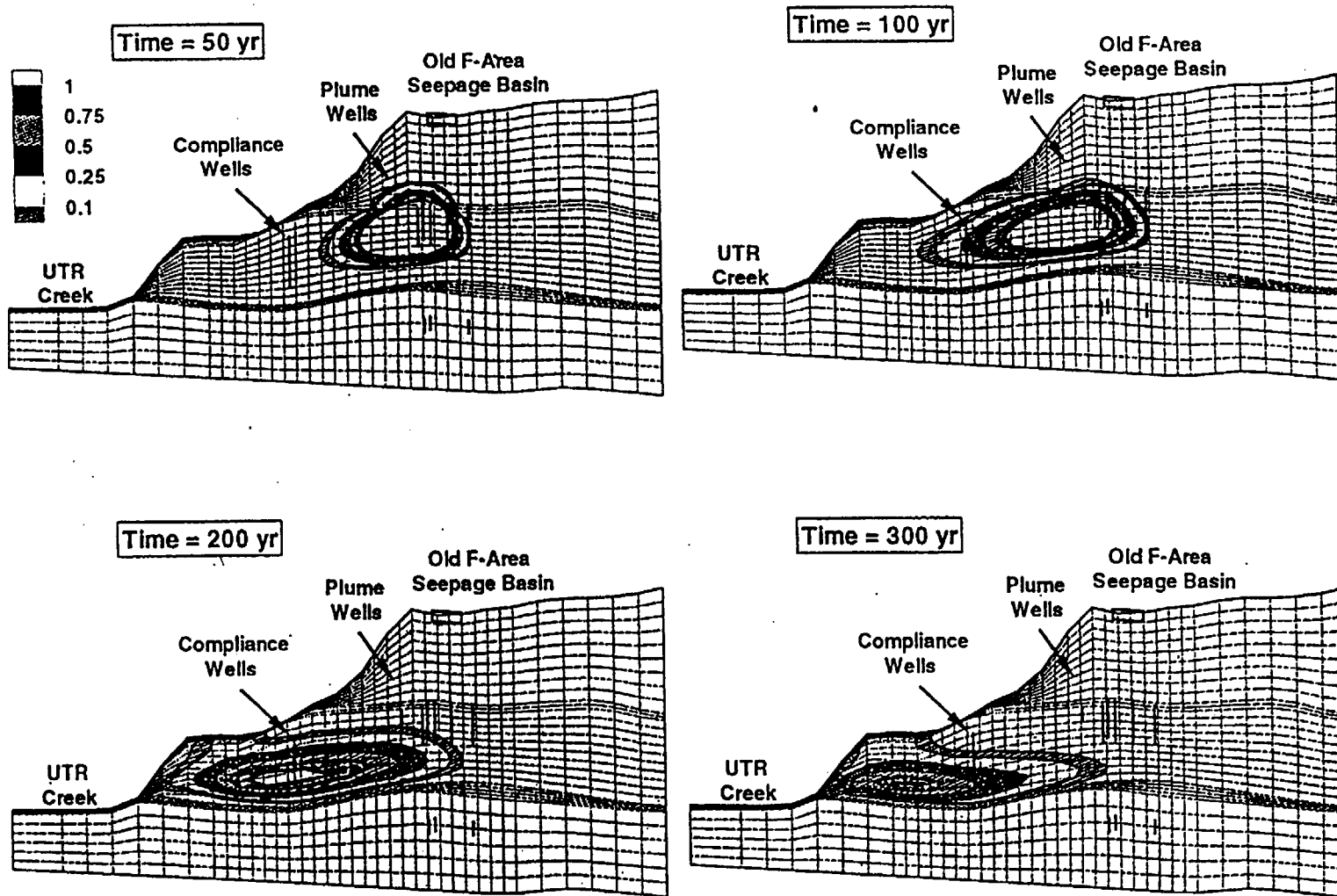


Figure A-16 Predicted iodine-129 plume conditions in 50, 100, 200, and 300 years (cross-sectional view).

# OLD F-AREA SEEPAGE BASIN

## Strontium-90 Concentration at Plume Boundary

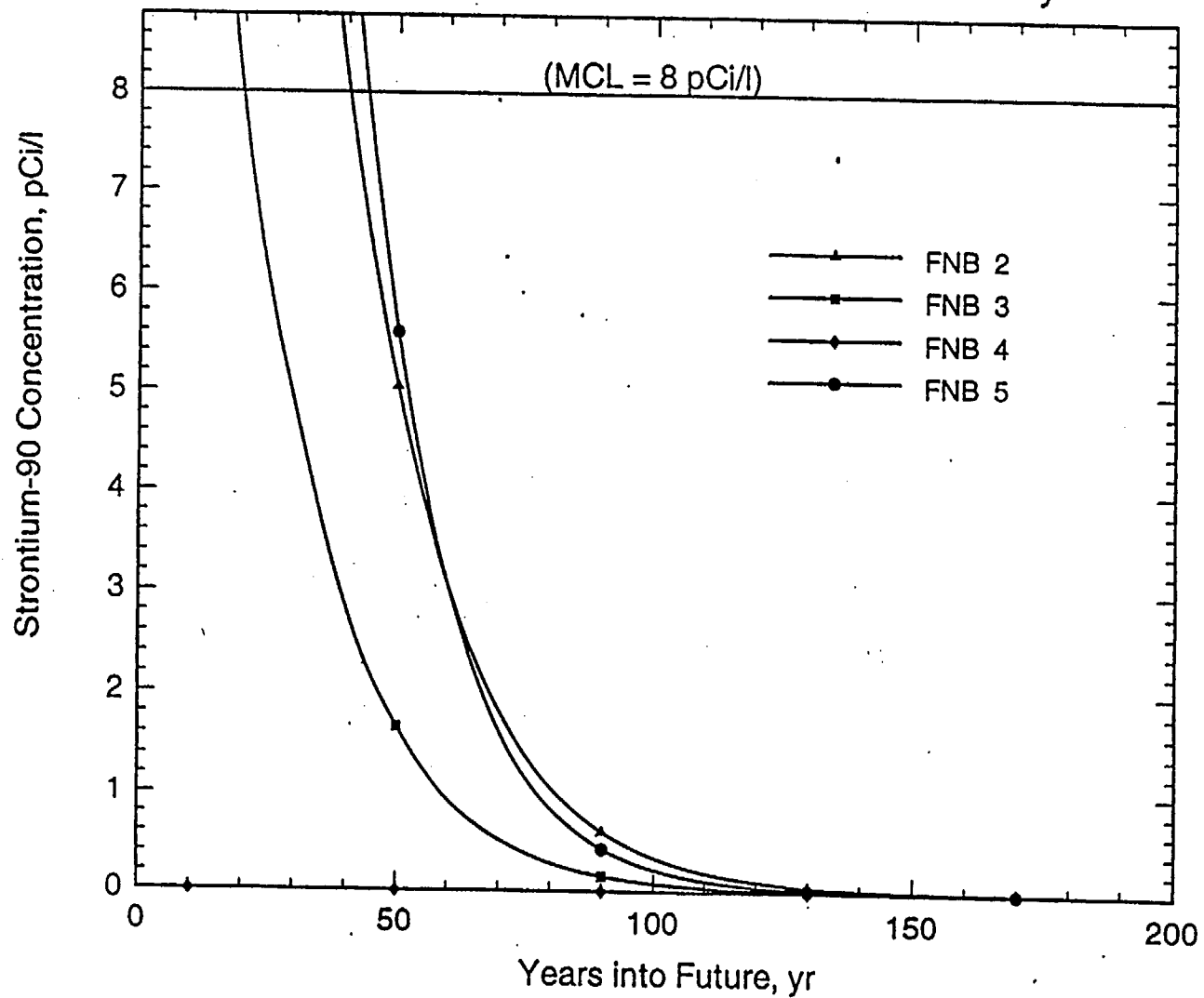


Figure A-17 Predicted strontium-90 concentration at FNB Point of Compliance wells.

# OLD F-AREA SEEPAGE BASIN

## Strontium Concentration at Compliance Boundary

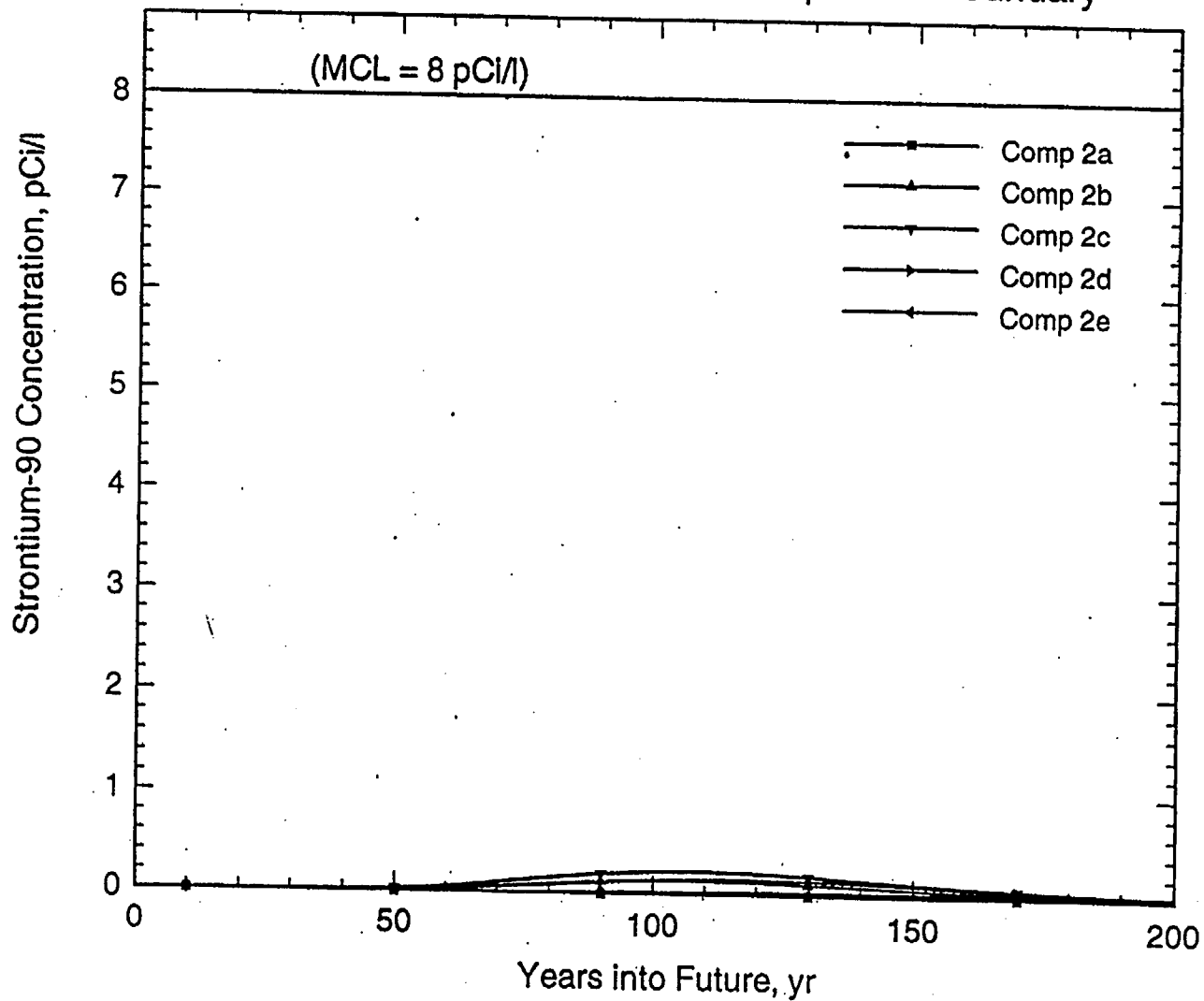


Figure A-18 Predicted strontium-90 concentration at Compliance Boundary.

# Strontium-90 Plume (pCi/l) in Upper Three Runs Aquifer Unit (IIB<sub>1</sub>)

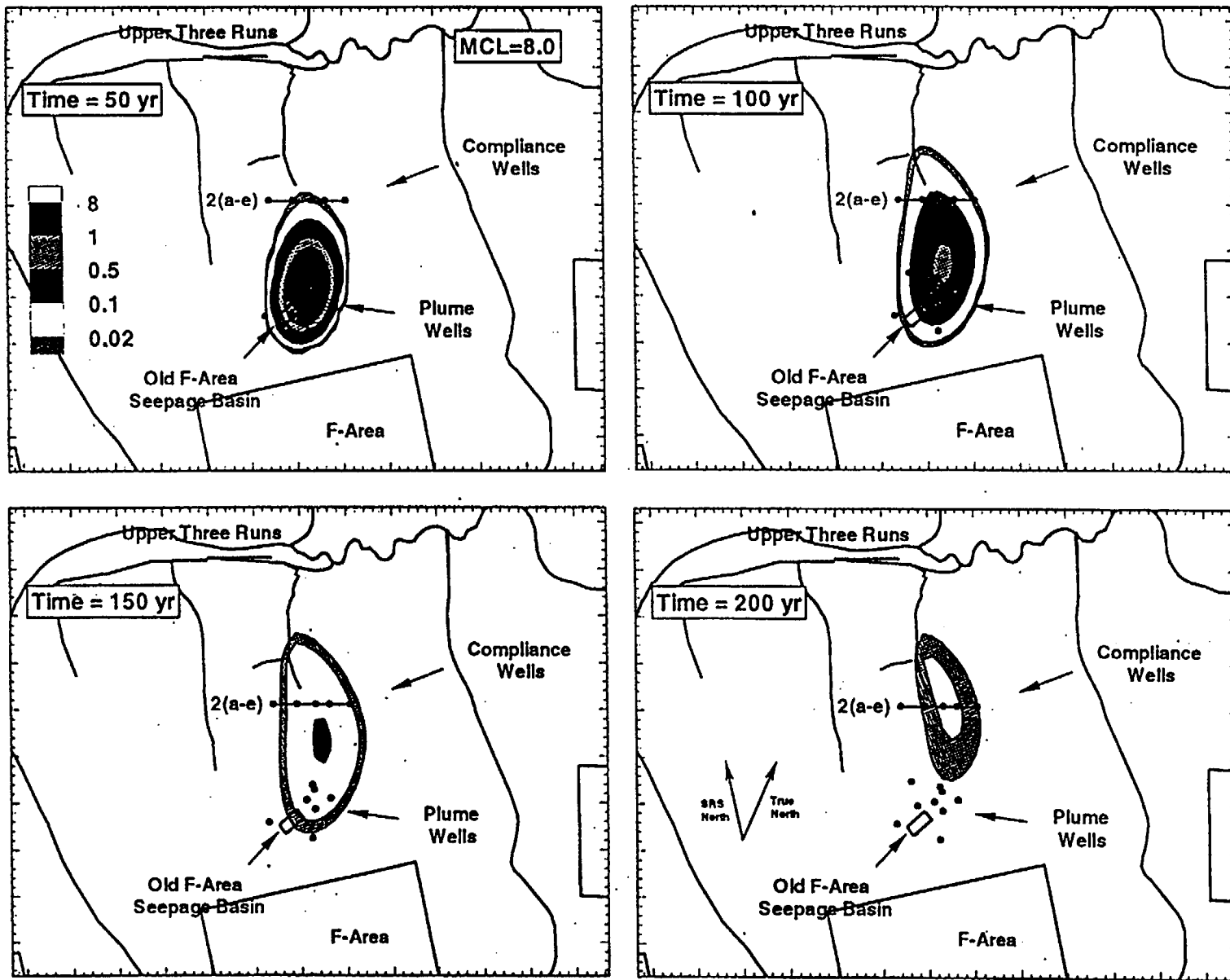


Figure A-19 Predicted strontium-90 plume conditions in 5, 100, 150, and 200 years (areal view).

# Strontium-90 Plume (pCi/l) in Upper Three Runs Aquifer Unit (IIB<sub>2</sub>&IIB<sub>1</sub>)

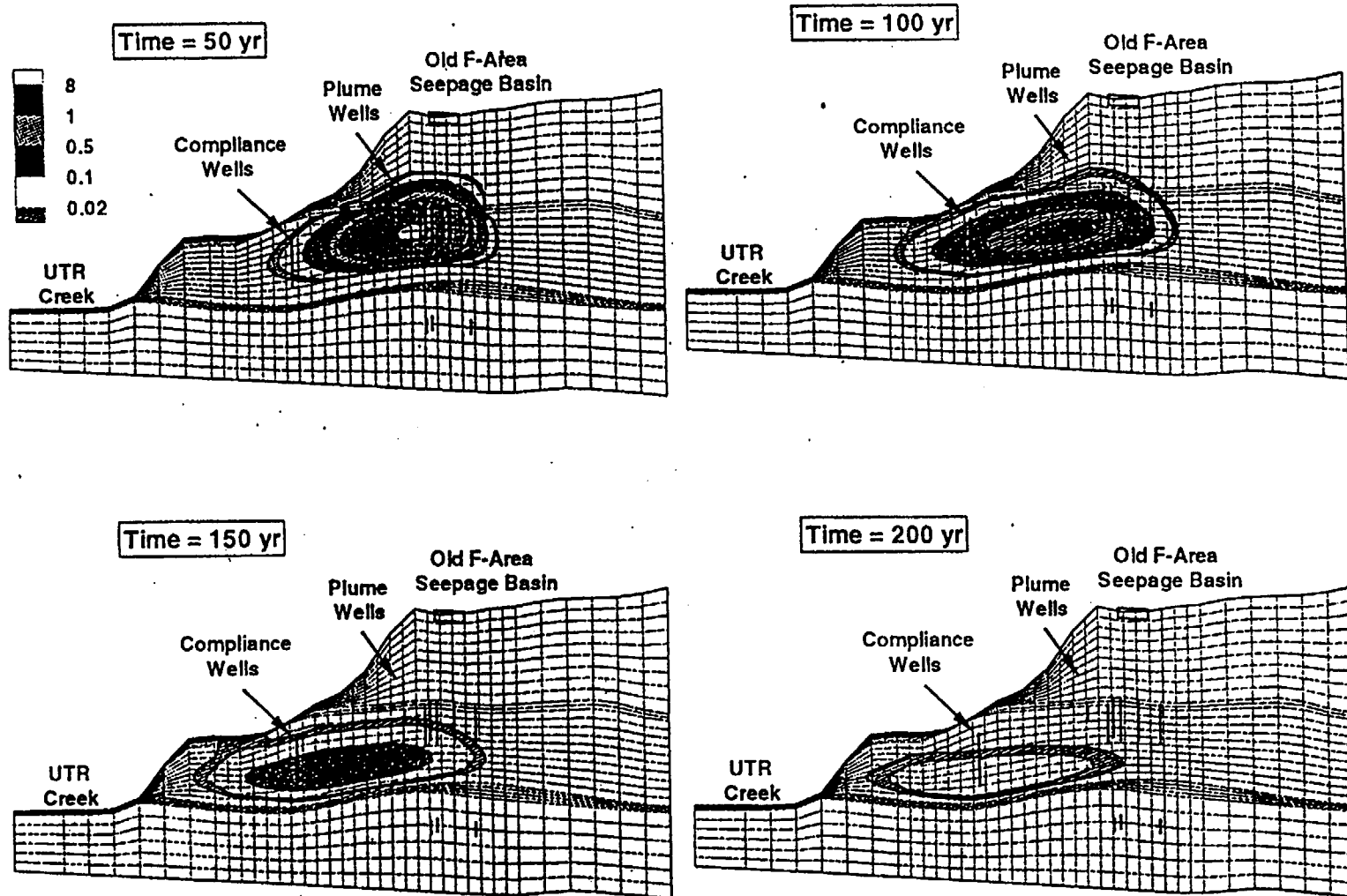


Figure A-20 Predicted strontium-90 plume conditions in 5, 100, 150, and 200 years (cross-sectional view).

# OLD F-AREA SEEPAGE BASIN

## Total Uranium Concentration at Plume Boundary

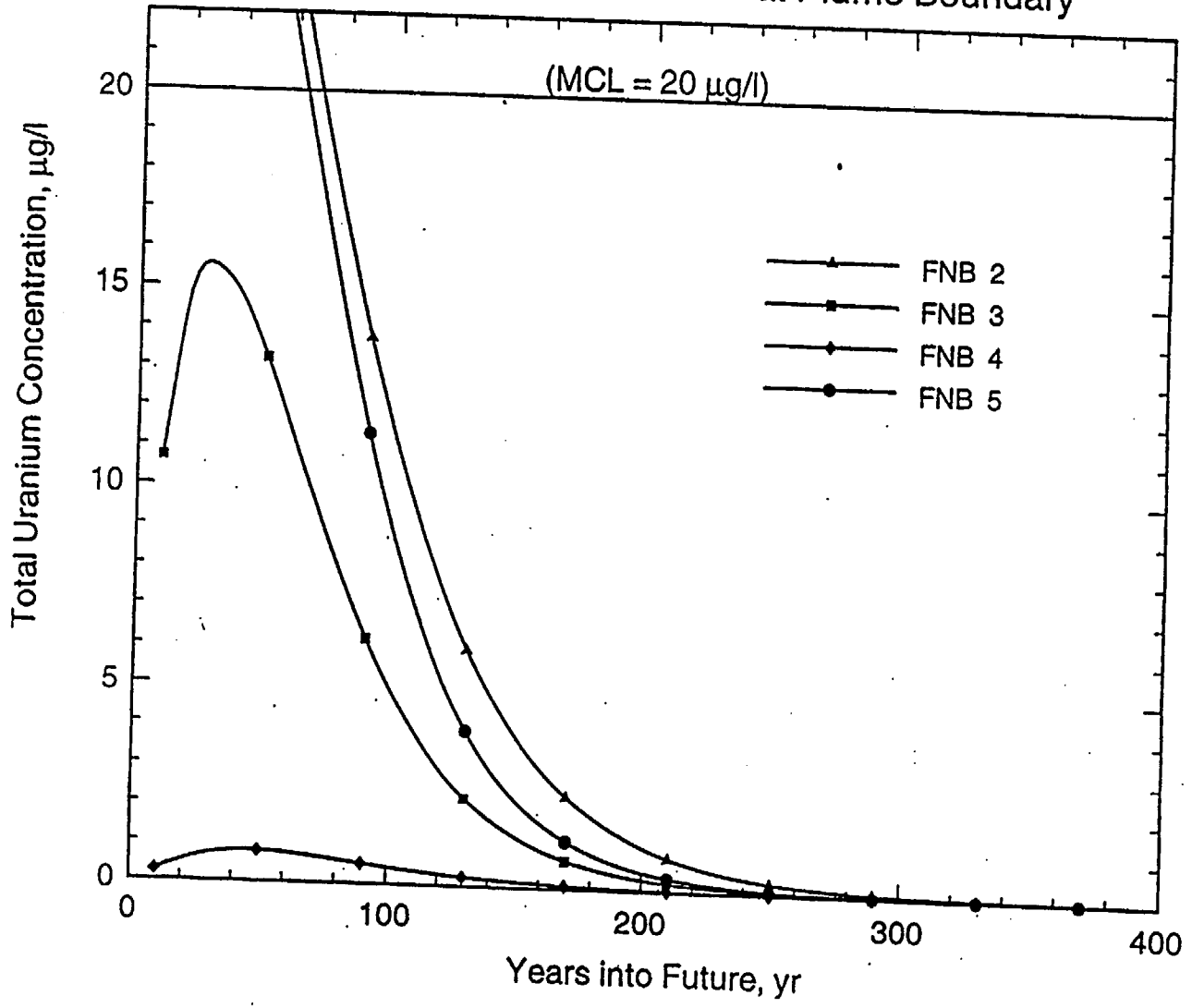


Figure A-21 Predicted uranium (total) concentration at FNB Point of Compliance wells.  
A-34

# OLD F-AREA SEEPAGE BASIN

## Total Uranium Concentration at Compliance Boundary

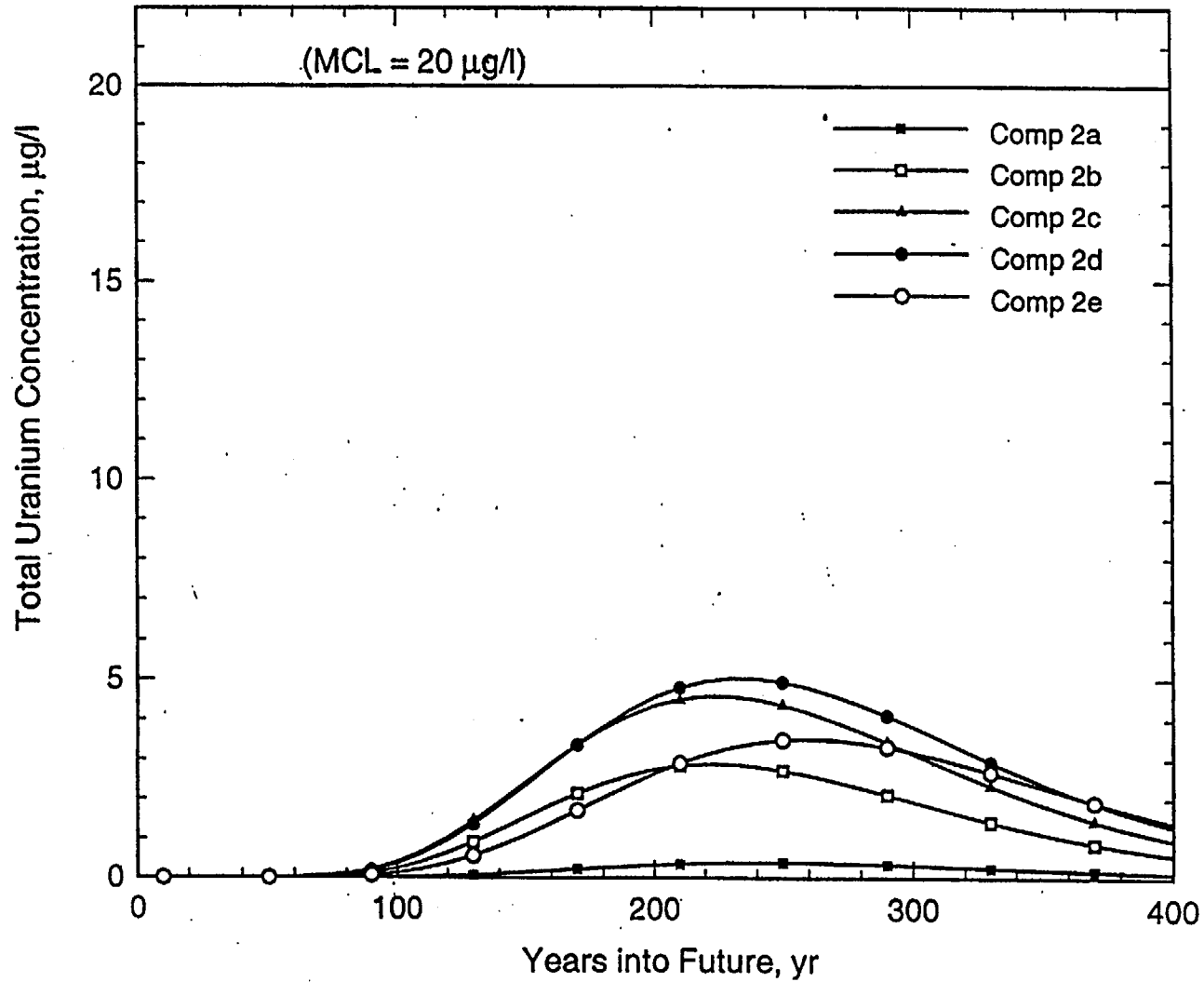


Figure A-22 Predicted uranium (total) concentration at Compliance Boundary.

# Total Uranium Plume ( $\mu\text{g/l}$ ) in Upper Three Runs Aquifer Unit (IIB<sub>1</sub>)

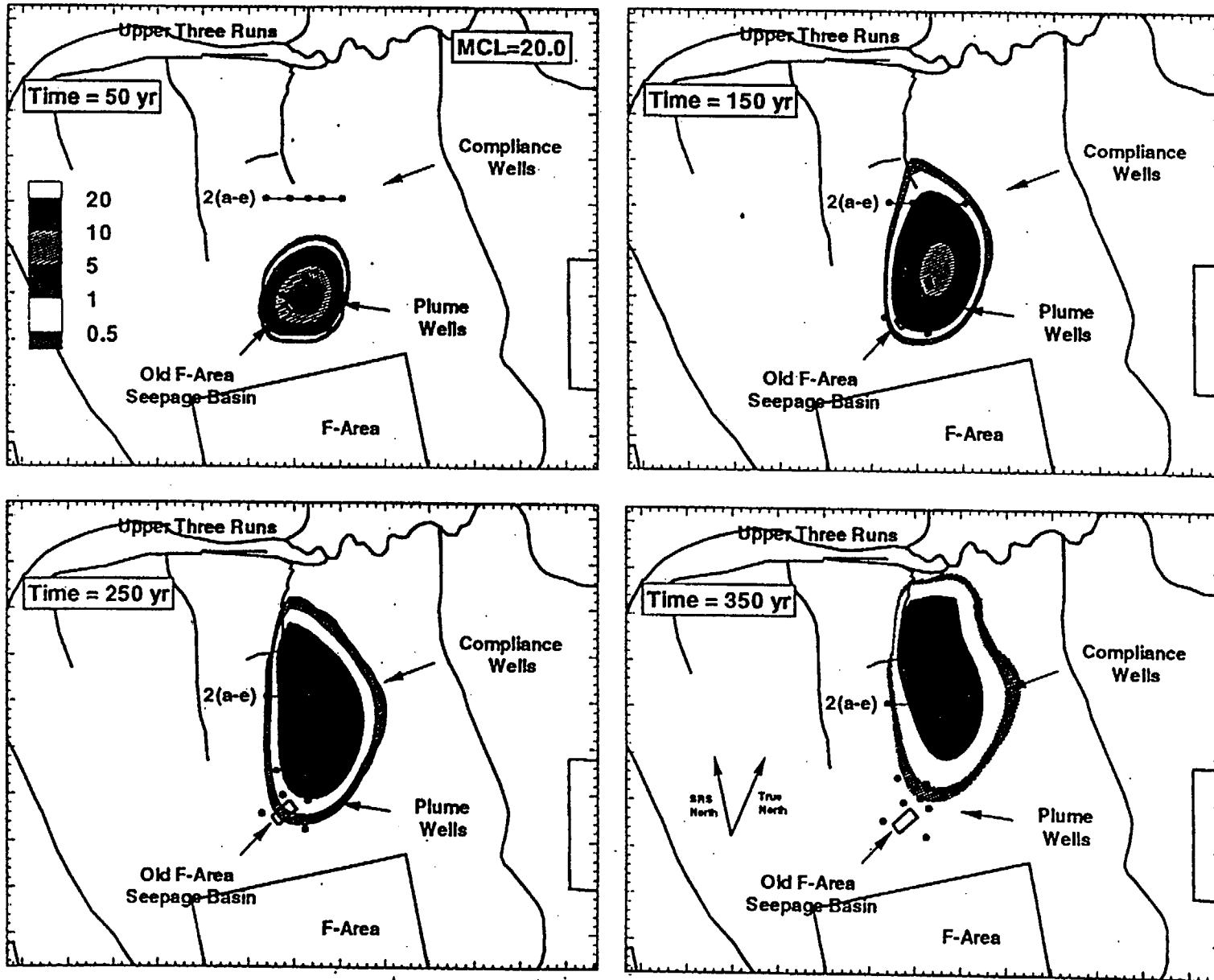


Figure A-23 Predicted uranium (total) plume conditions in 50, 150, 250, and 350 years (areal view).

# Total Uranium Plume ( $\mu\text{g/l}$ ) in Upper Three Runs Aquifer Unit (IIB<sub>2</sub>&IIB<sub>1</sub>)

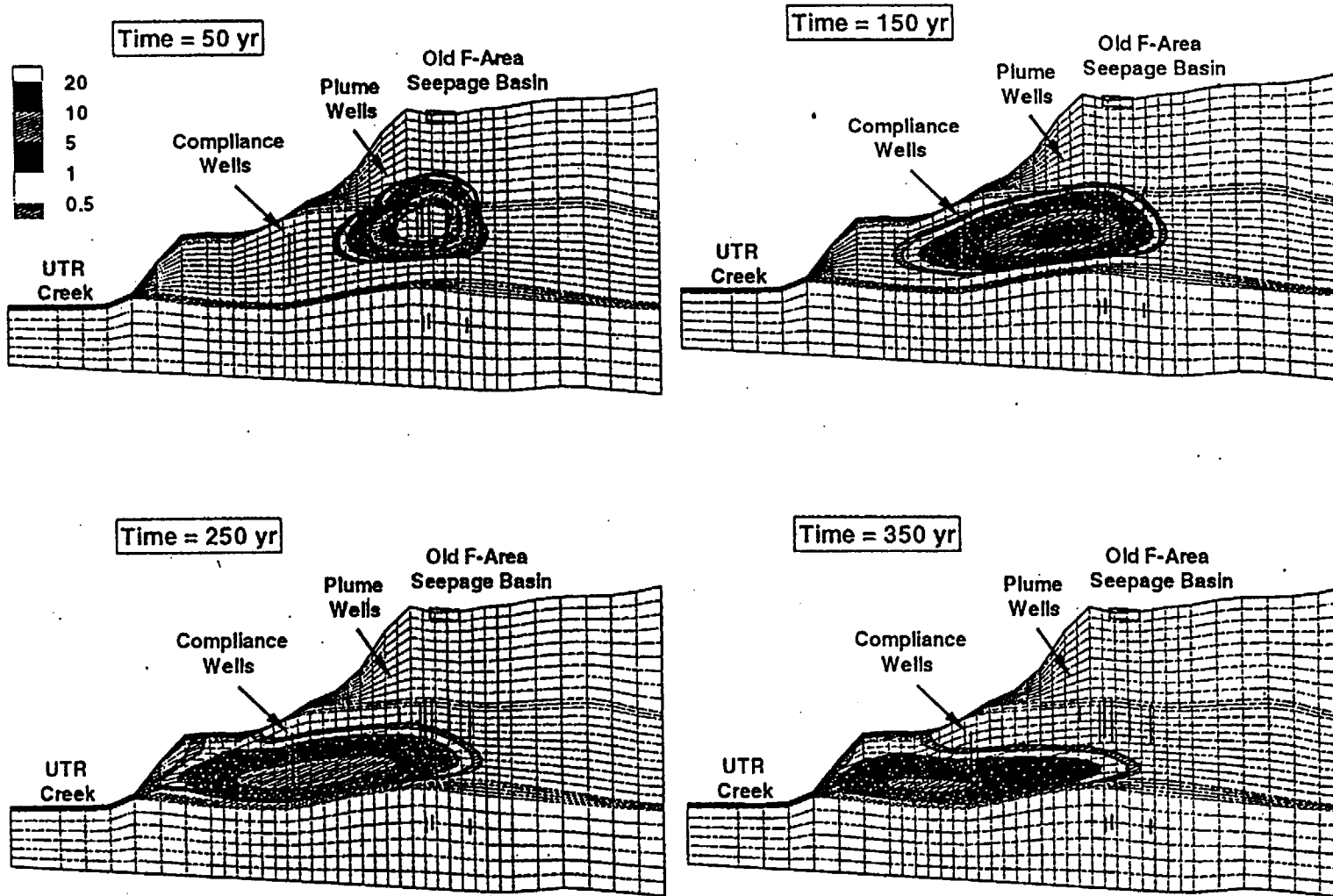


Figure A-24 Predicted uranium (total) plume conditions in 50, 150, 250, and 350 years (cross-sectional view).

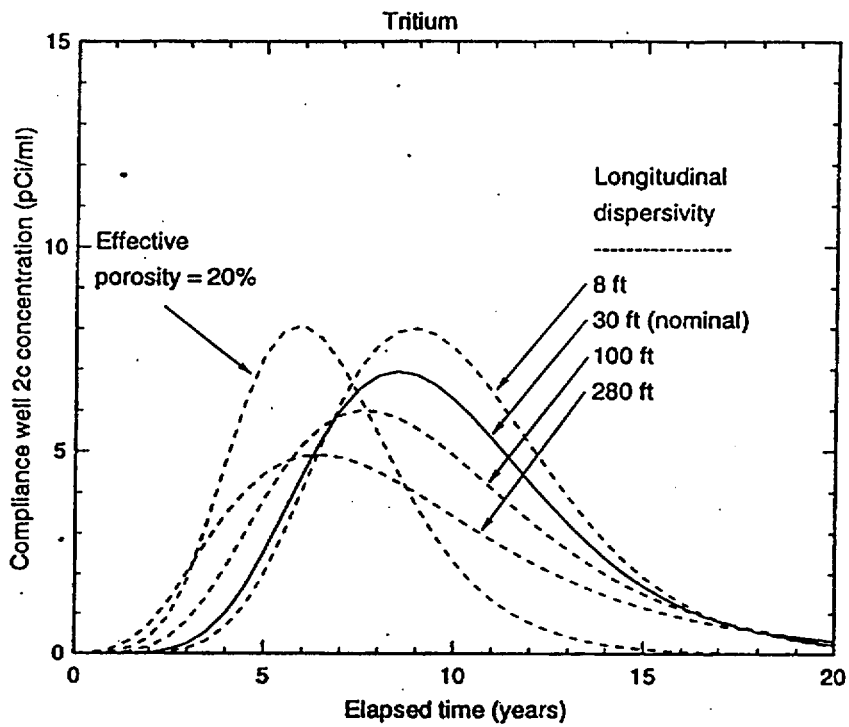


Figure A-25 Results of sensitivity study for tritium.  
A-38

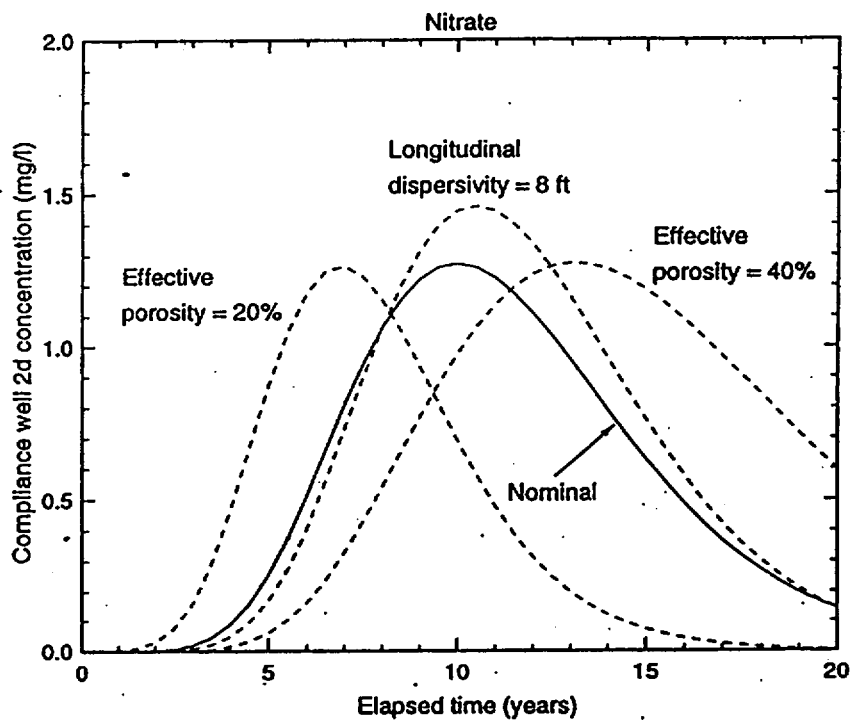


Figure A-26 Results of sensitivity study for nitrate.

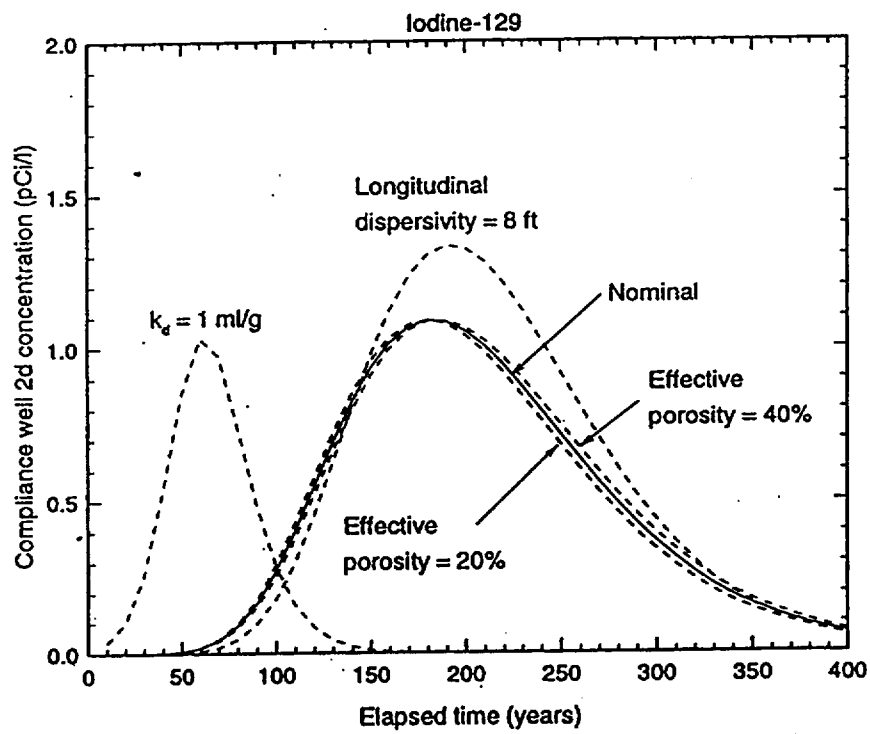


Figure A-27 Results of sensitivity study for iodine-129.  
A-40

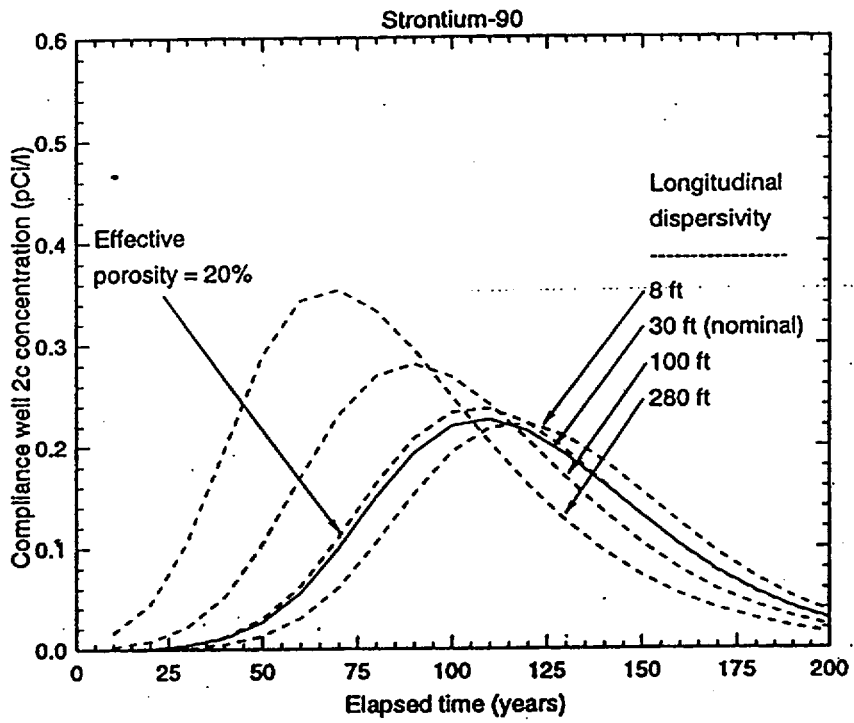


Figure A-28 Results of sensitivity study for strontium-90.

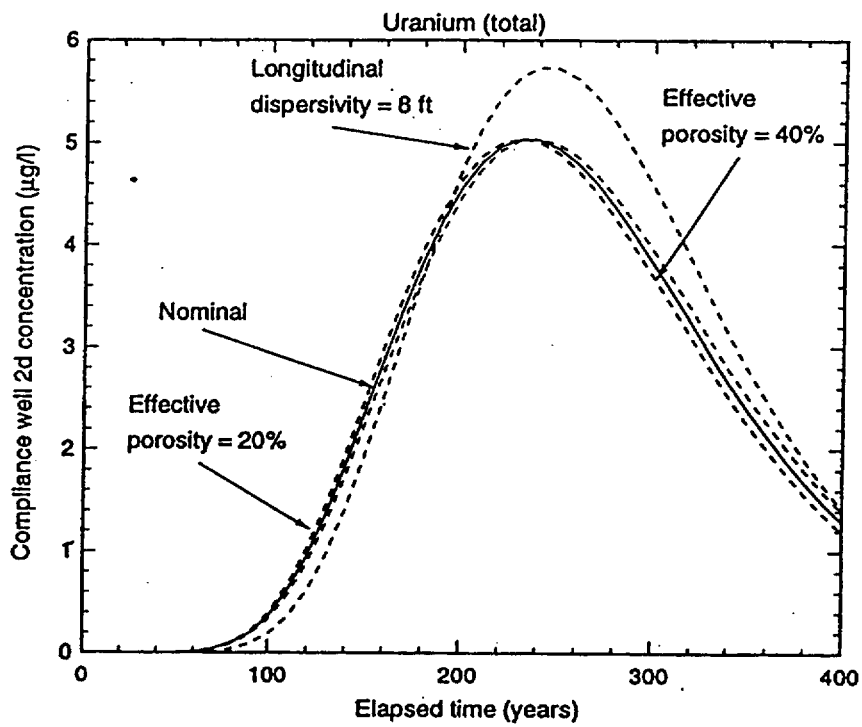


Figure A-29 Results of sensitivity study for uranium.  
A-42

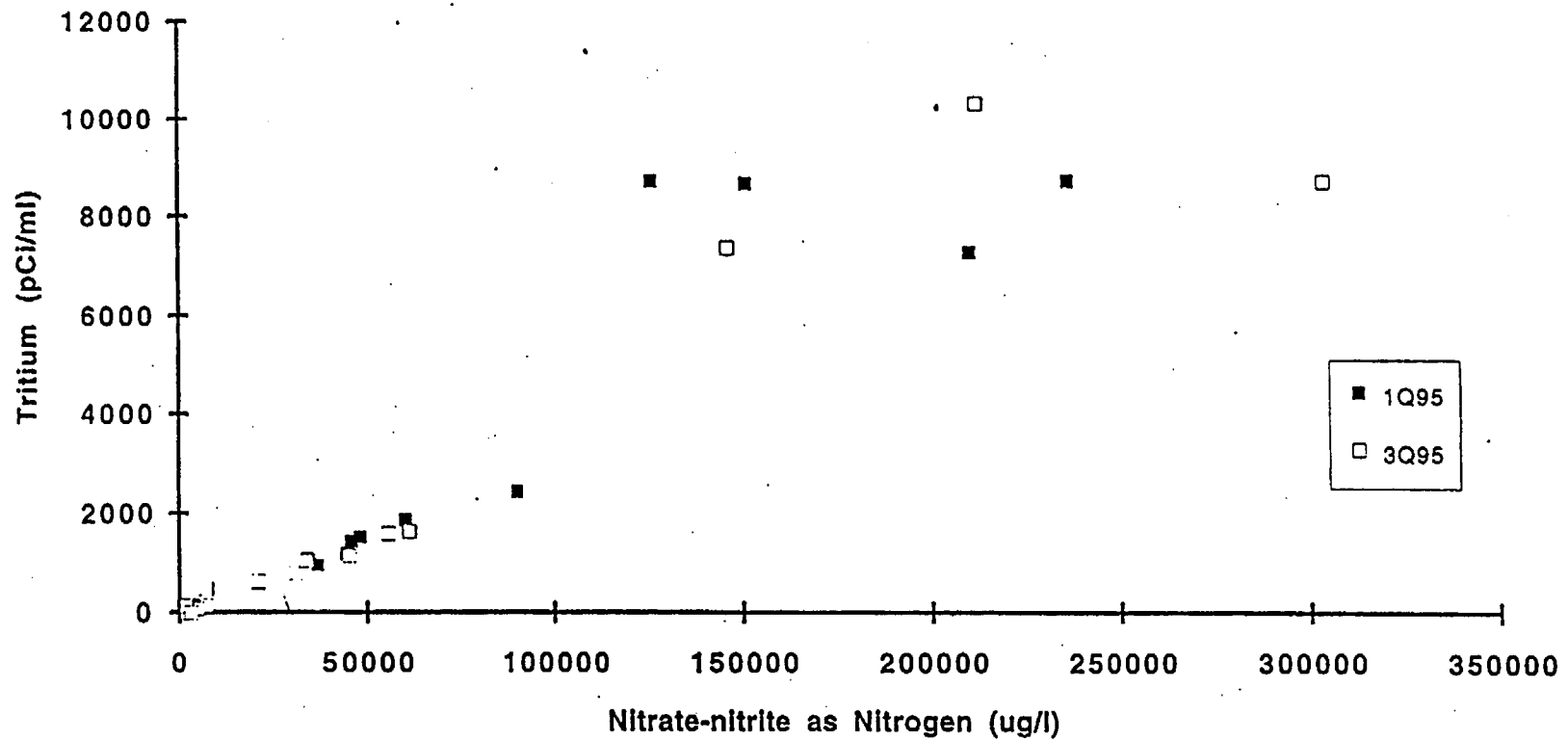


Figure A-30: Plot of tritium versus nitrate in groundwater of water table wells at F-Area Seepage Basin.

Measured Hydraulic Head in Upper Three Runs Aquifer (IIB<sub>1</sub> and IIB<sub>2</sub>)

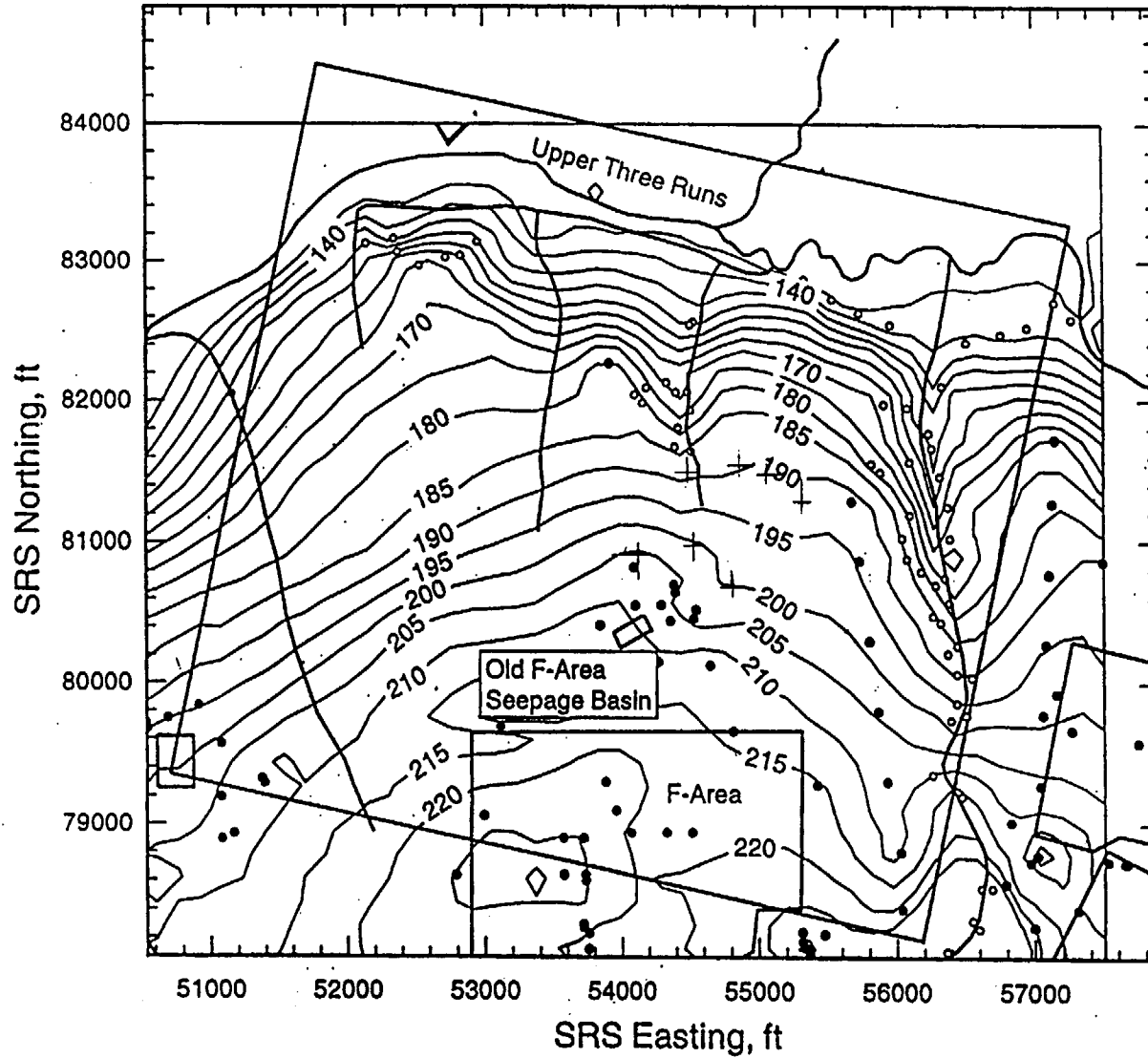


Figure A-31: Contour plot of measured hydraulic head data from Upper Three Runs aquifer (IIB<sub>1</sub> and IIB<sub>2</sub>).

Simulated Hydraulic Head in "Lower" Aquifer Zone (IIB<sub>1</sub>)

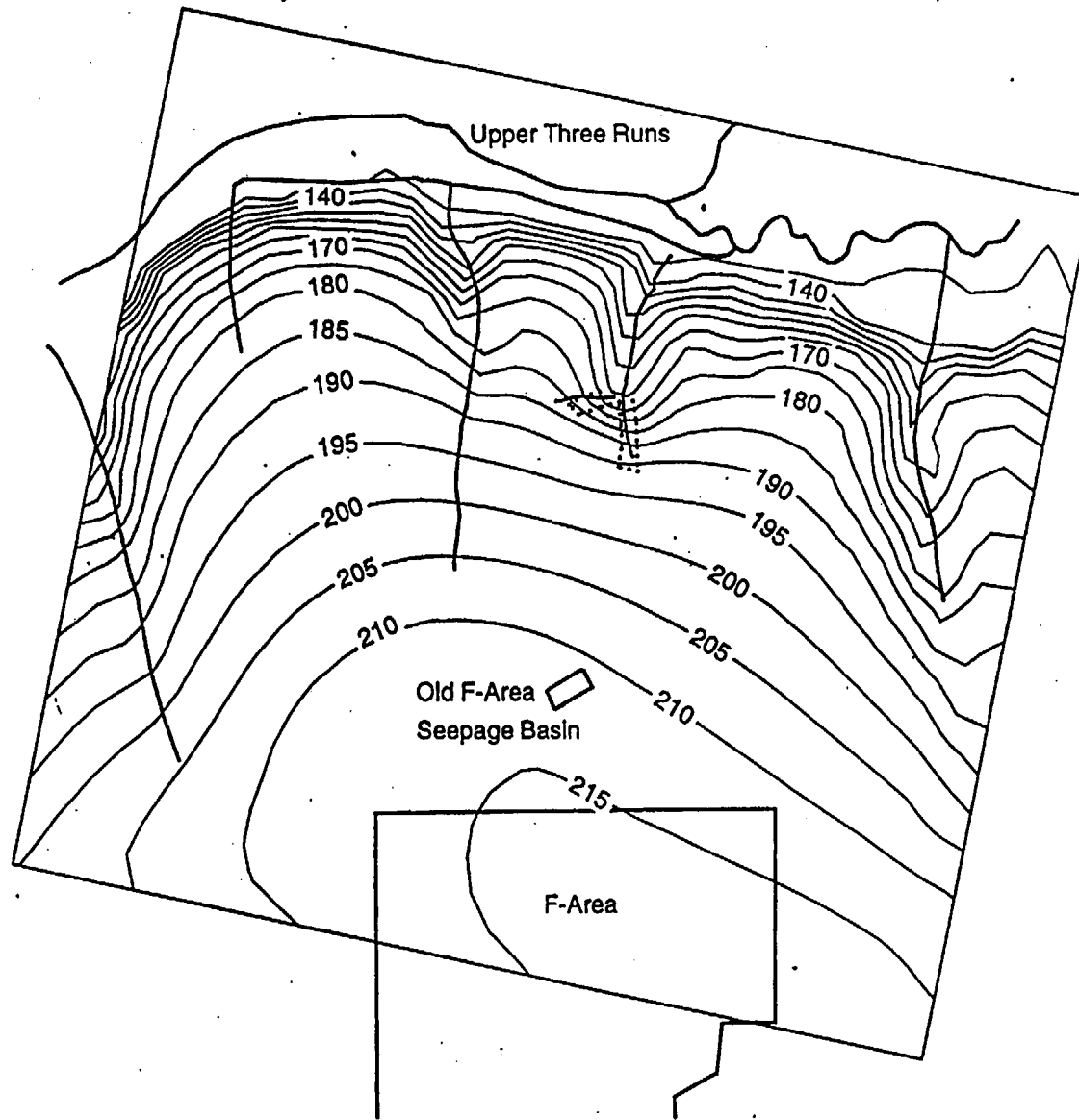


Figure A-32: Contour plot of simulated hydraulic head in the "lower" aquifer zone (IIB<sub>1</sub>).

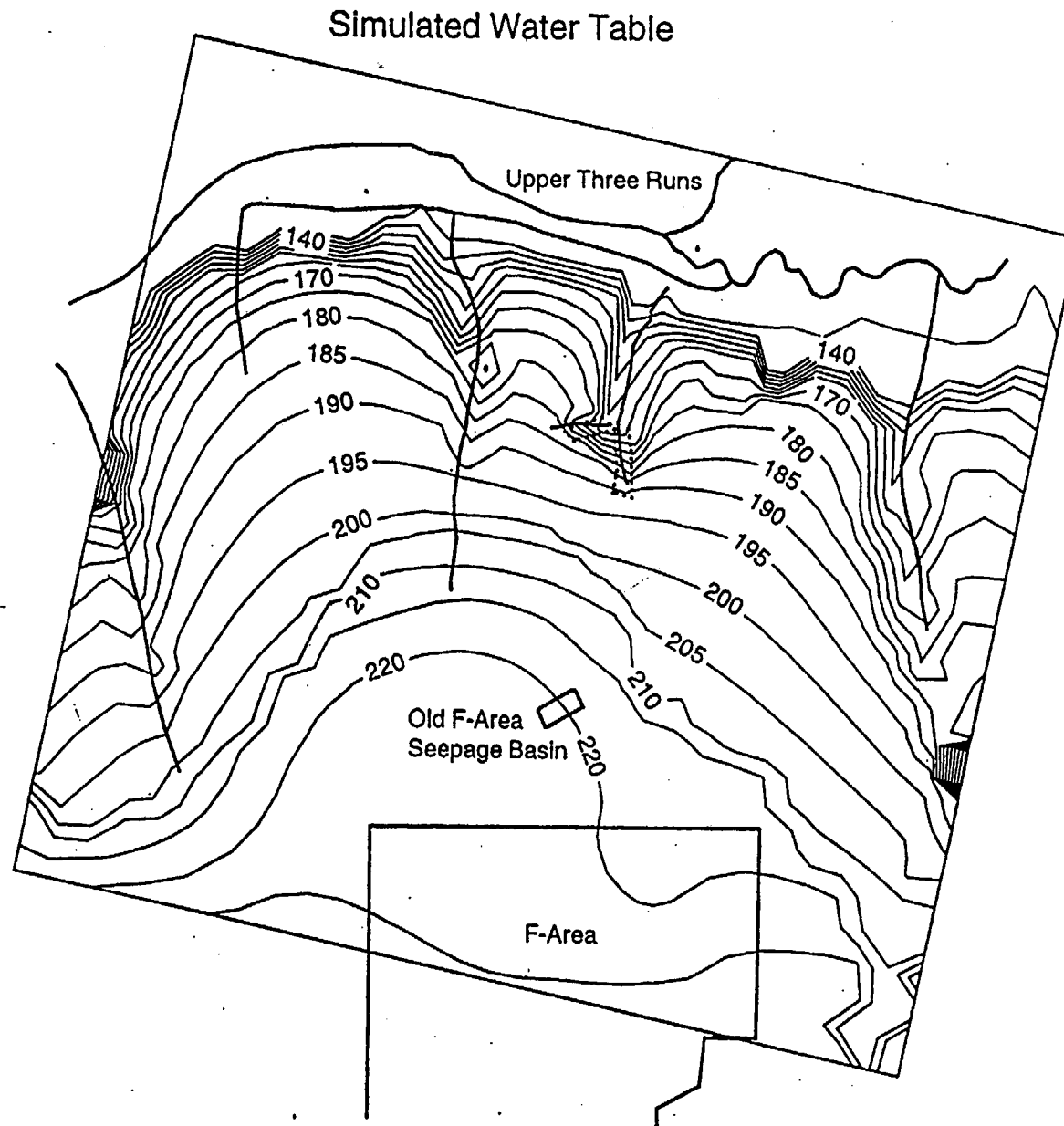


Figure A-33: Contour plot of simulated water table surface.  
A-46

### Restoration Times for Upper Three Runs Aquifer Unit

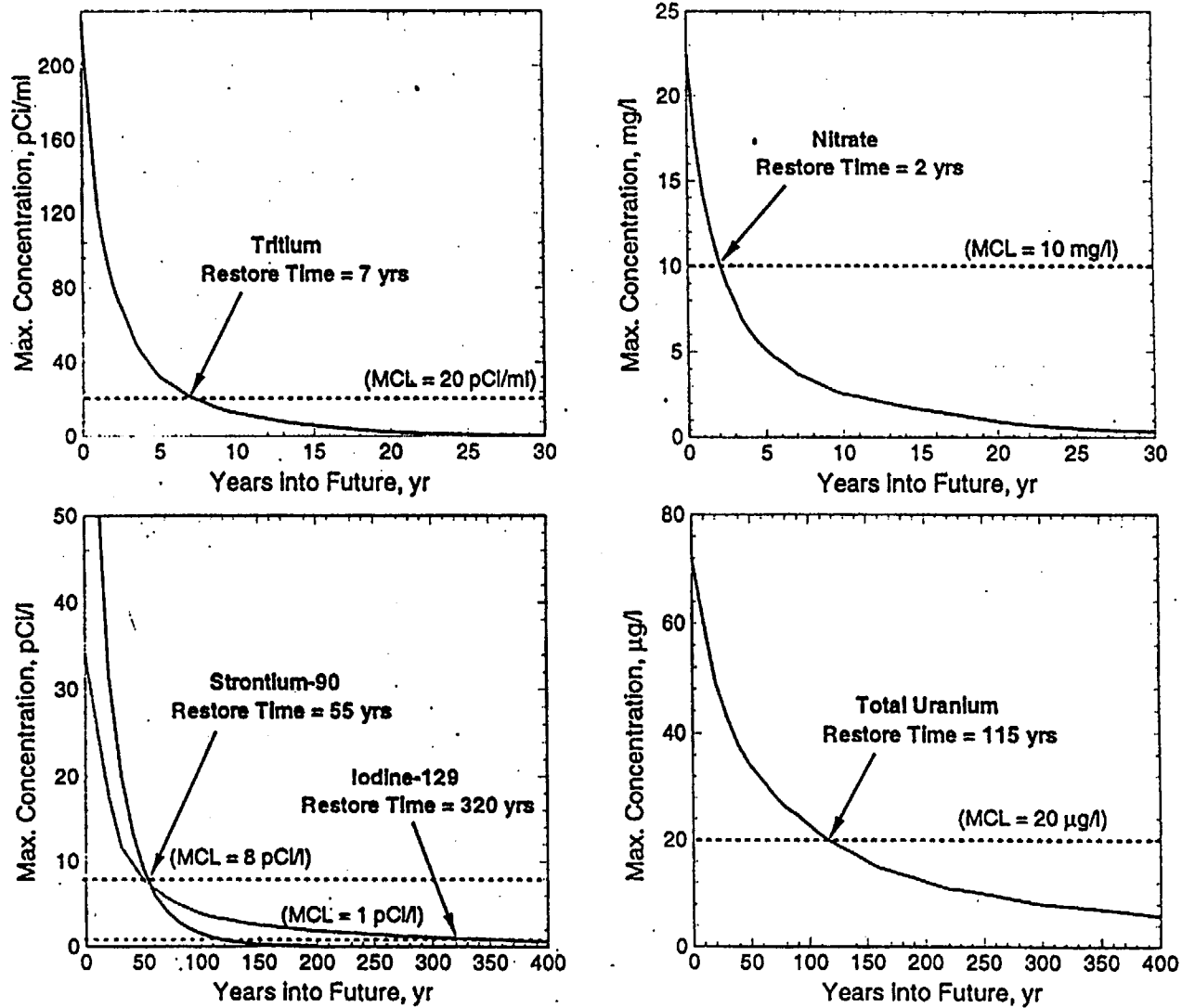


Figure A-34: Restoration times based on natural attenuation of aquifer unit.